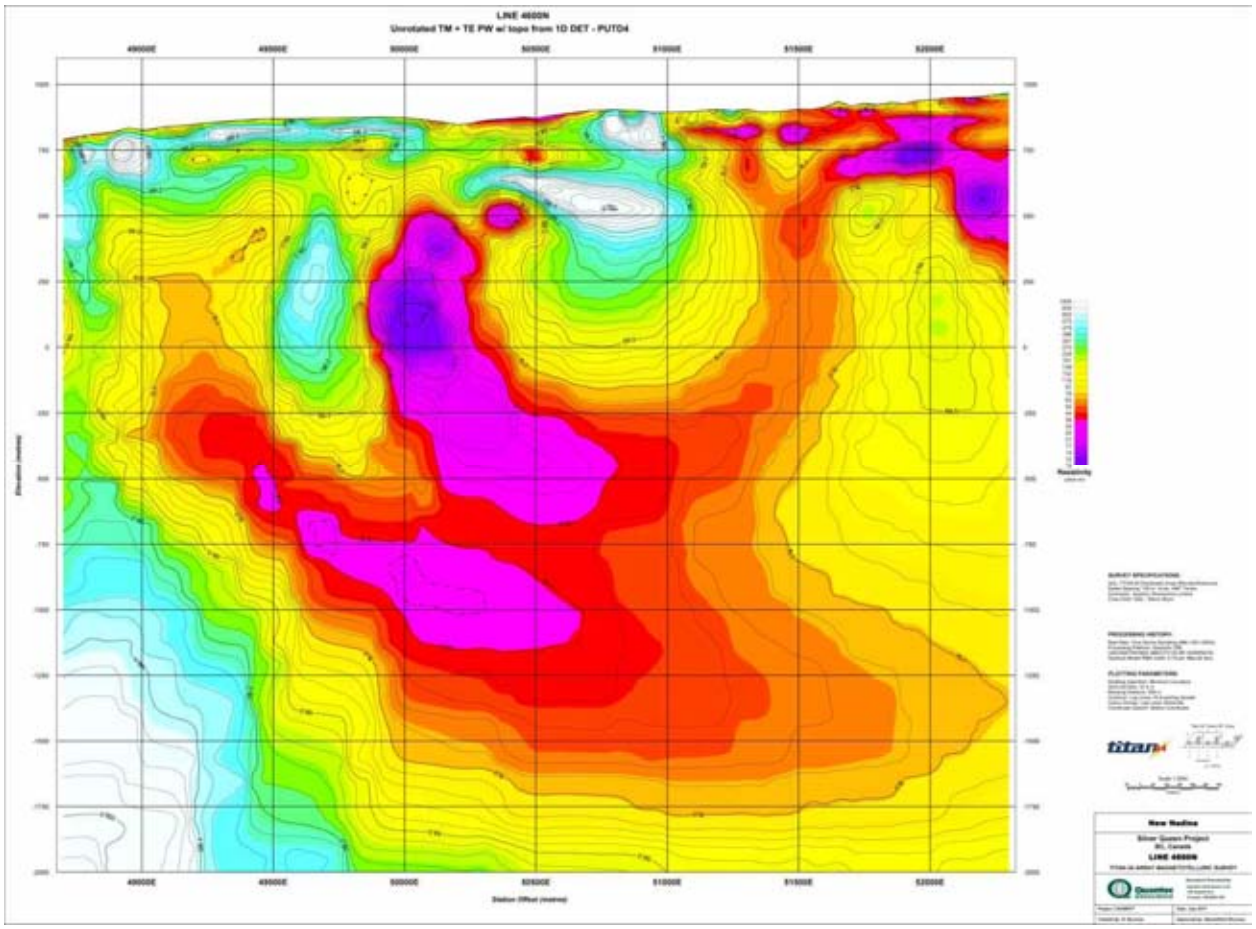

Line 4600N –MT- PWM Resistivity 2D Model

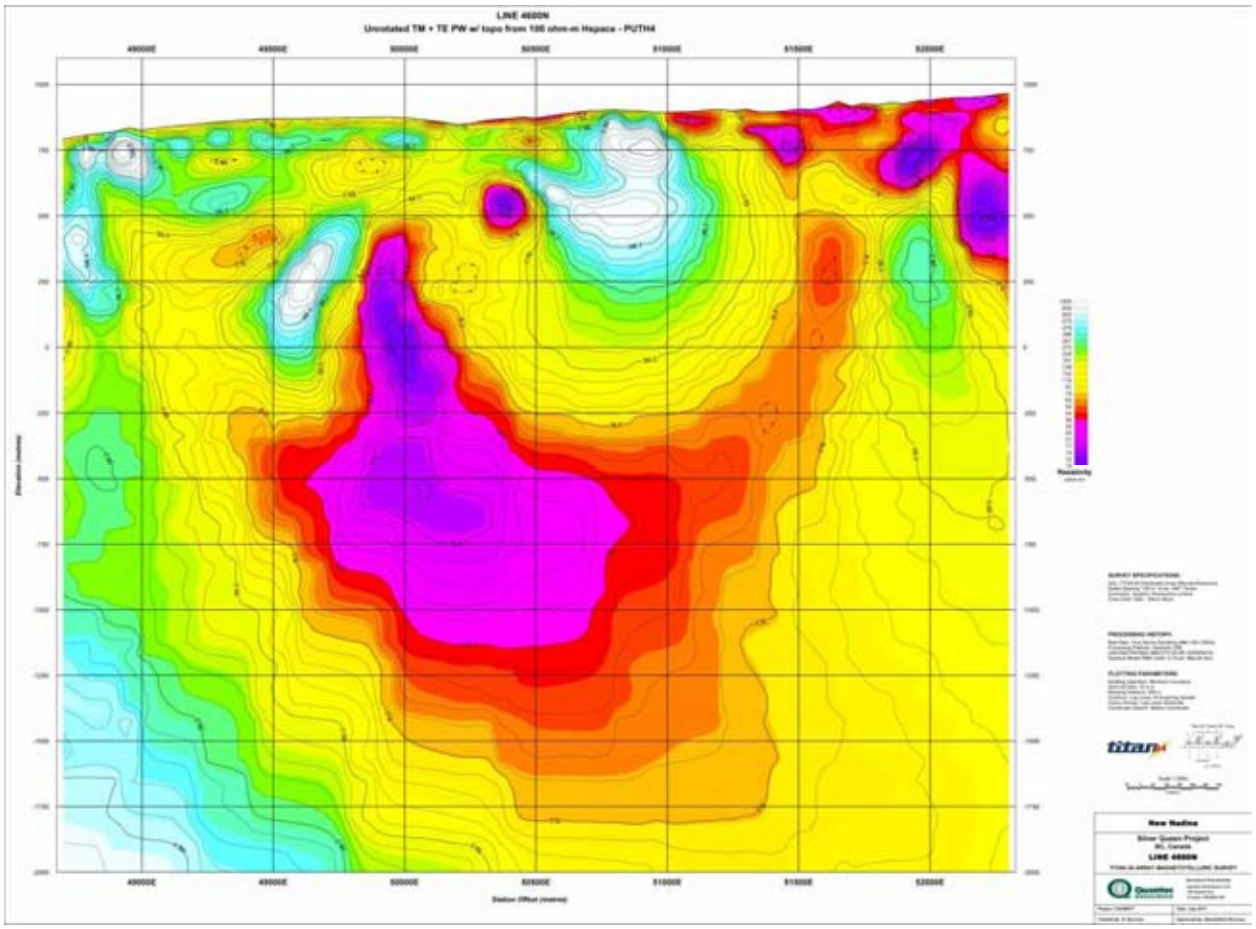

Line 4600N –MT- PWM Resistivity 2D Model

J.6 LINE 4900N

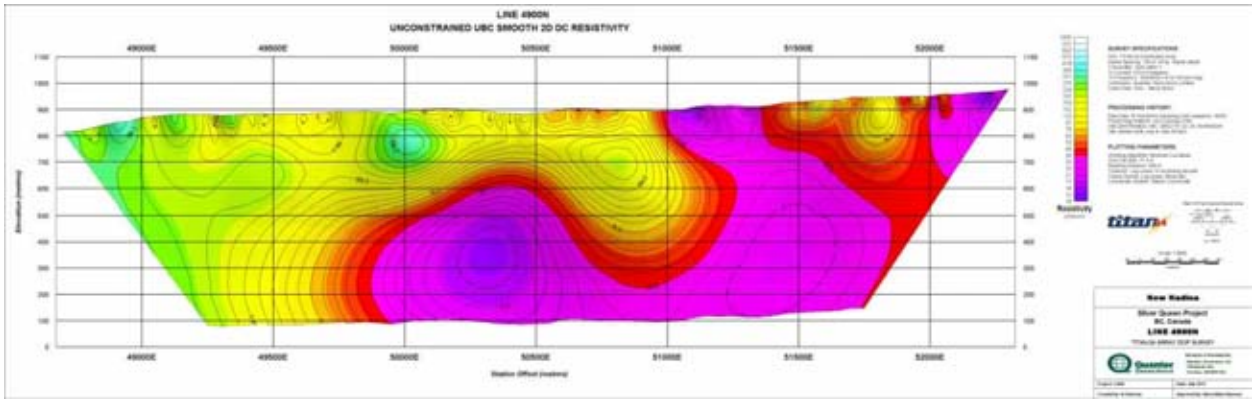

Line 4900N –DC Resistivity 2D Model

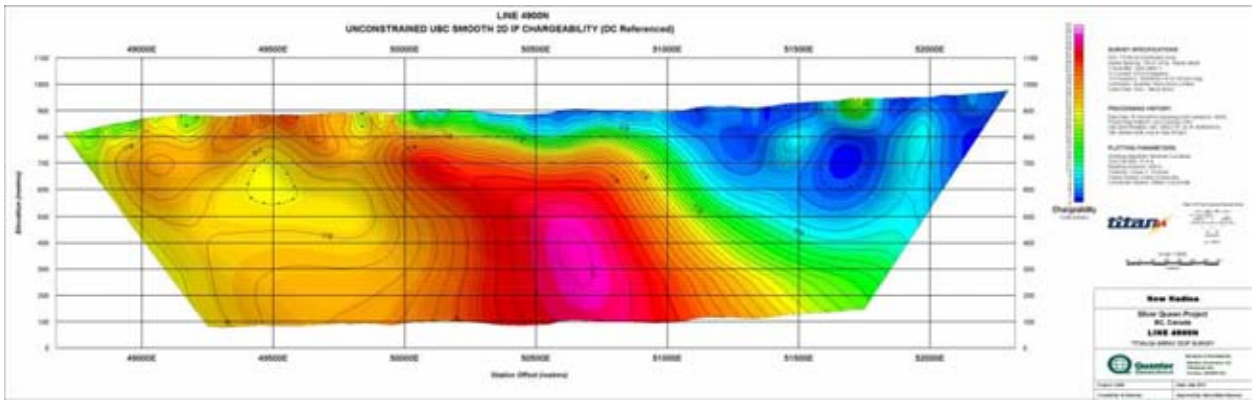

Line 4900N –IP Chargeability 2D Model

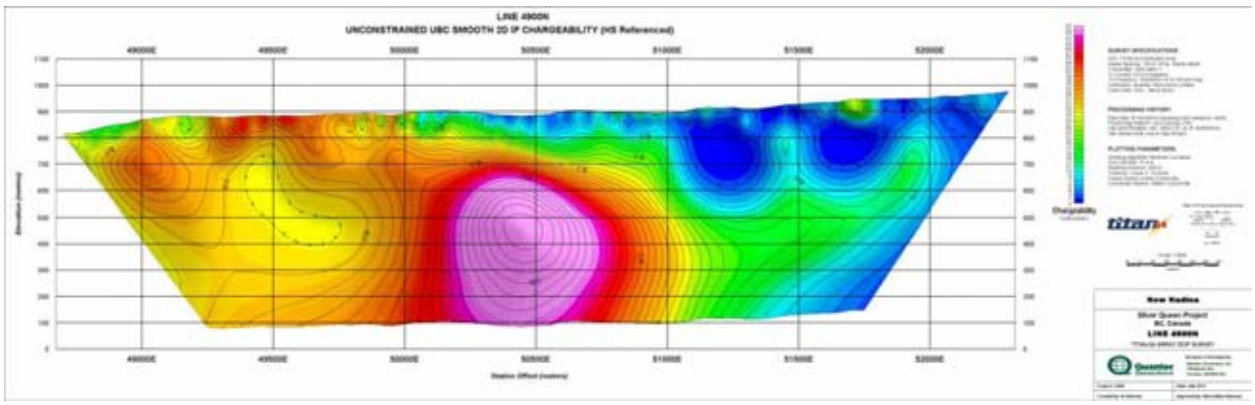

Line 4900N –IP Chargeability 2D Model

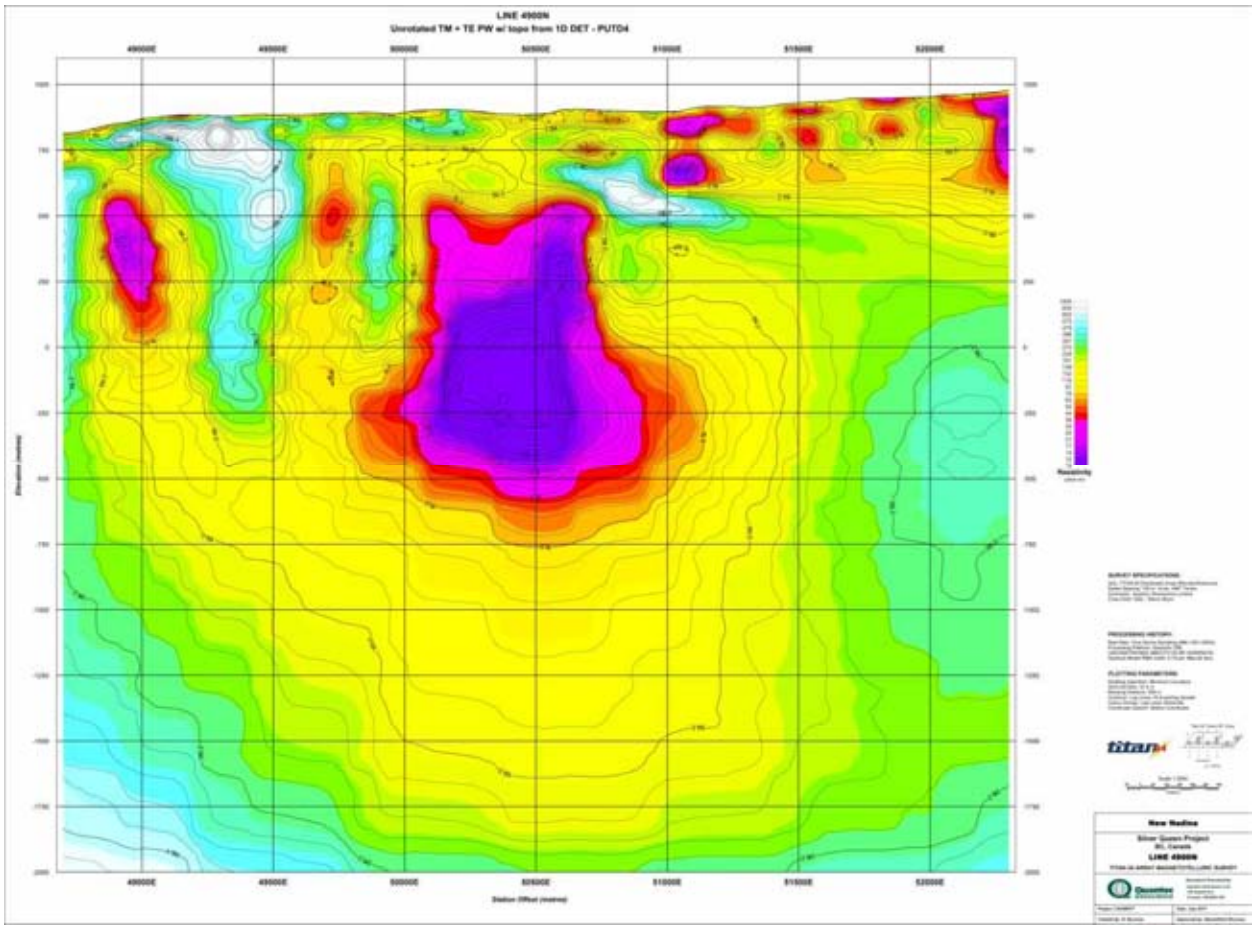

Line 4900N –MT- PWM Resistivity 2D Model

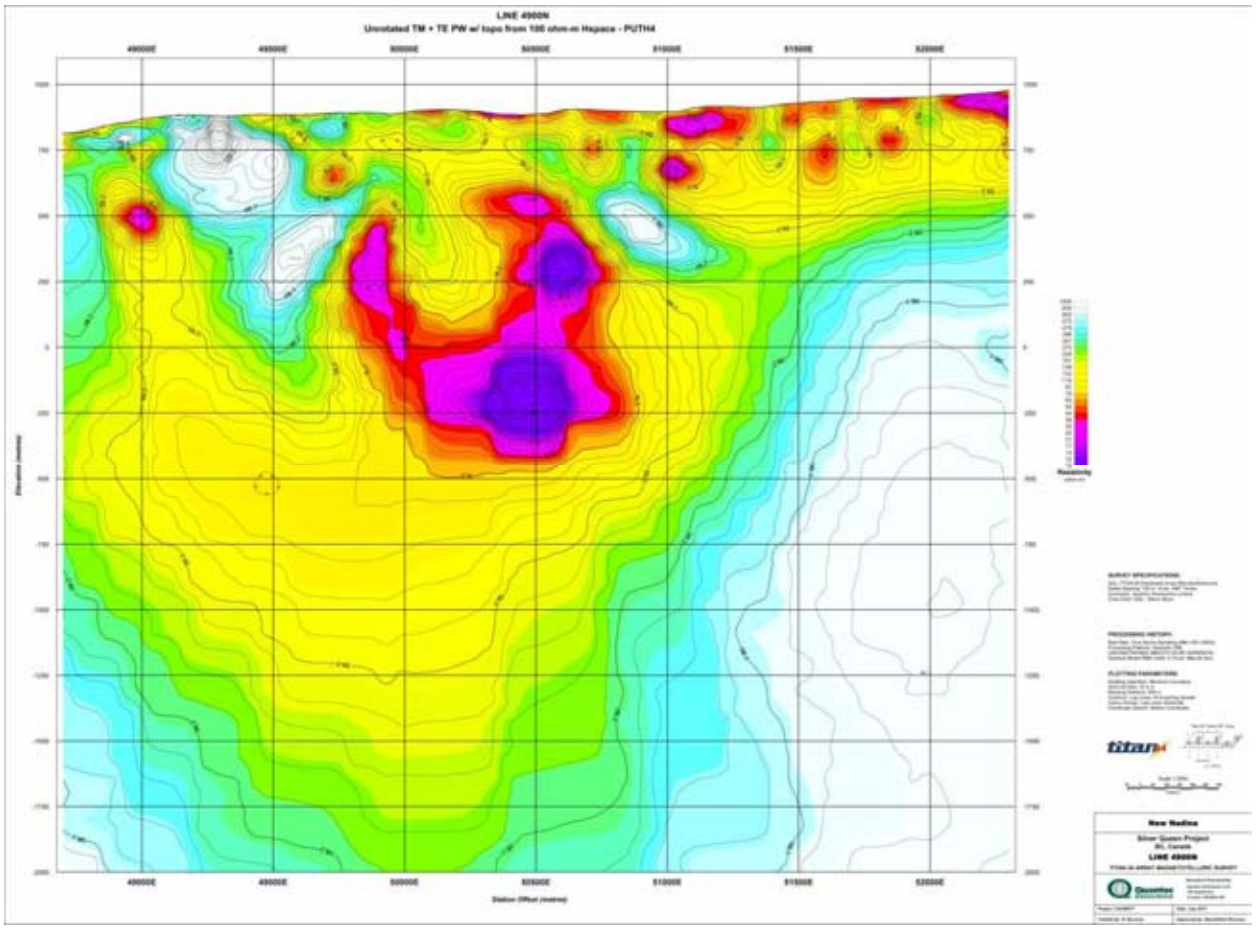

Line 4900N –MT- PWM Resistivity 2D Model

J.7 LINE 5750N

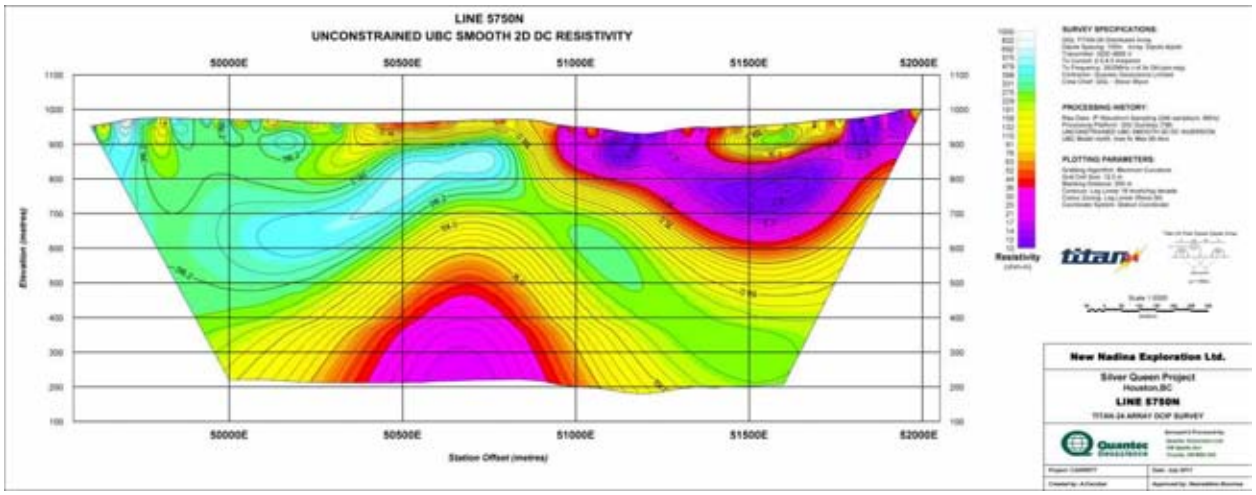

Line 5750N –DC Resistivity 2D Model

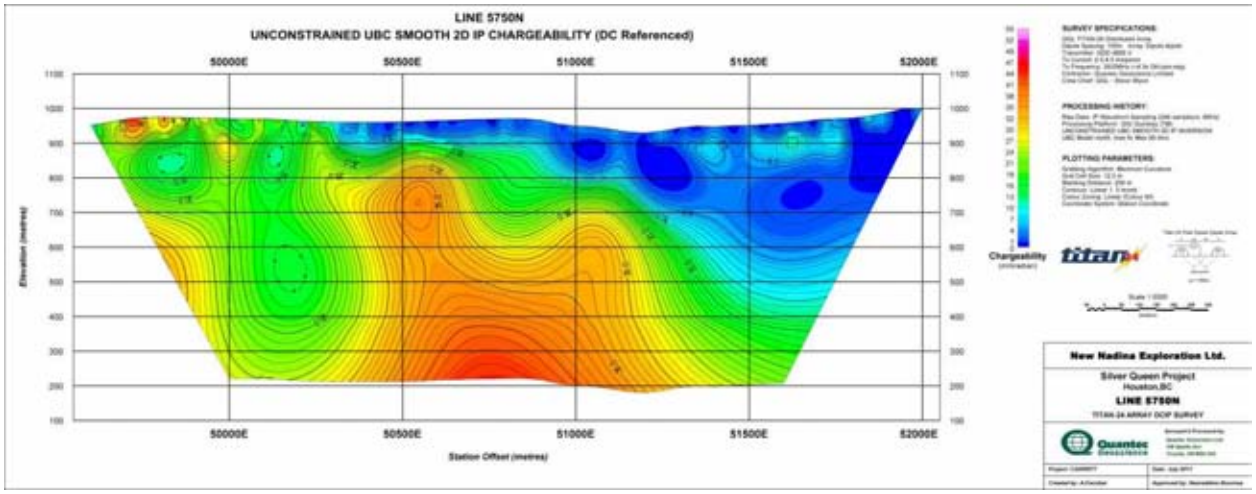

Line 5750N –IP Chargeability 2D Model

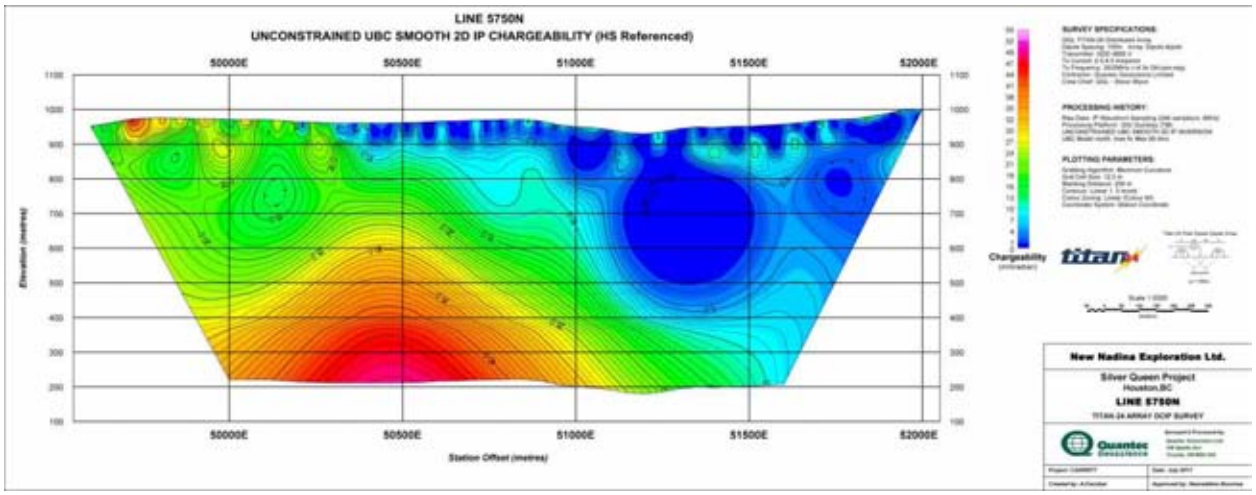

Line 5750N –IP Chargeabilit 2D Model

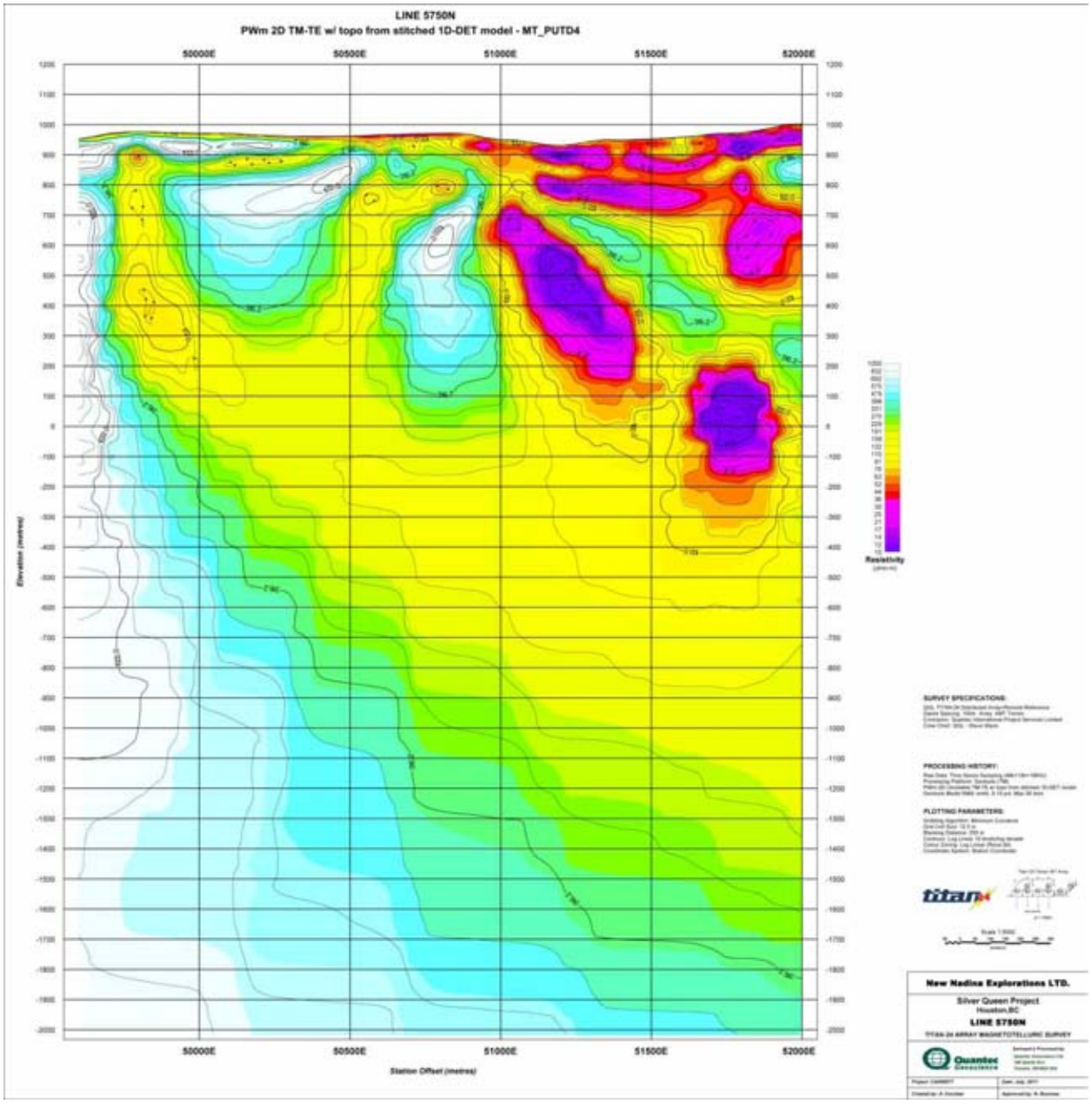

Line 5750N –MT- PWM Resistivity 2D Model

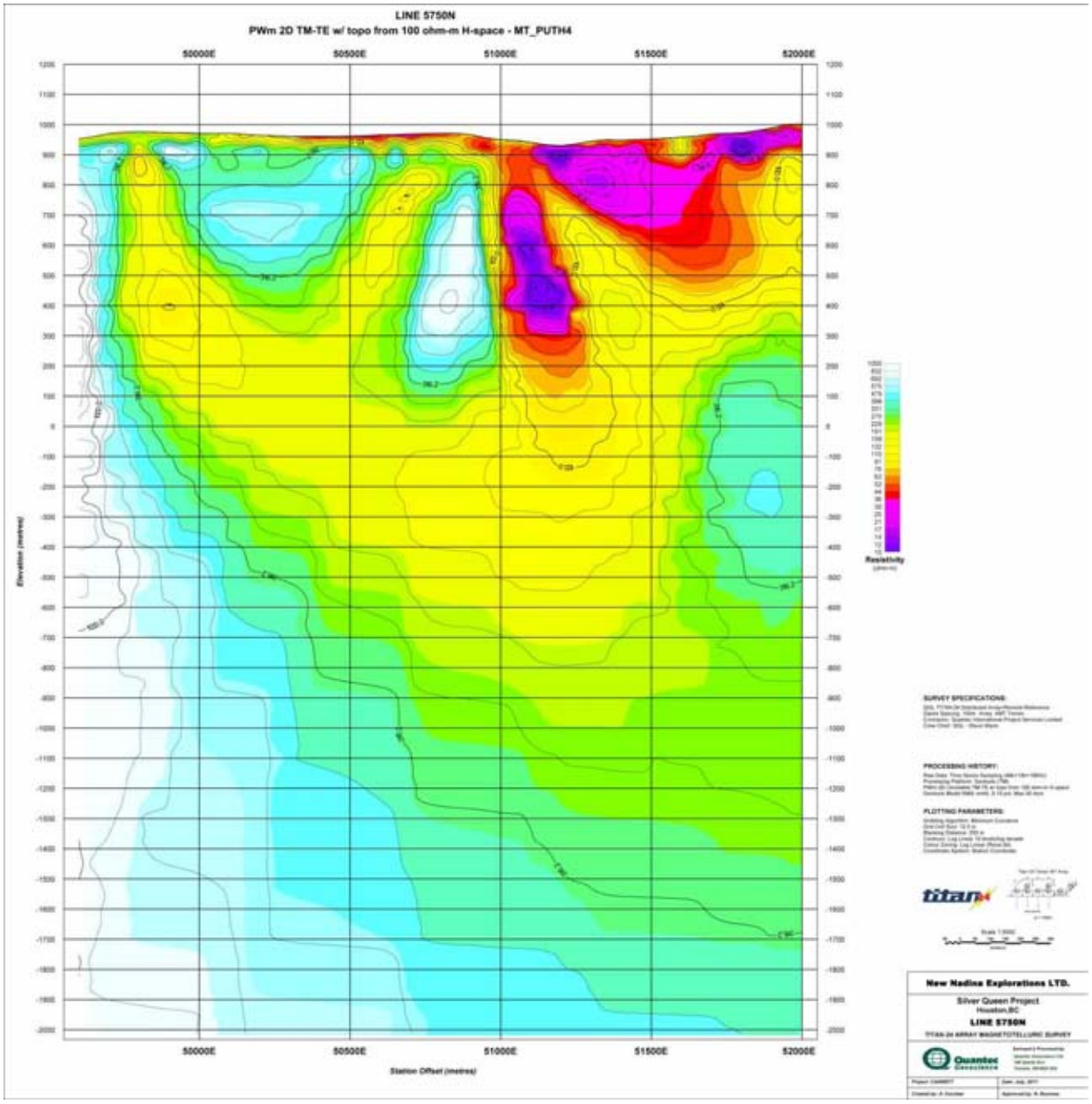

Line 5750N –MT- PWM Resistivity 2D Model

J.8 LINE 5900N

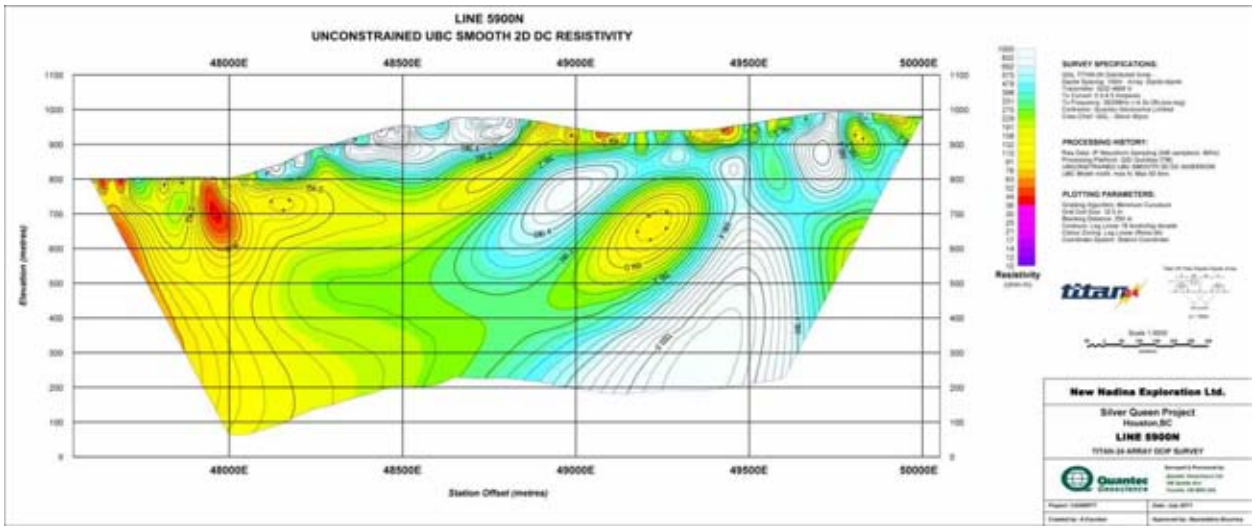

Line 5900N –DC Resistivity 2D Model

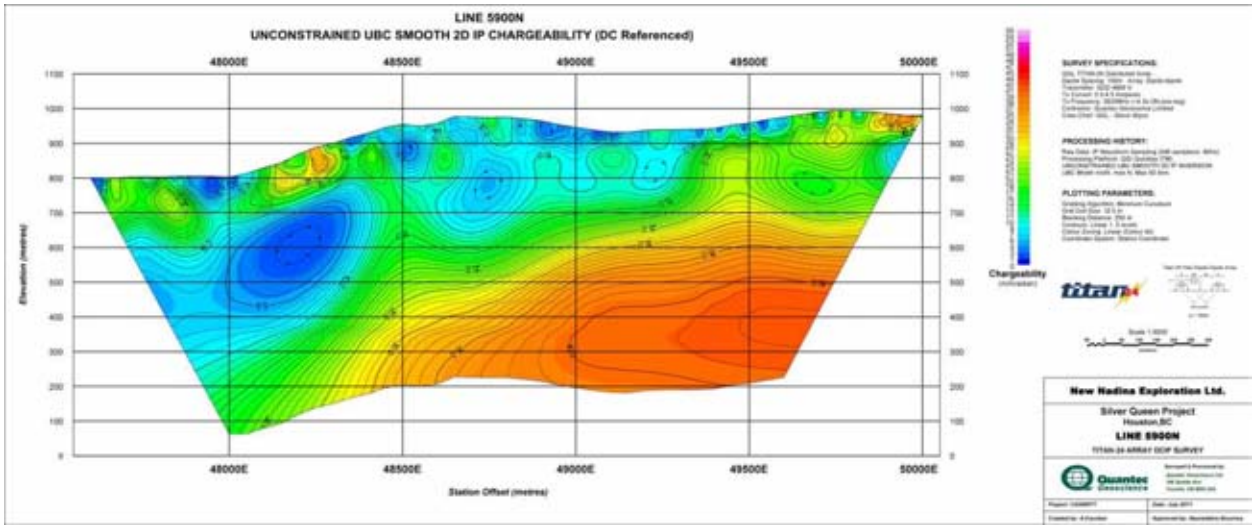

Line 5900N –IP Chargeability 2D Model

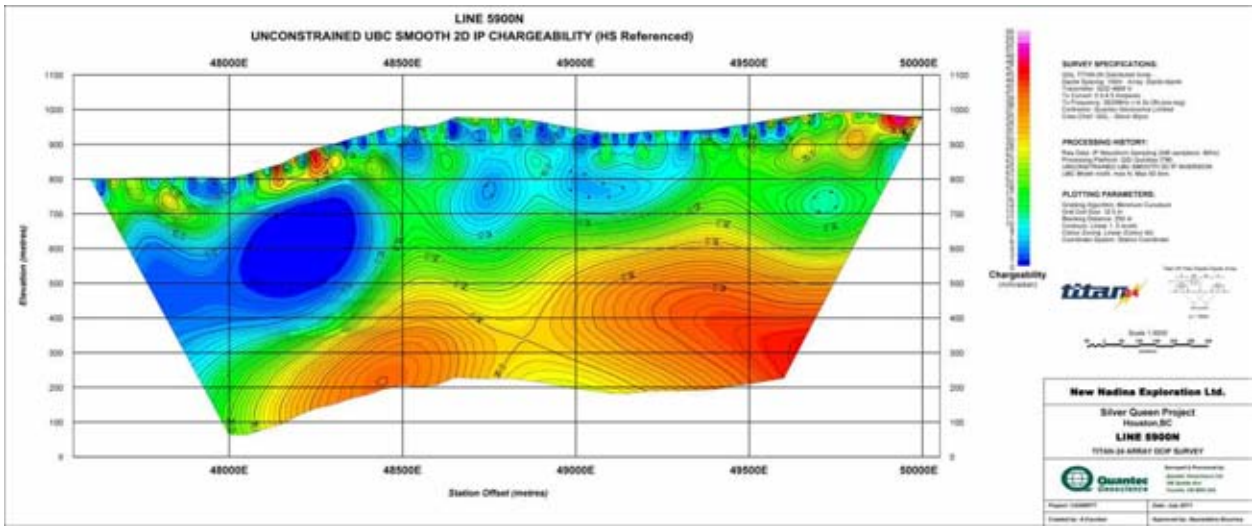

Line 5900N –IP Chargeability 2D Model

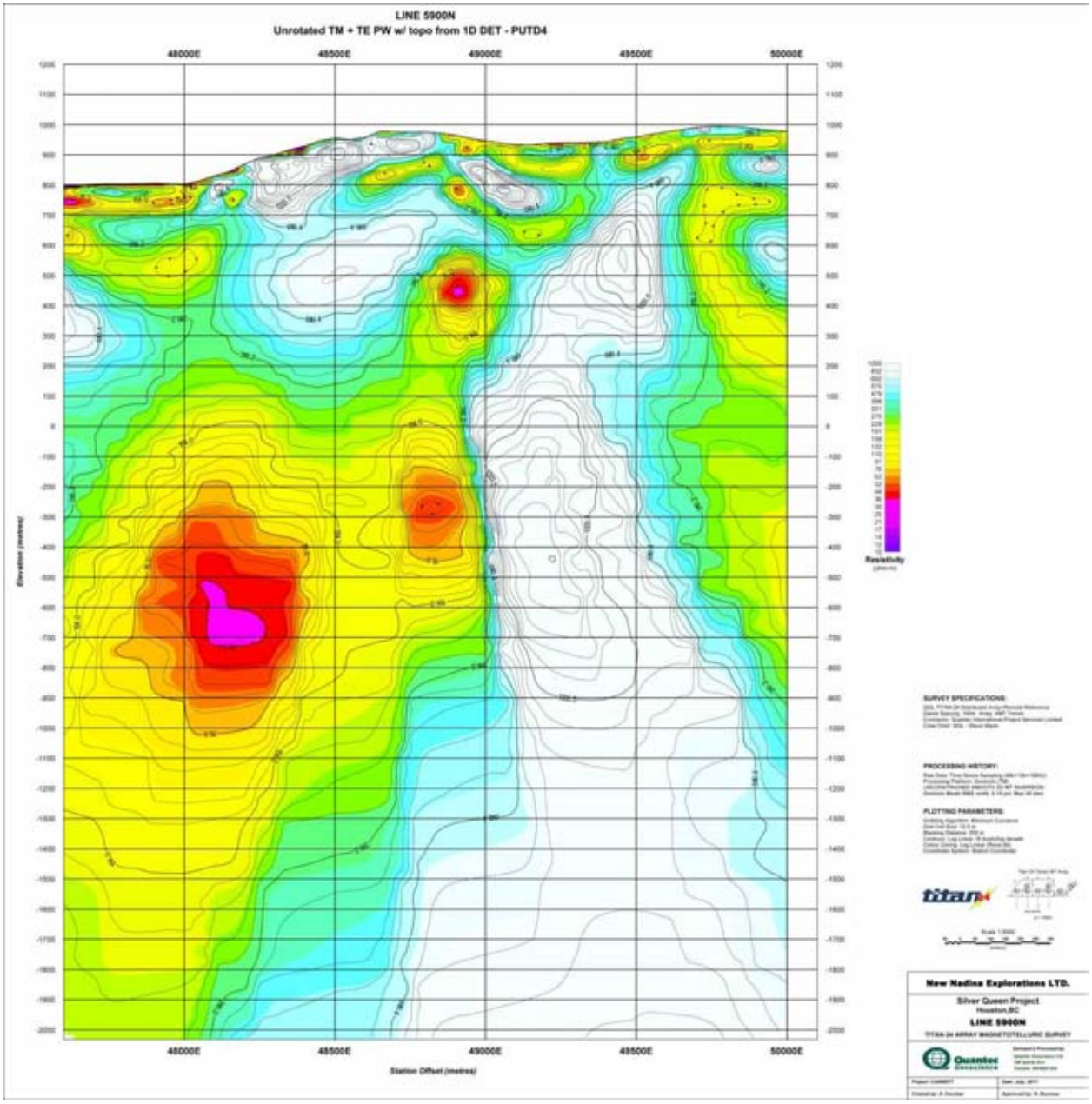

Line 5900N –MT- PWM Resistivity 2D Model

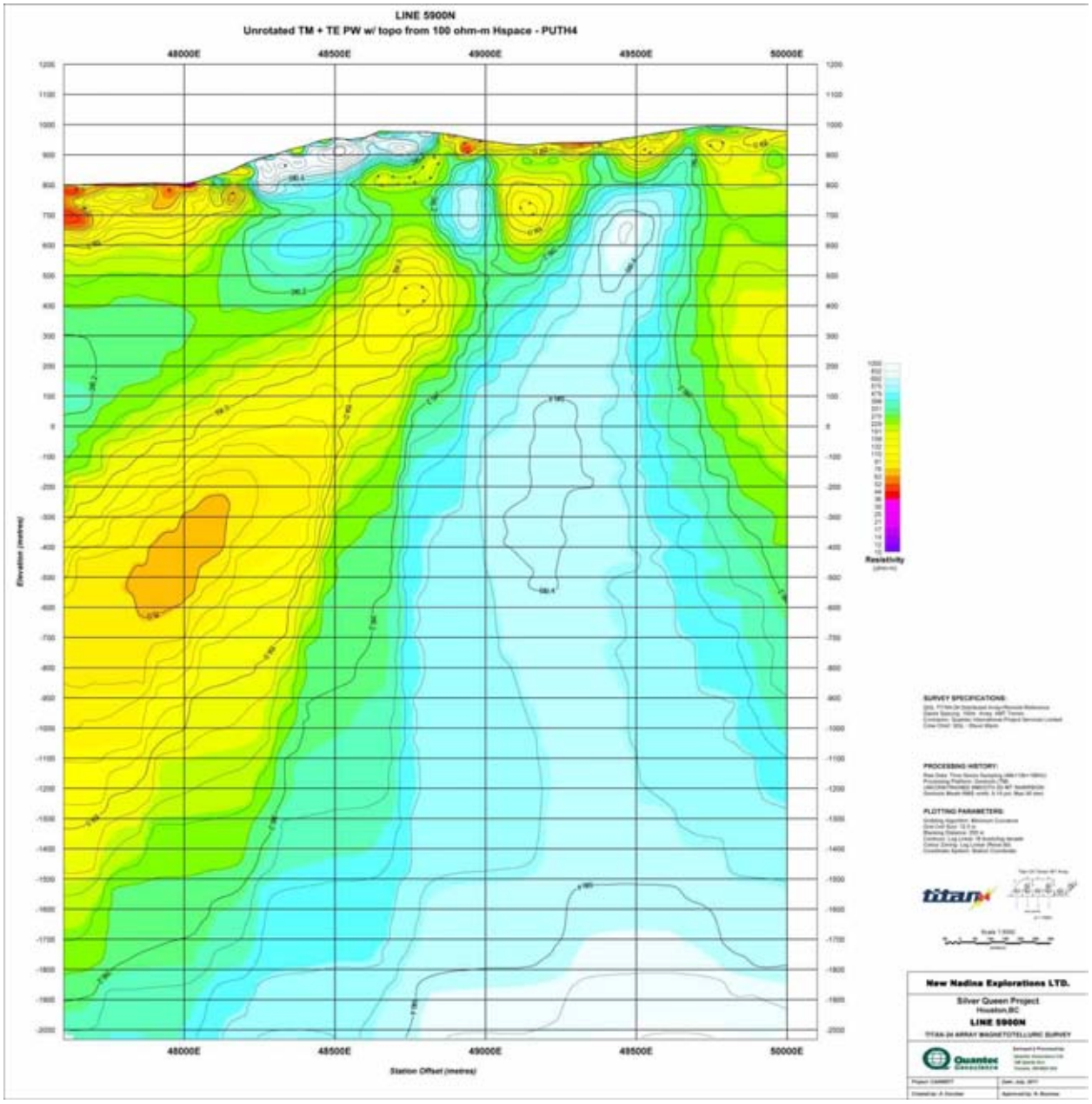

Line 5900N –MT- PWM Resistivity 2D Model

K GEOSOFT PLAN MAPS OF THE 2D MODELS

K.1 PLAN MAP AT -1500M ELEVATION

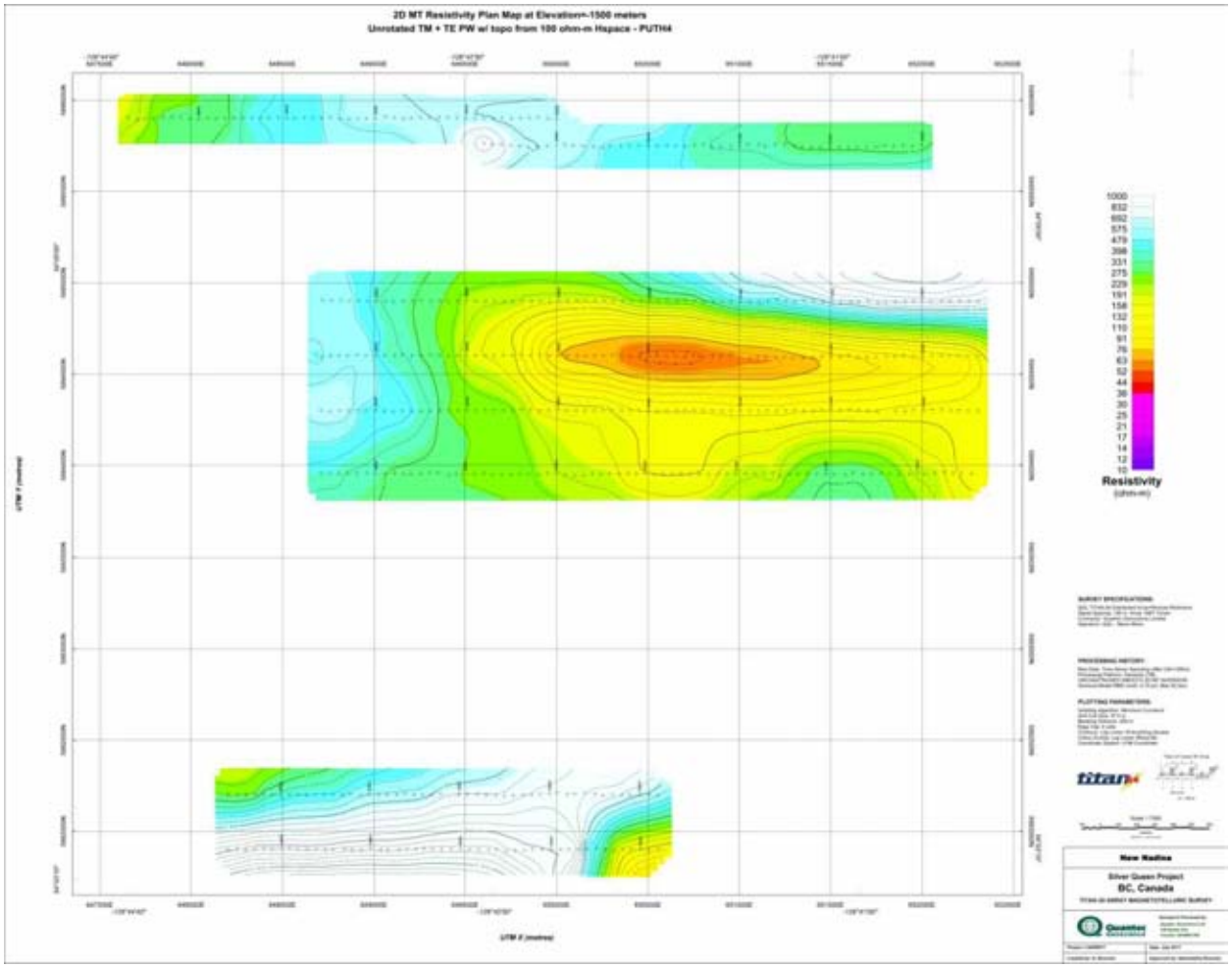

Plan Map at -1500m Elevation of MT PWM Resistivity

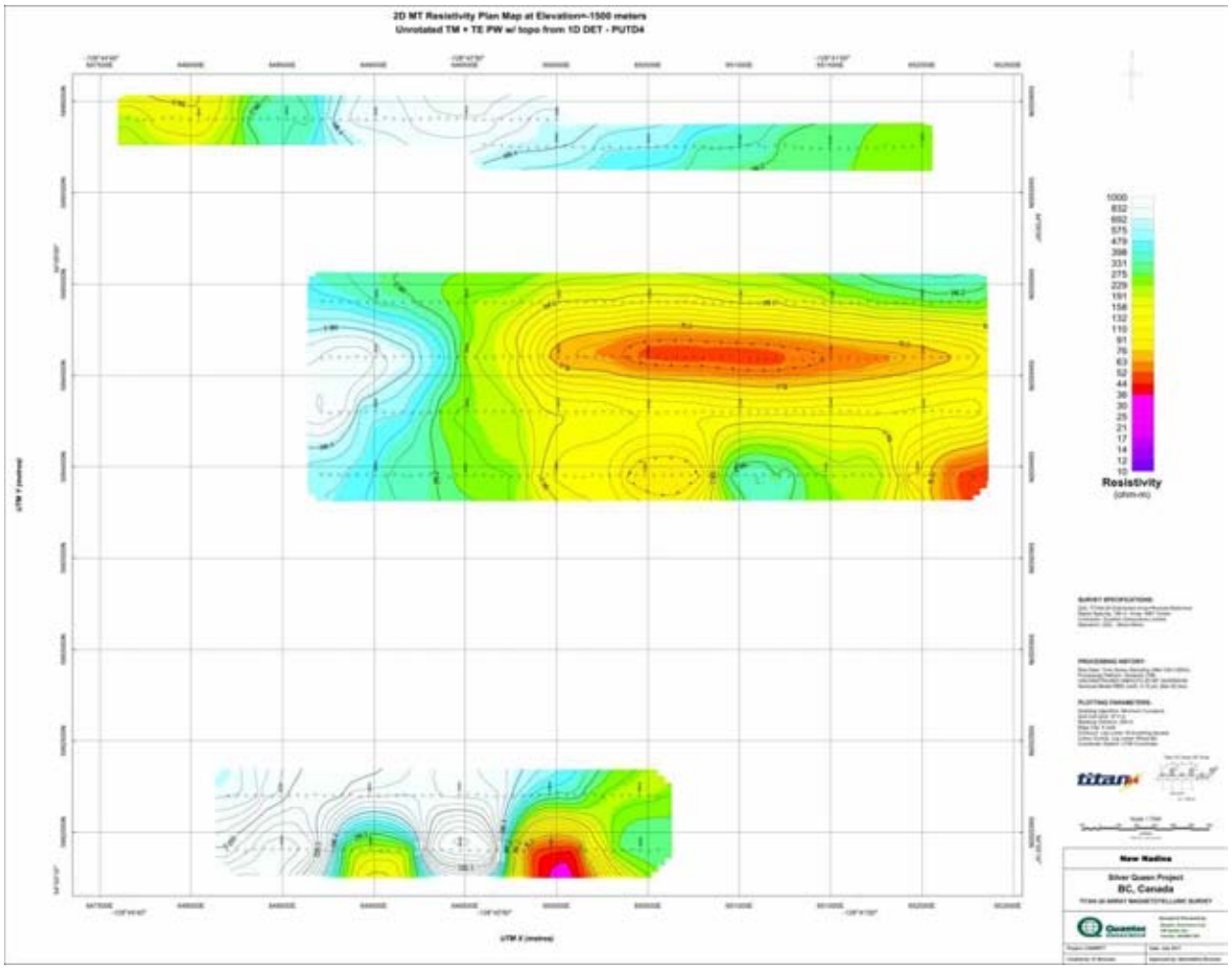

Plan Map at -1500m Elevation of MT PWM Resistivity

K.2 PLAN MAP AT -1250M ELEVATION

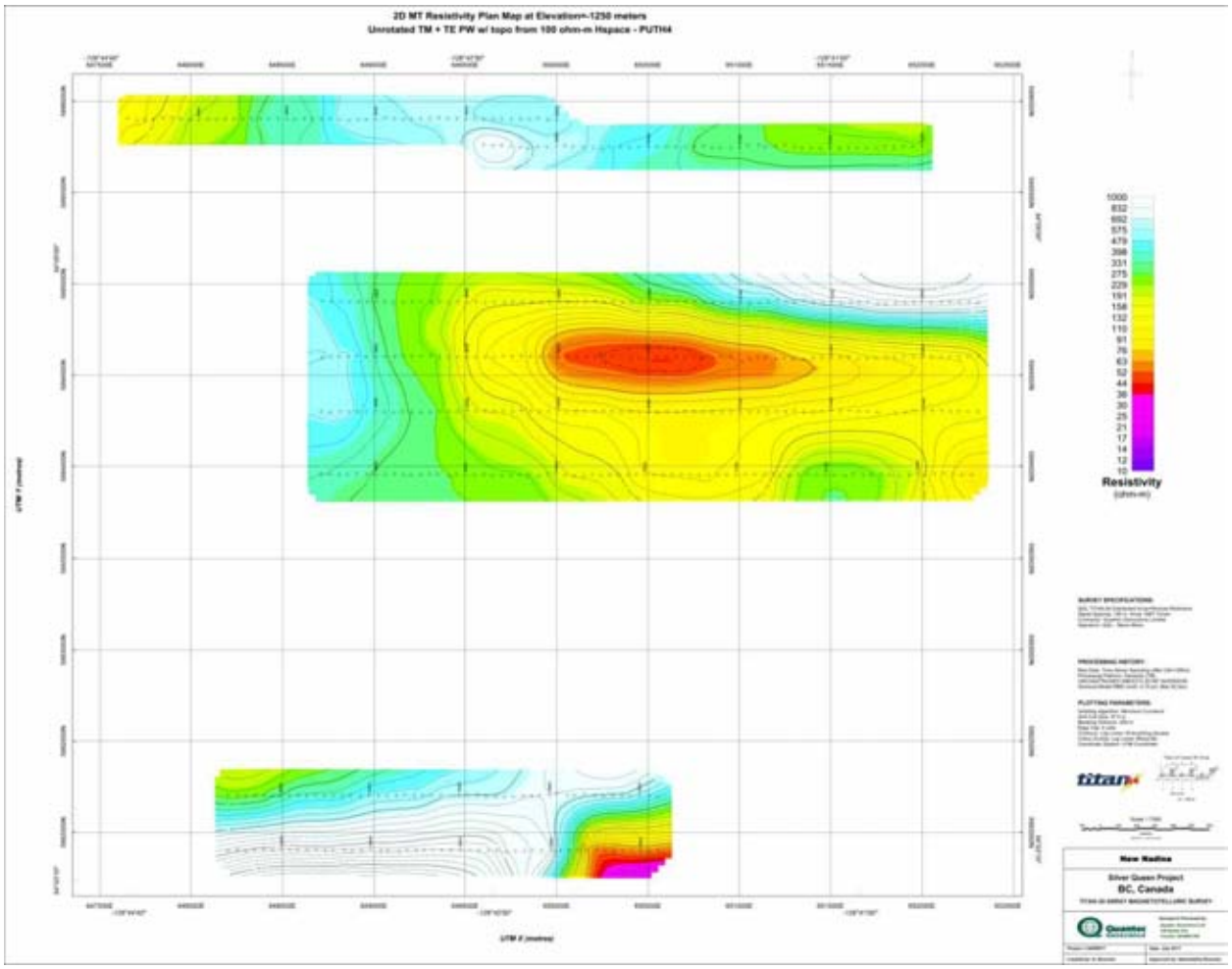

Plan Map at -1250m Elevation of MT PWM Resistivity

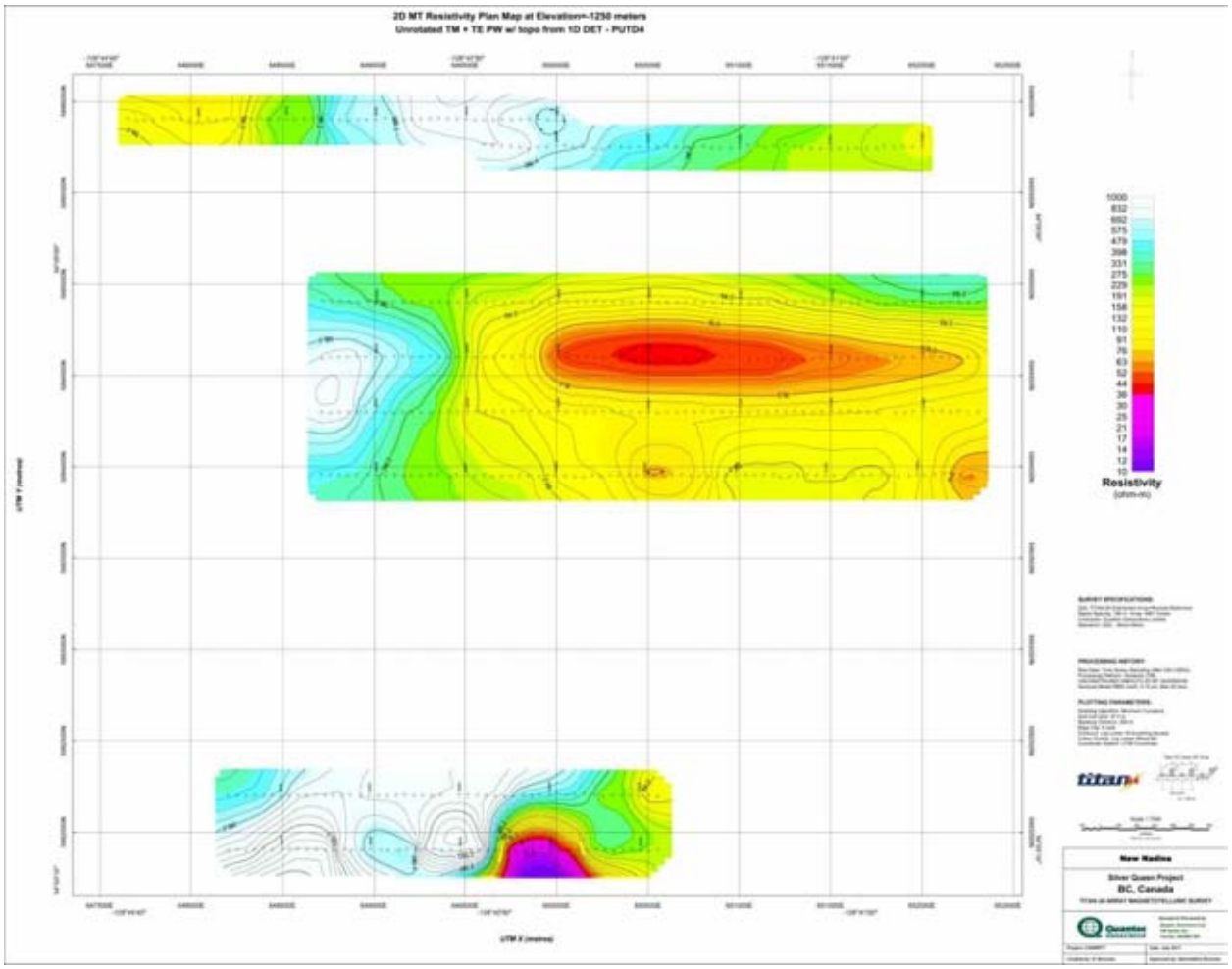

Plan Map at -1250m Elevation of MT PWM Resistivity

K.3 PLAN MAP AT -1000M ELEVATION

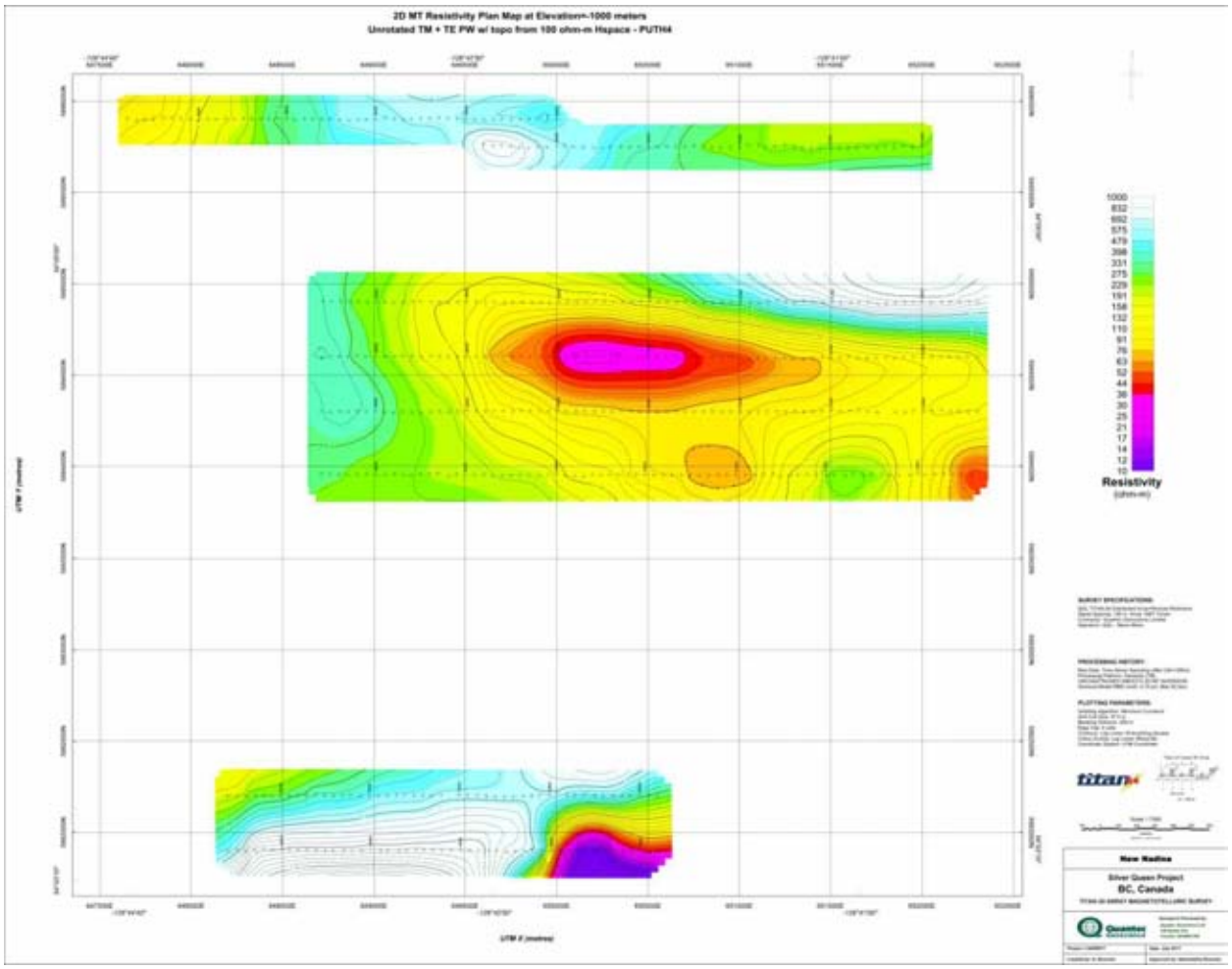

Plan Map at -1000m Elevation of MT PWM Resistivity

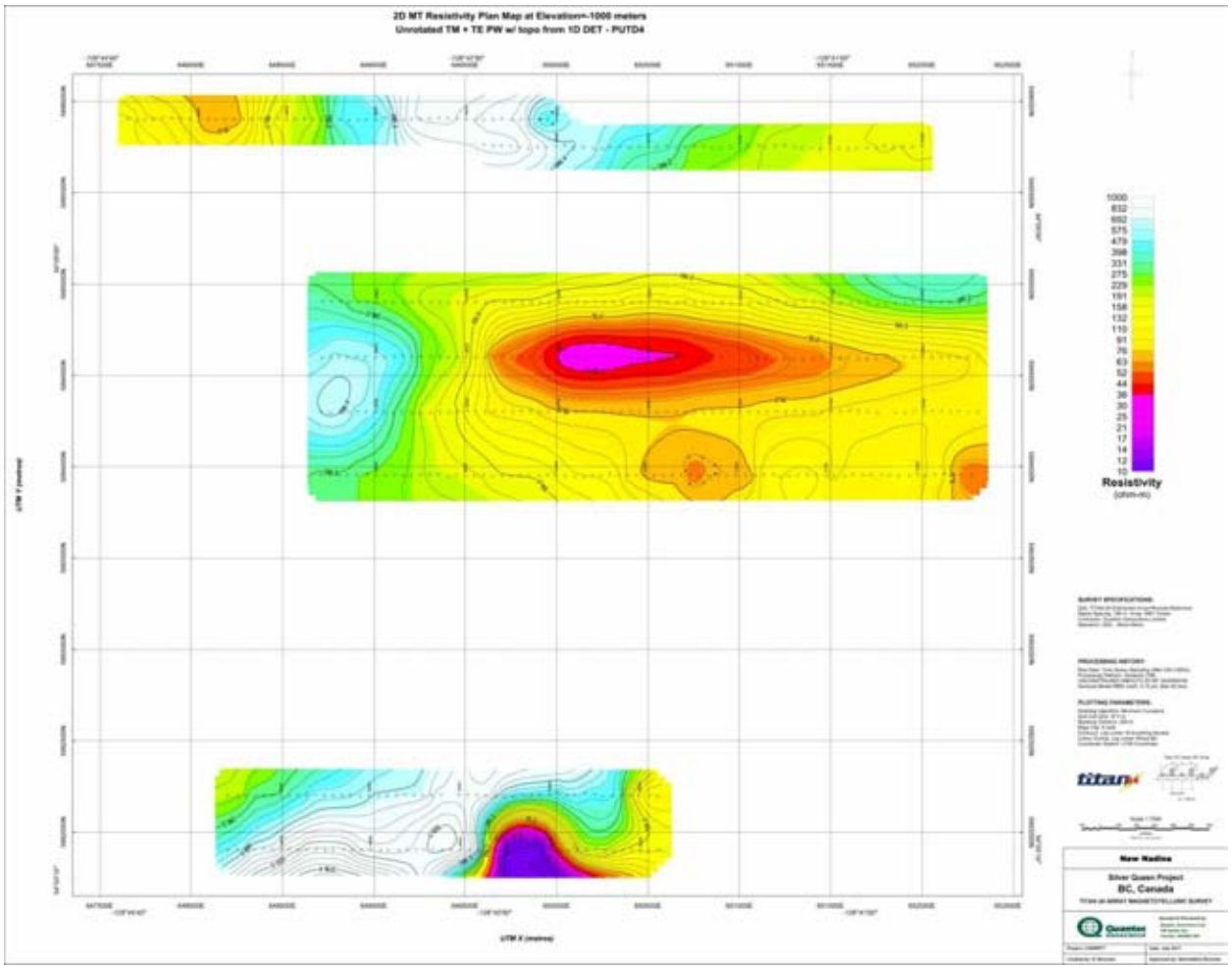

Plan Map at -1000m Elevation of MT PWM Resistivity

K.4 PLAN MAP AT -750M ELEVATION

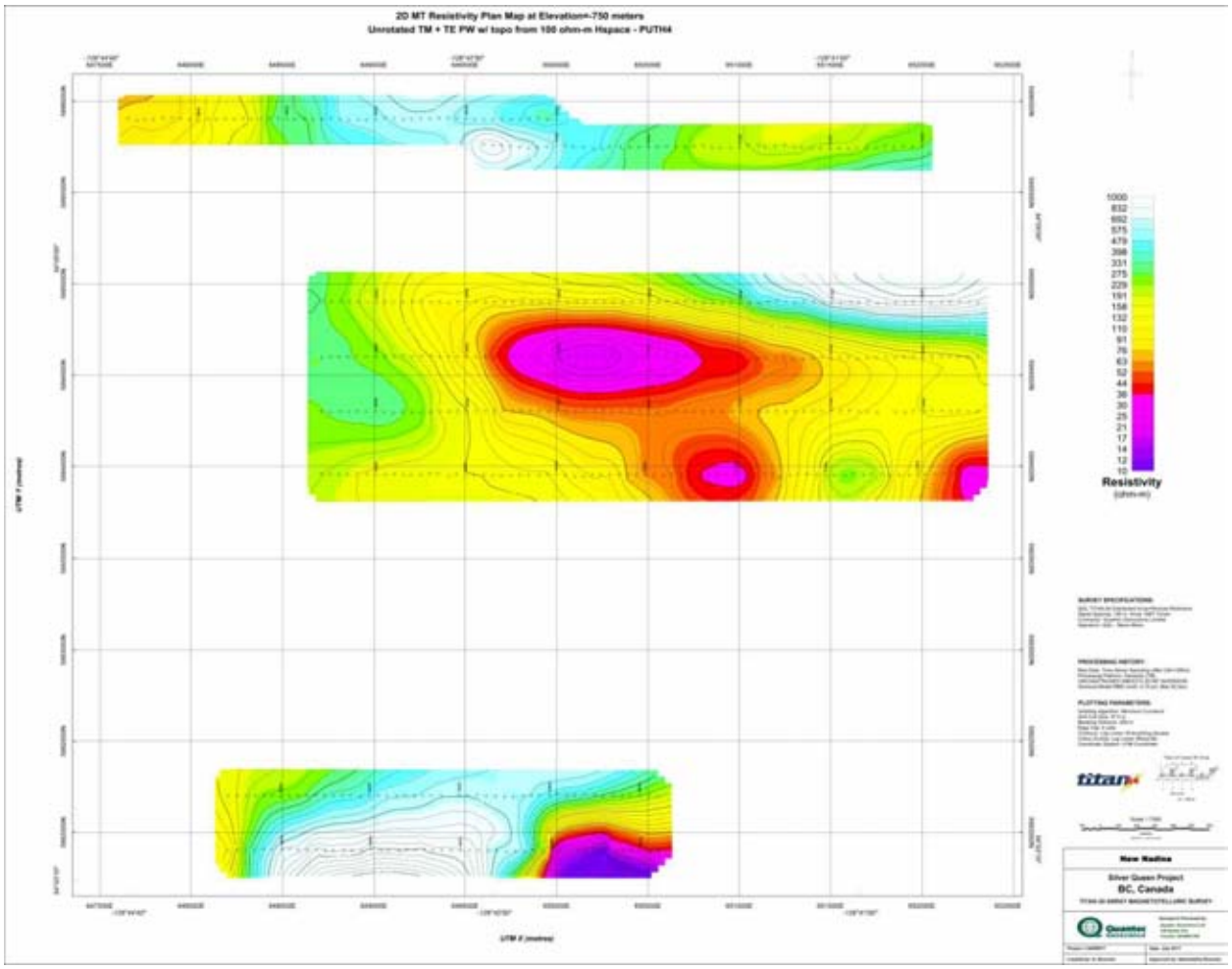

Plan Map at -750m Elevation of MT PWM Resistivity

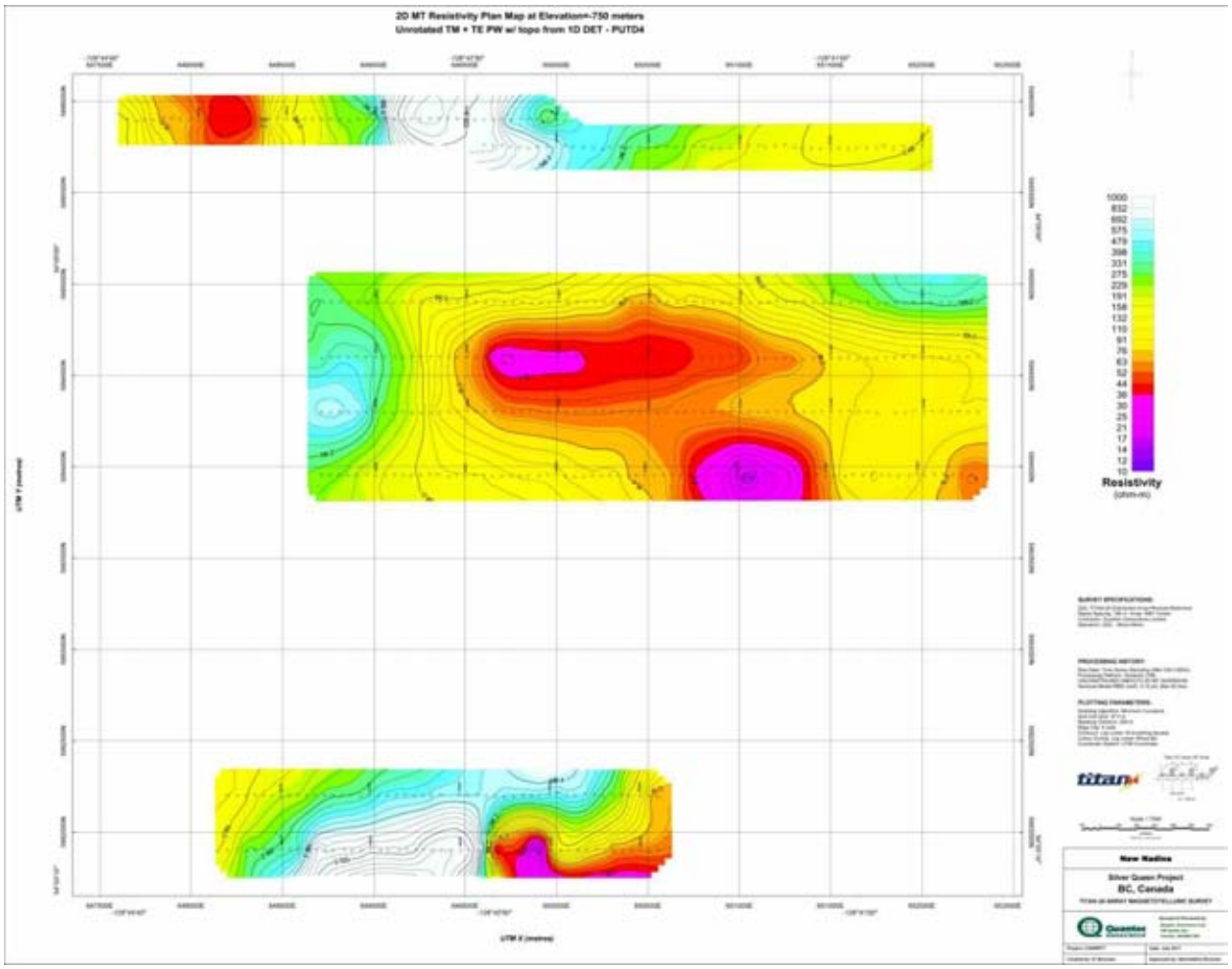

Plan Map at -750m Elevation of MT PWM Resistivity

K.5 PLAN MAP AT -500M ELEVATION

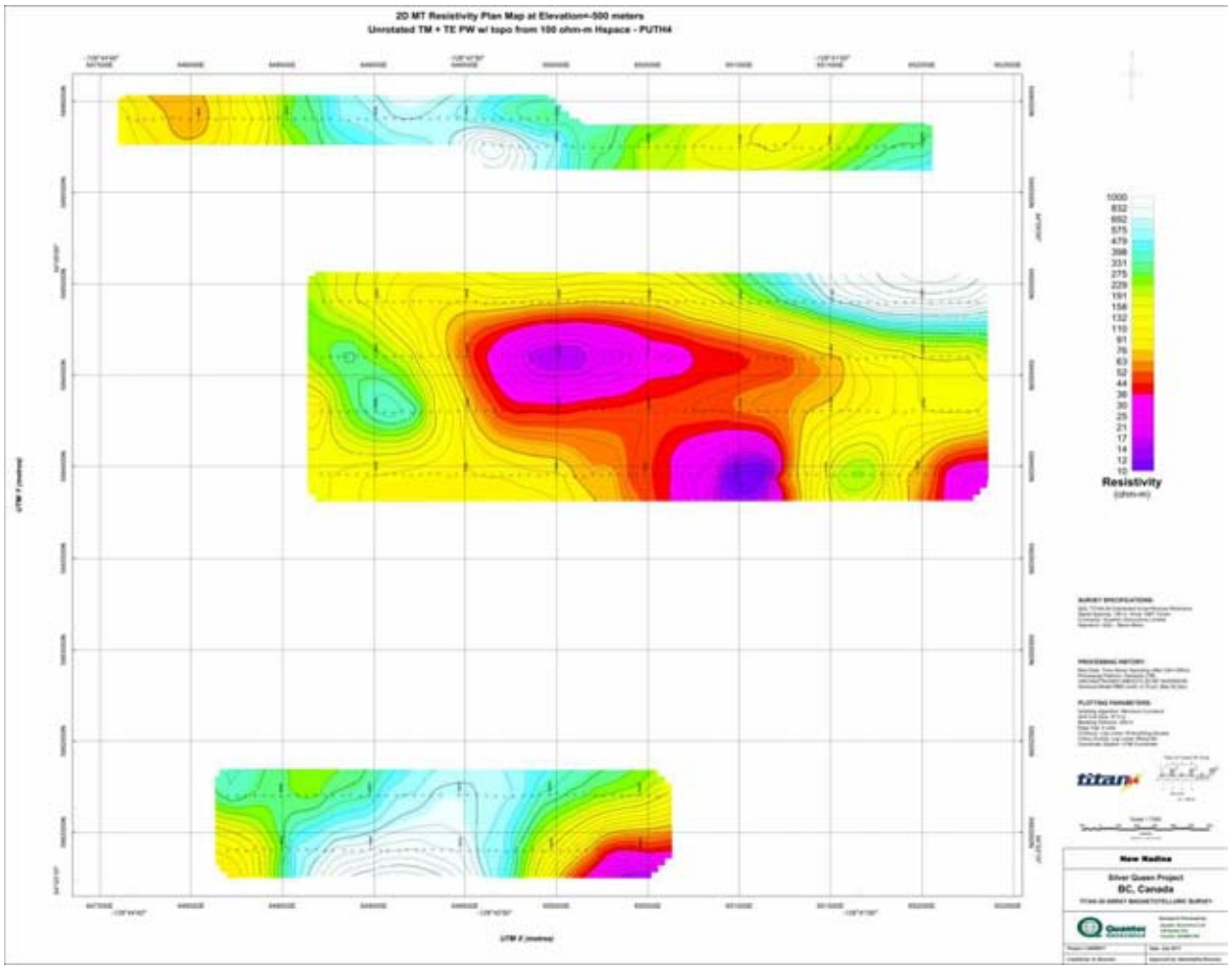

Plan Map at -500m Elevation of MT PWM Resistivity

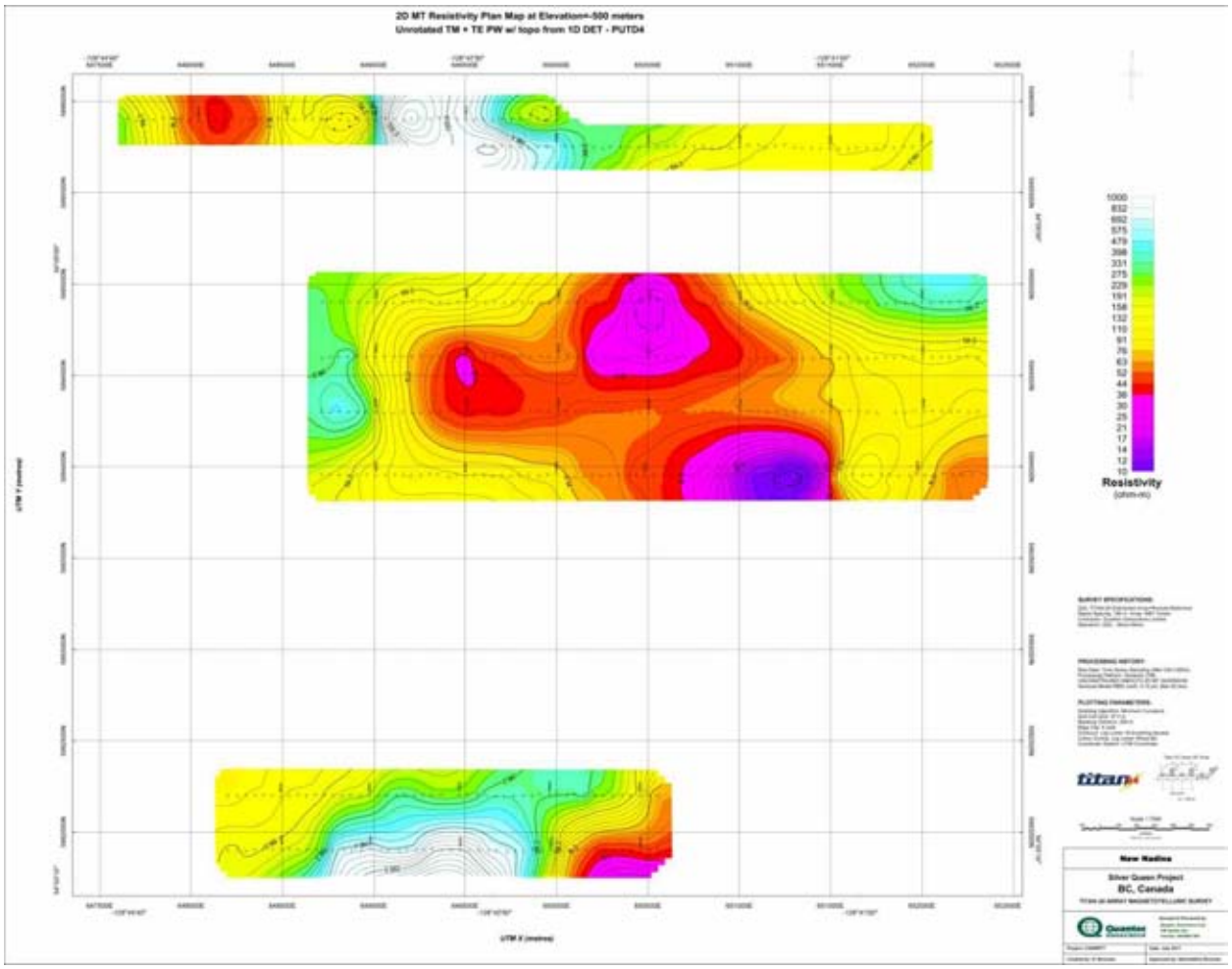

Plan Map at -500m Elevation of MT PWM Resistivity

K.6 PLAN MAP AT -250M ELEVATION

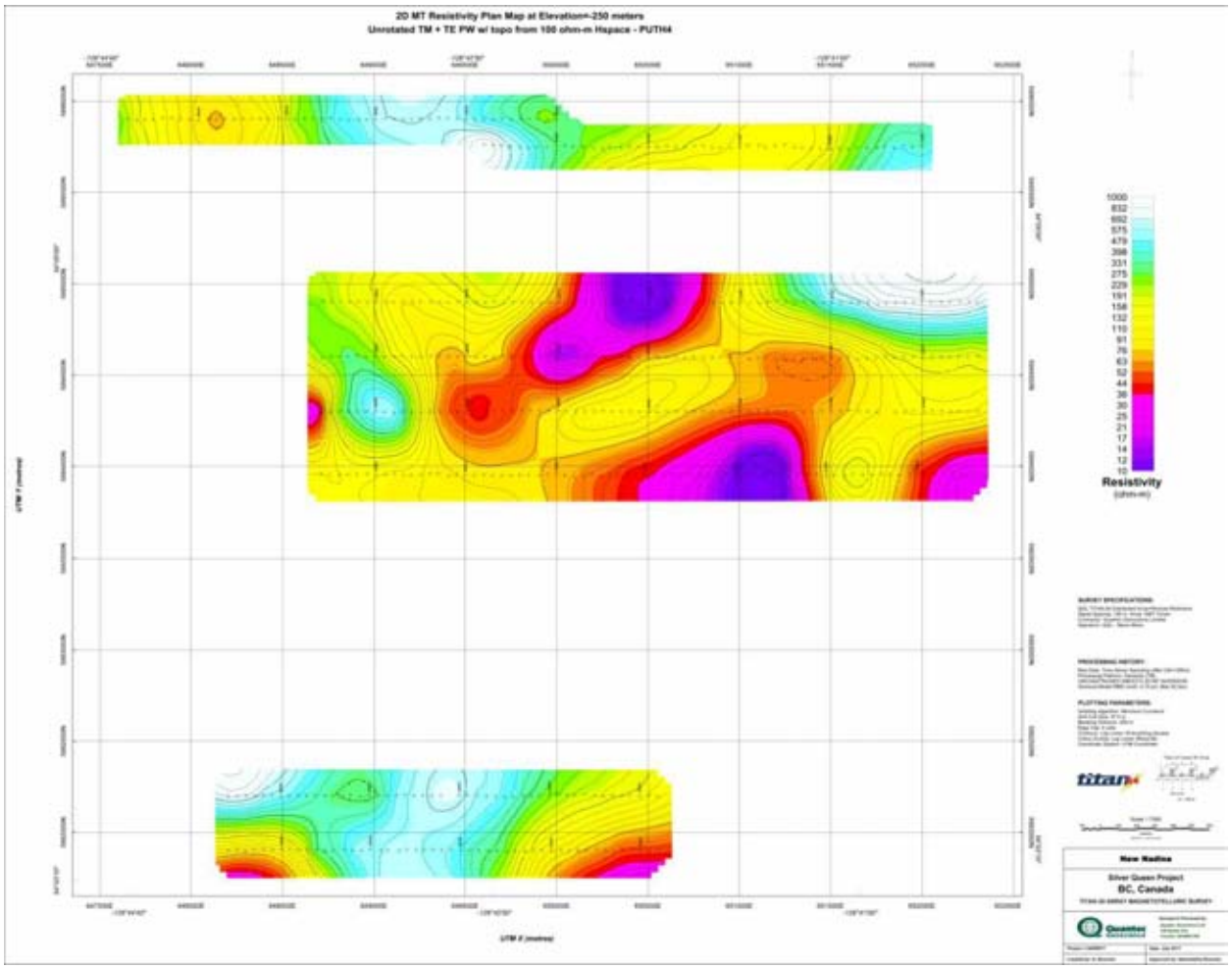

Plan Map at -250m Elevation of MT PWM Resistivity

K.7 PLAN MAP AT -250M ELEVATION

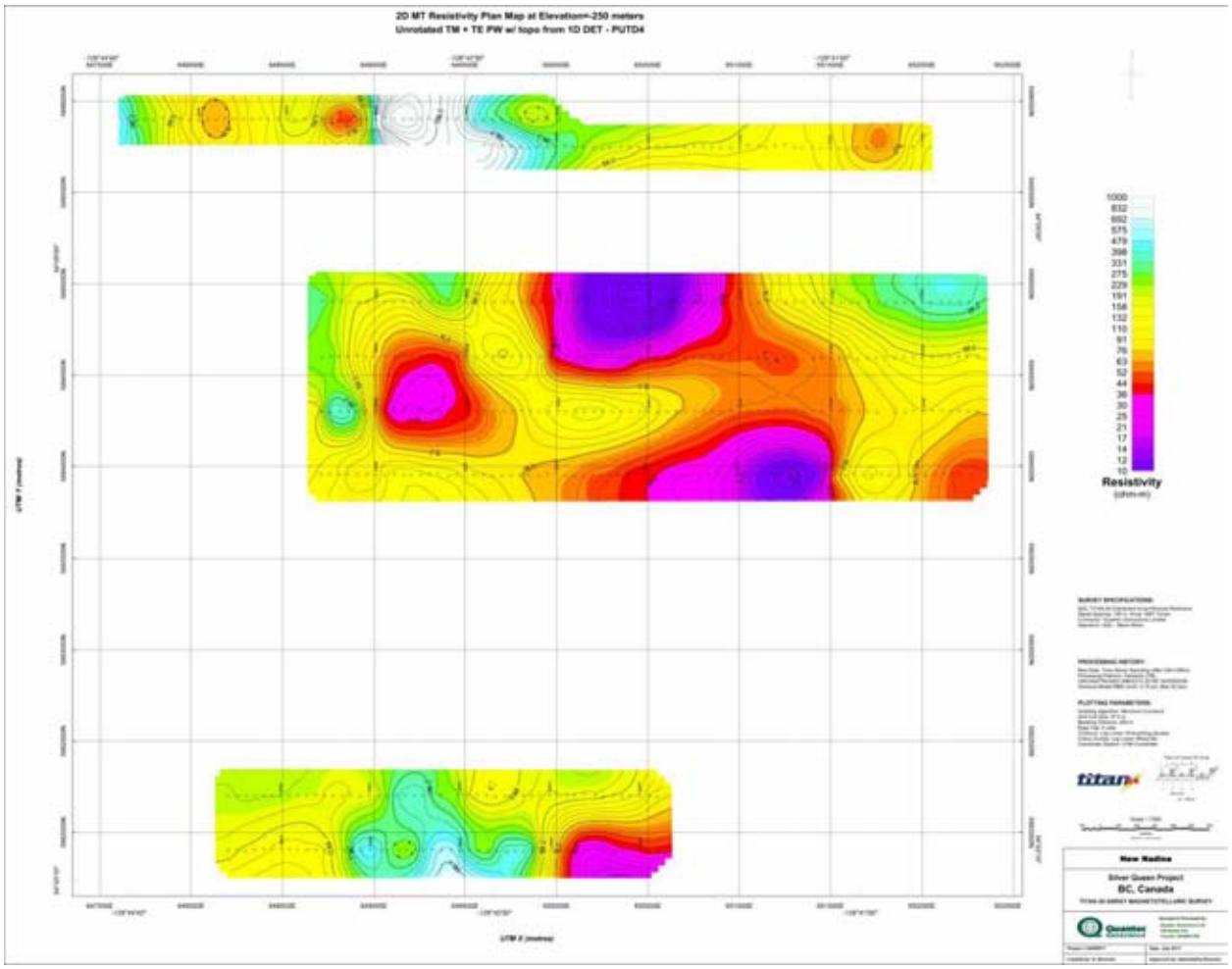

Plan Map at -250m Elevation of MT PWM Resistivity

K.8 PLAN MAP AT 0M ELEVATION

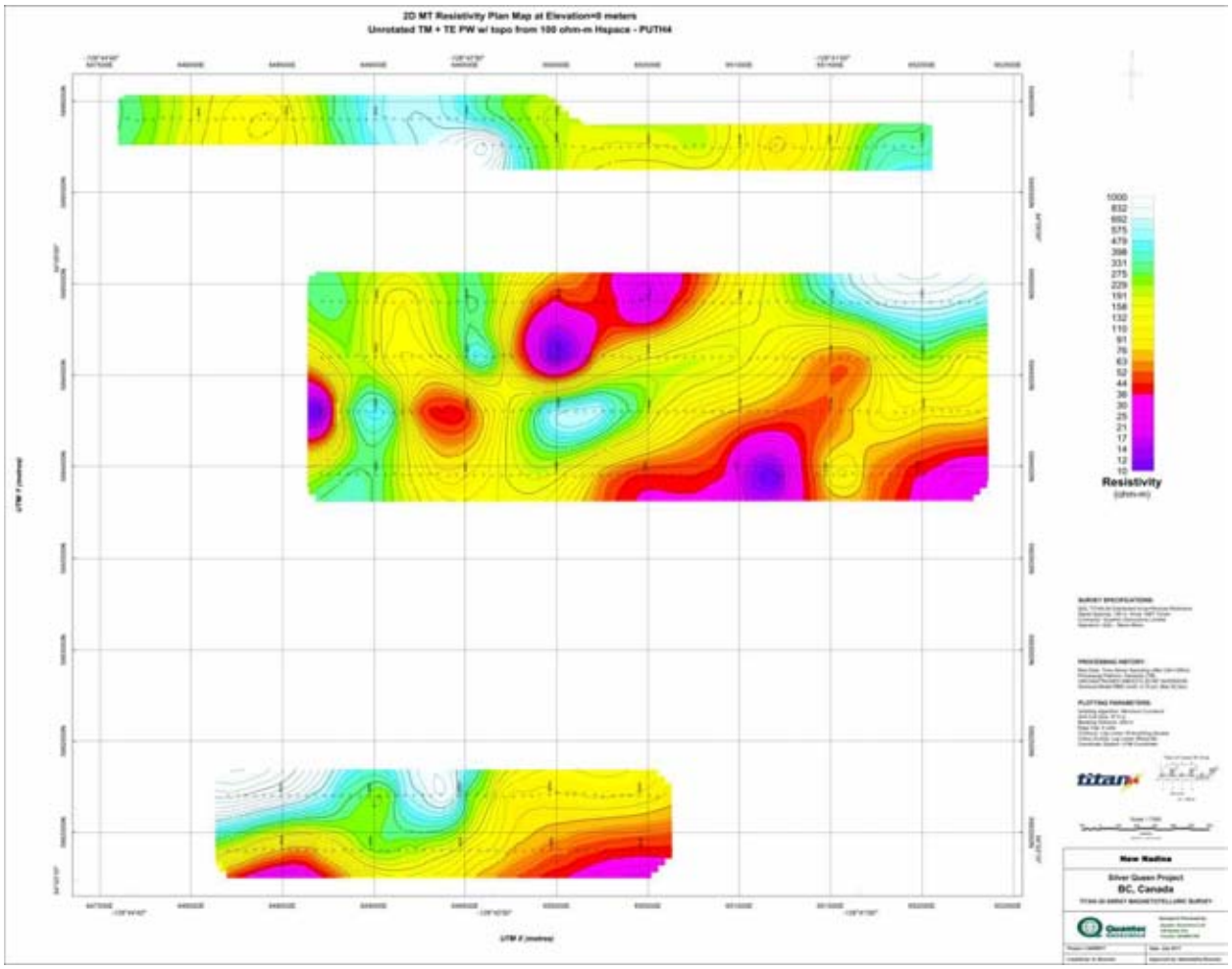

Plan Map at 0m Elevation of MT PWM Resistivity

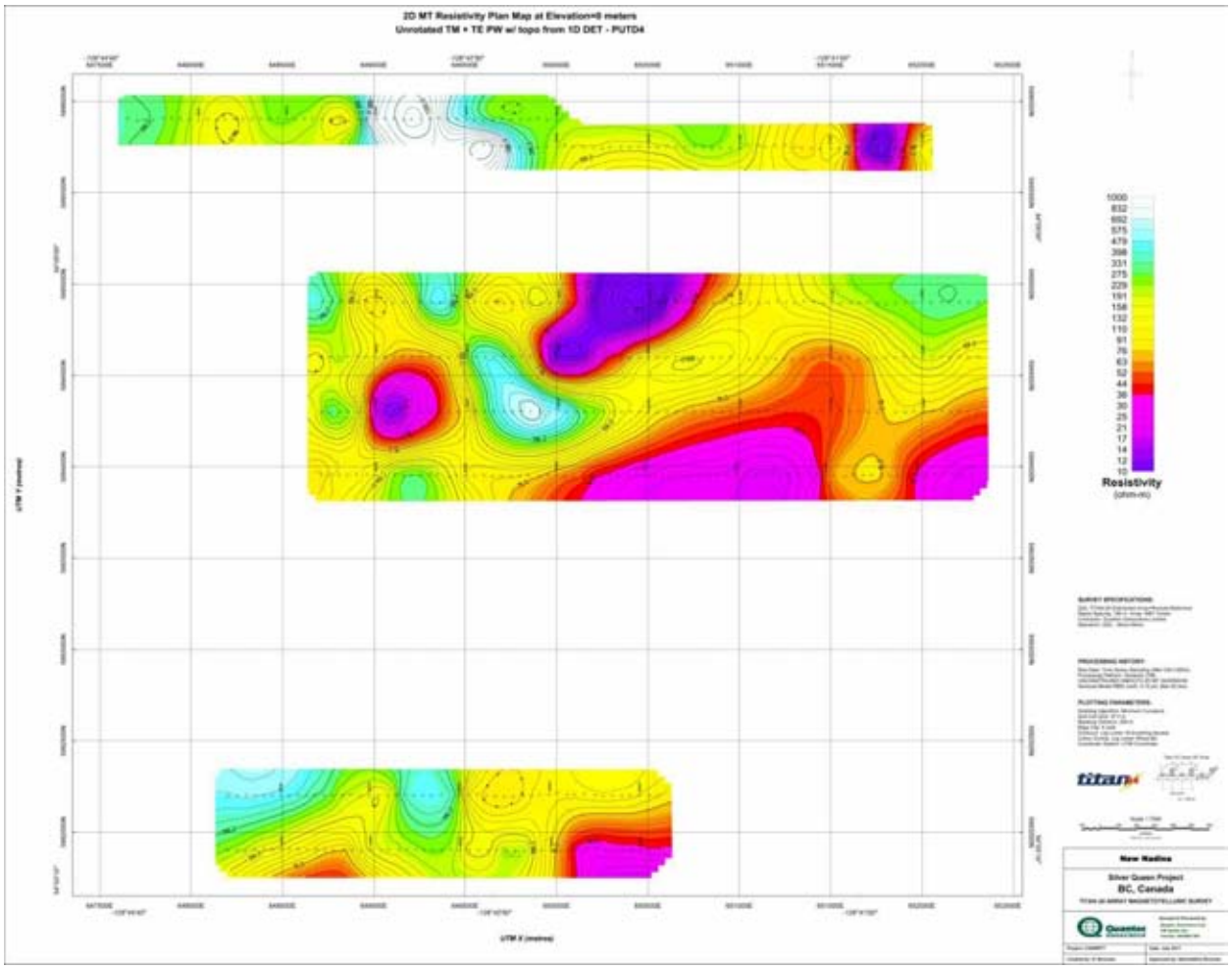

Plan Map at 0m Elevation of MT PWM Resistivity

K.9 PLAN MAP AT 100M ELEVATION

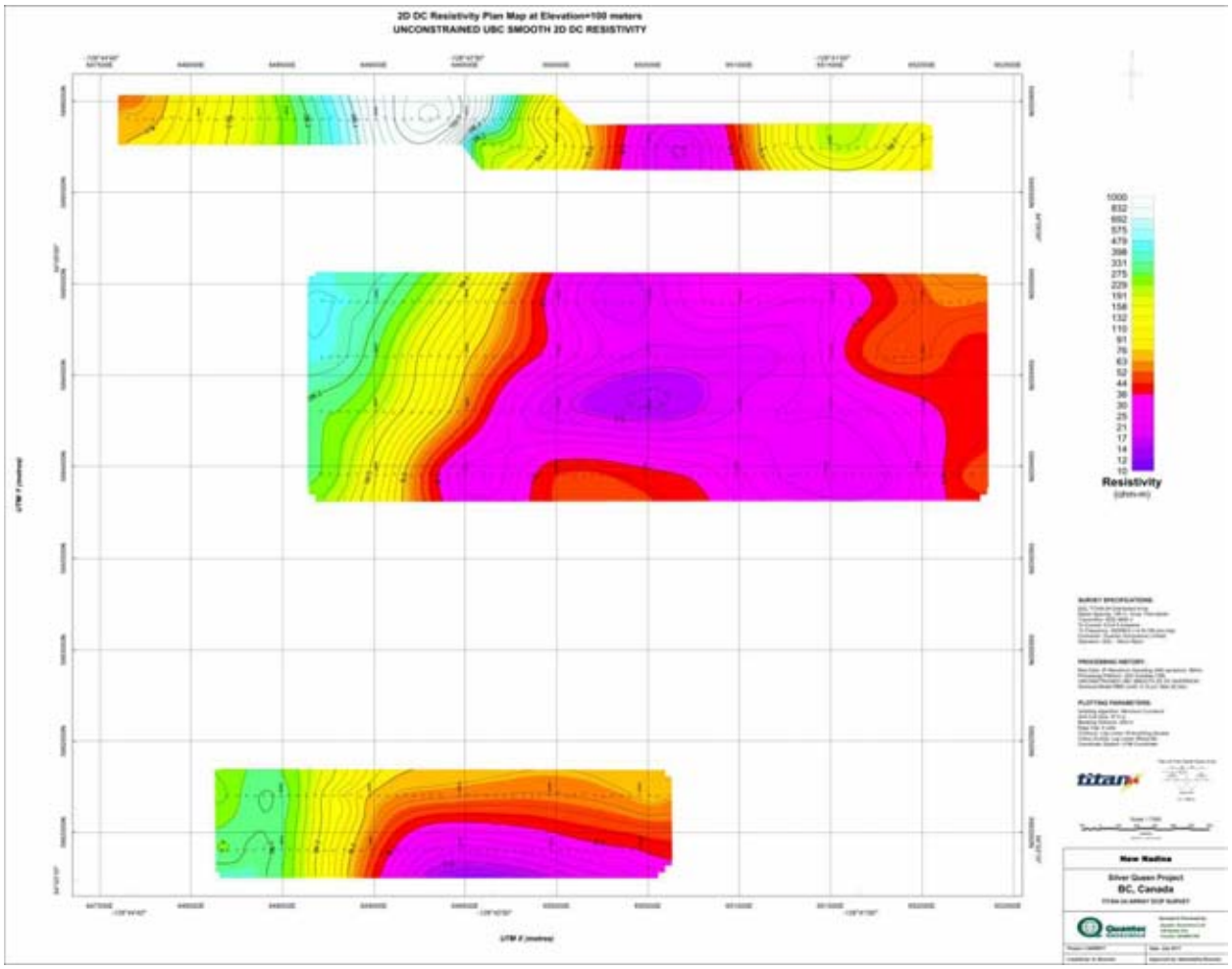

Plan Map at 100m Elevation of DC Resistivity.

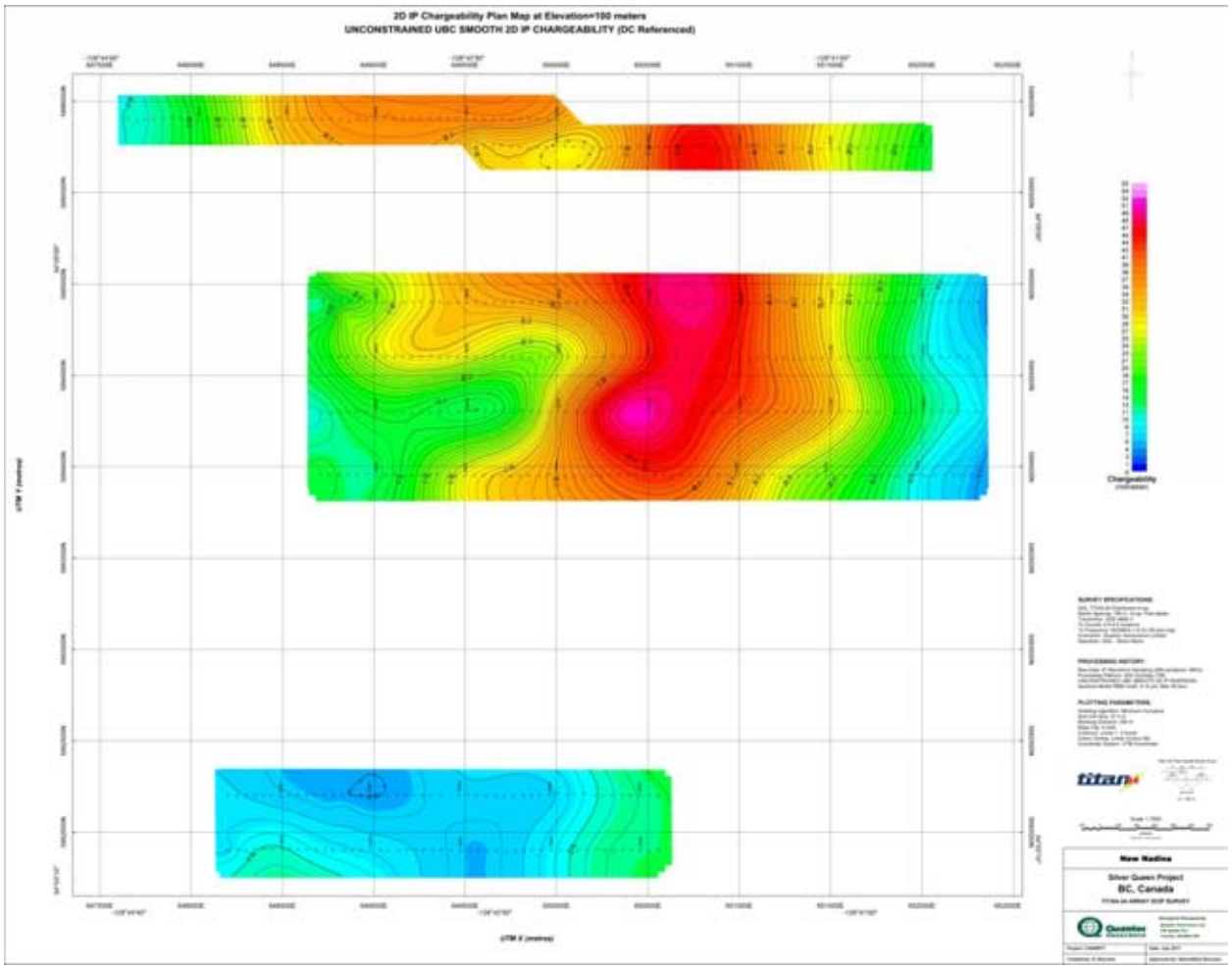

Plan Map at 100m Elevation of IP Chargeability.

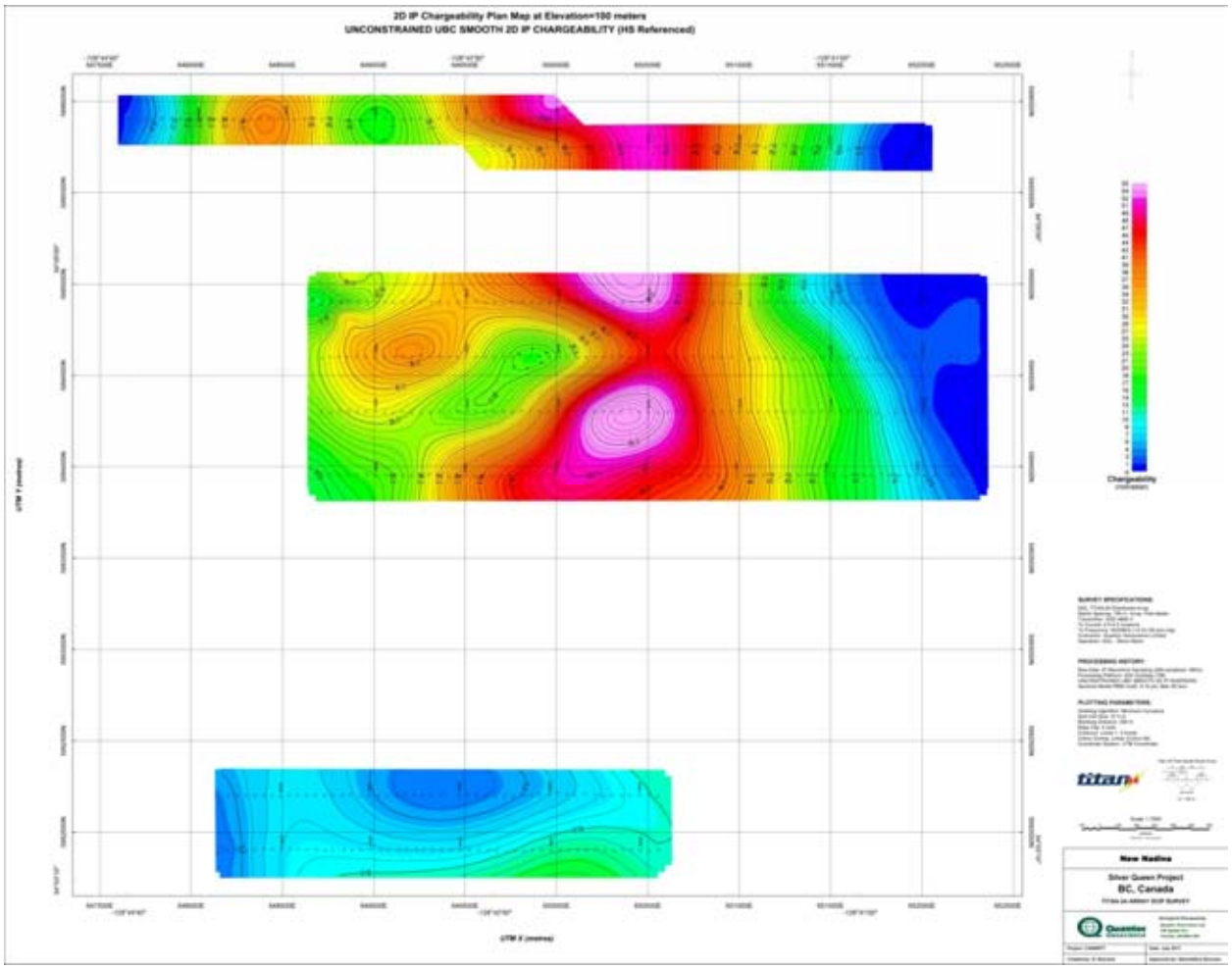

Plan Map at 100m Elevation of IP Chargeability.

K.10 PLAN MAP AT 200M ELEVATION

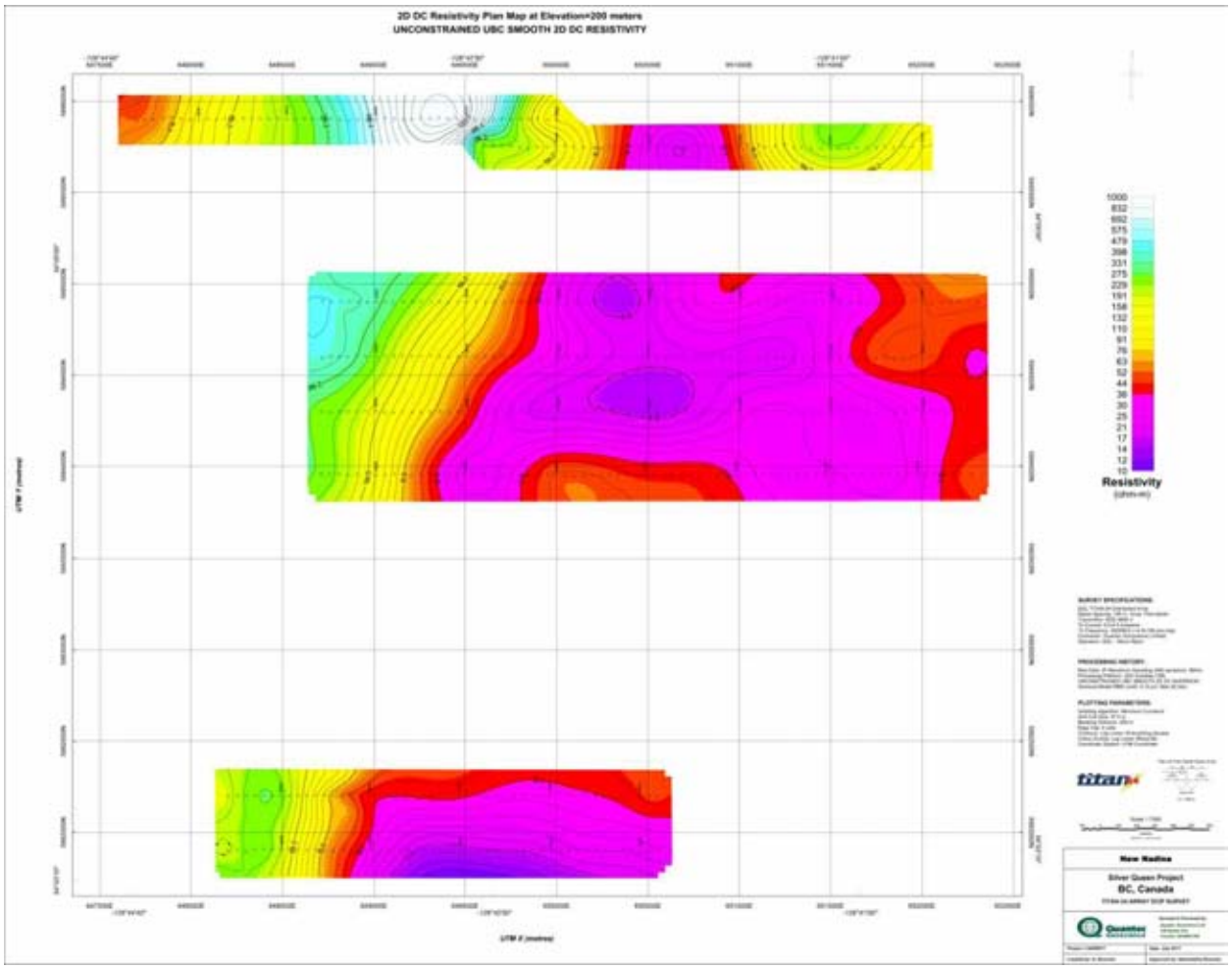

Plan Map at 200m Elevation of DC Resistivity.

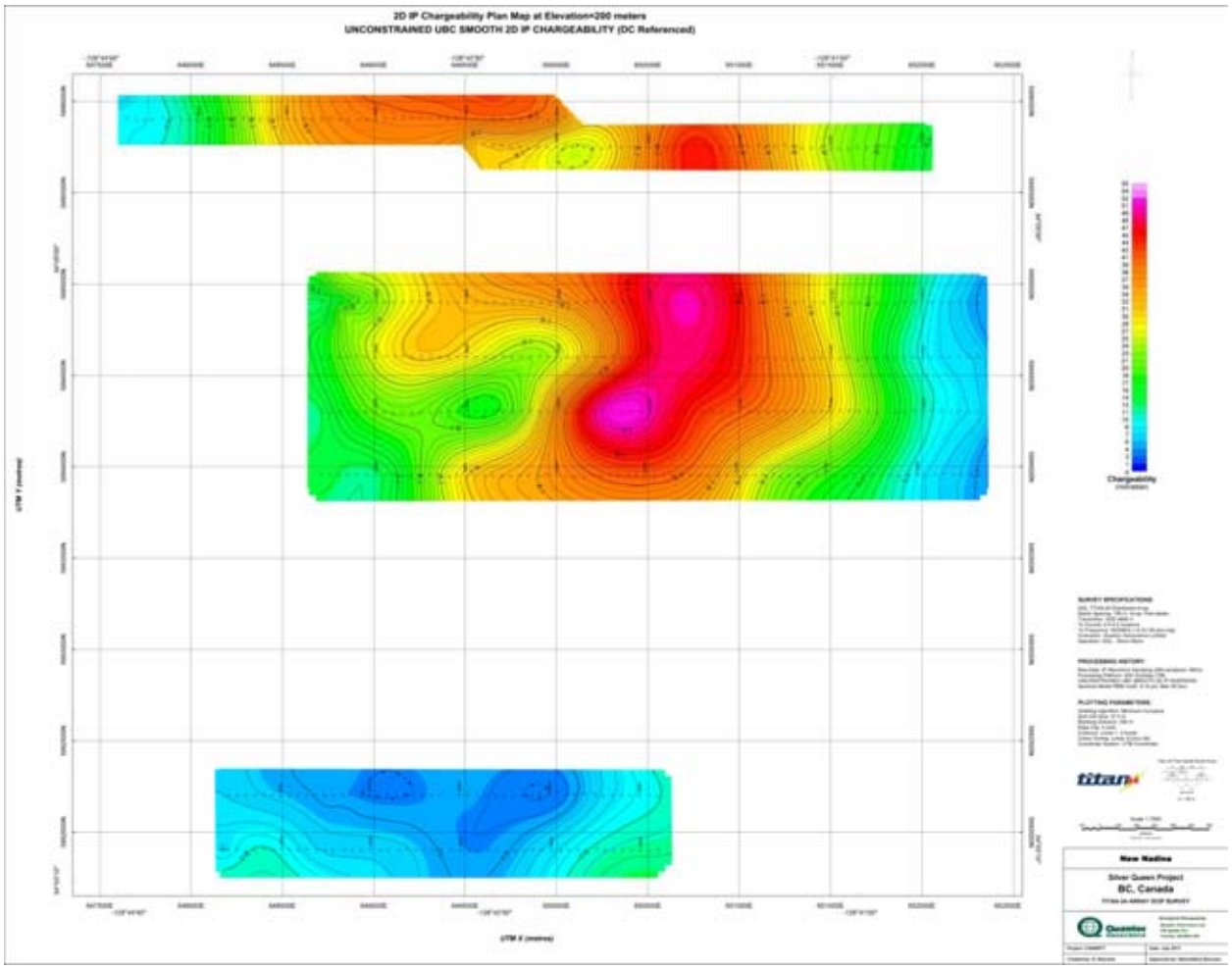

Plan Map at 200m Elevation of IP Chargeability.

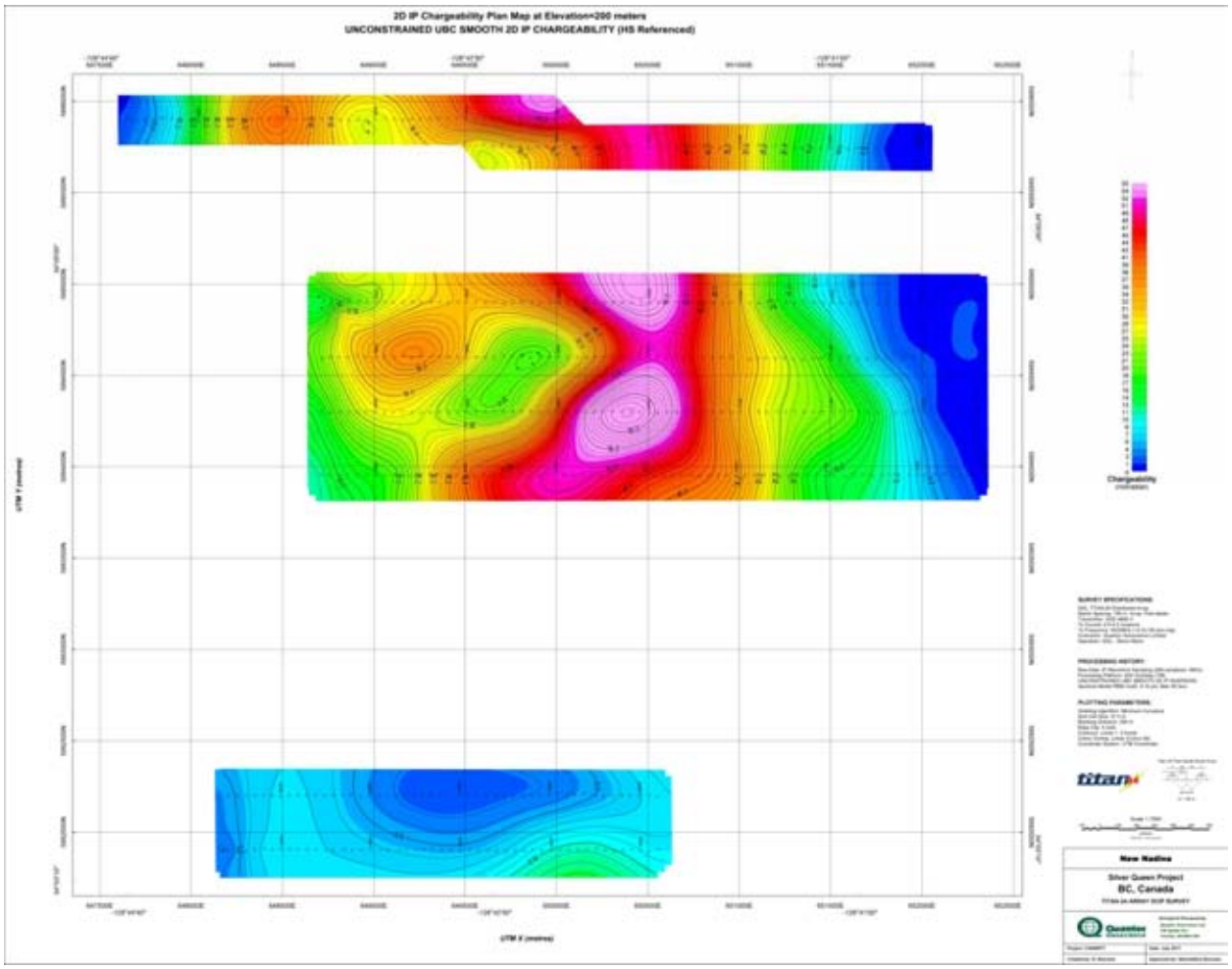

Plan Map at 200m Elevation of IP Chargeability.

K.11 PLAN MAP AT 250M ELEVATION

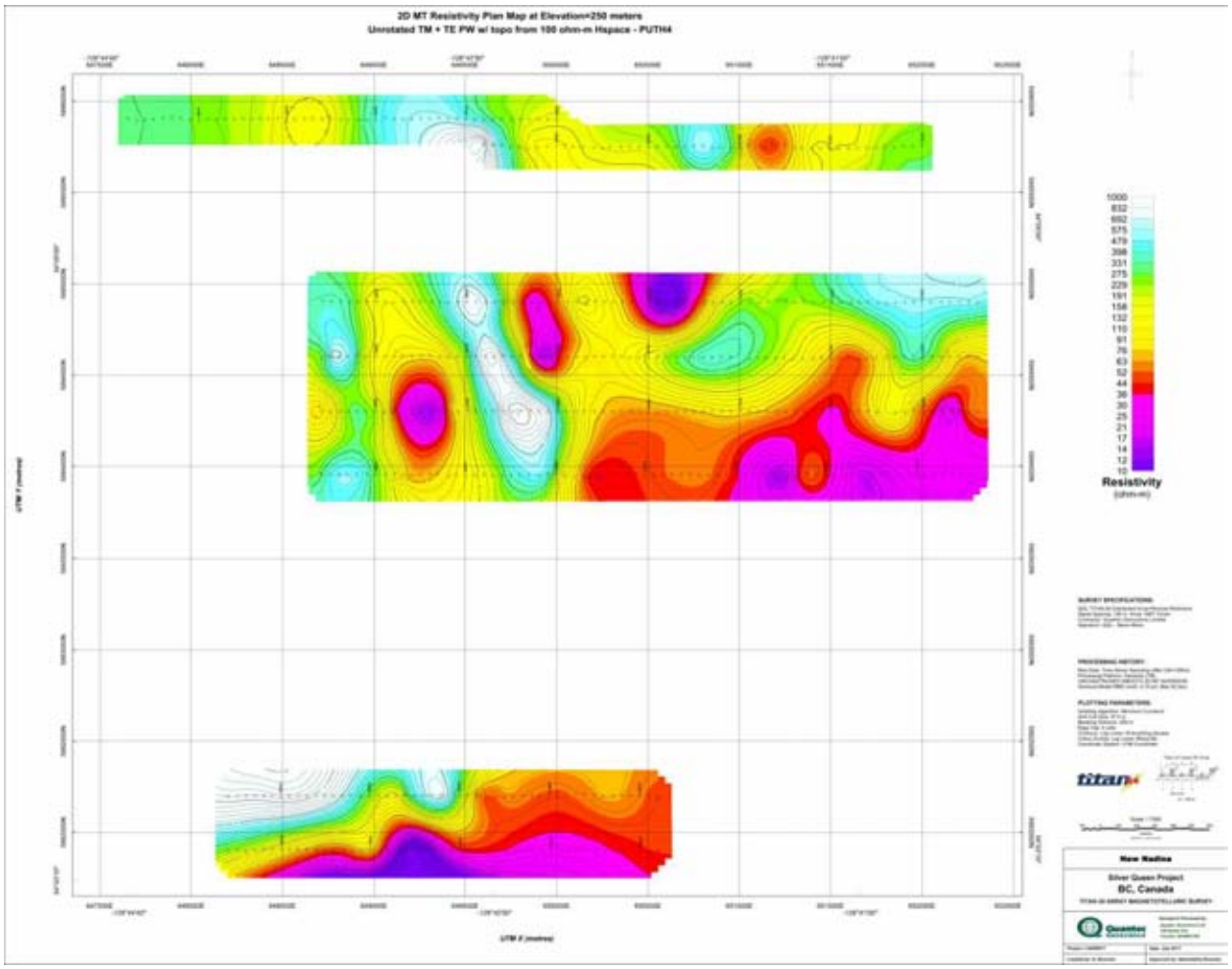

Plan Map at 250m Elevation of MT PWM Resistivity

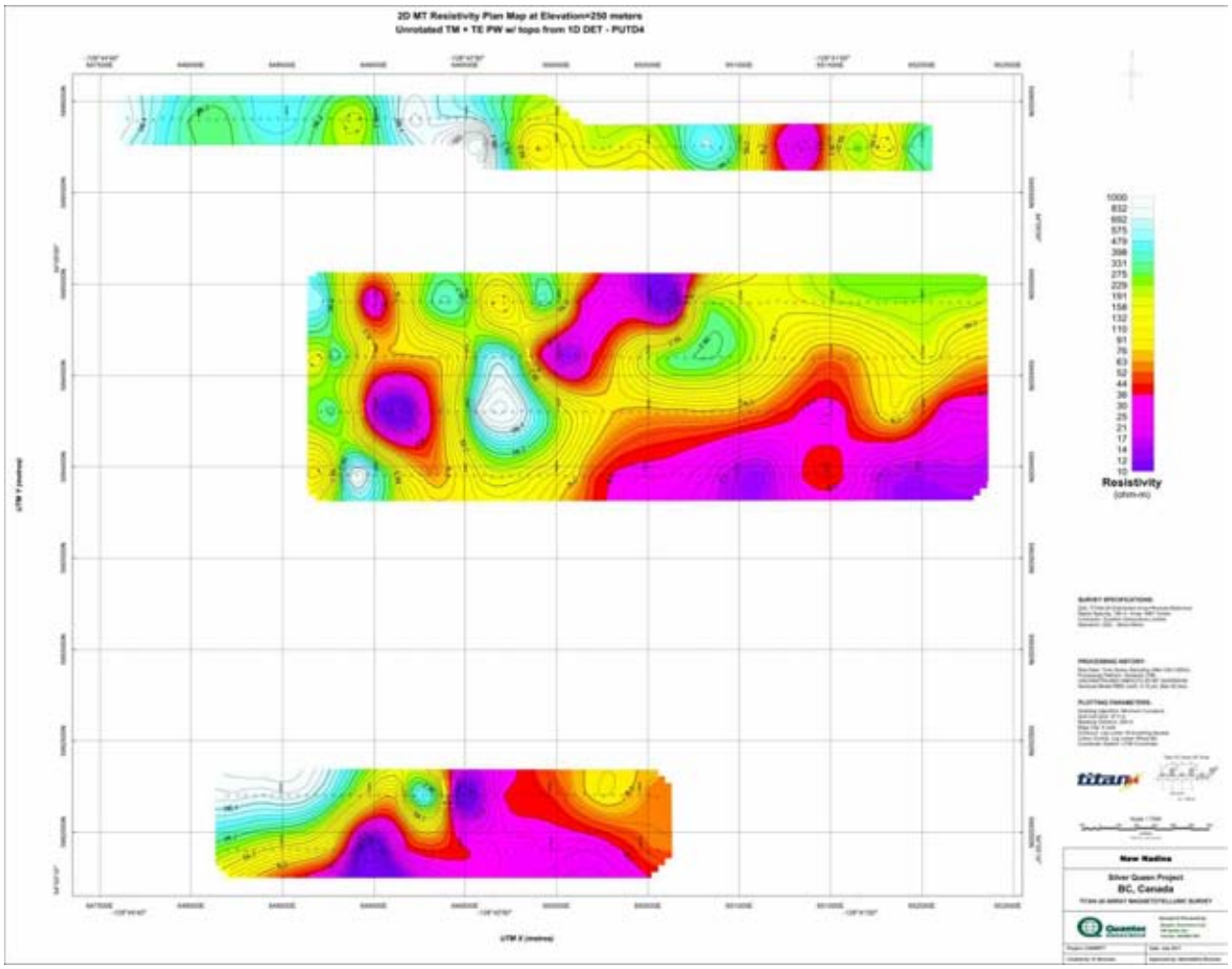

Plan Map at 250m Elevation of MT PWM Resistivity

K.12 PLAN MAP AT 300M ELEVATION

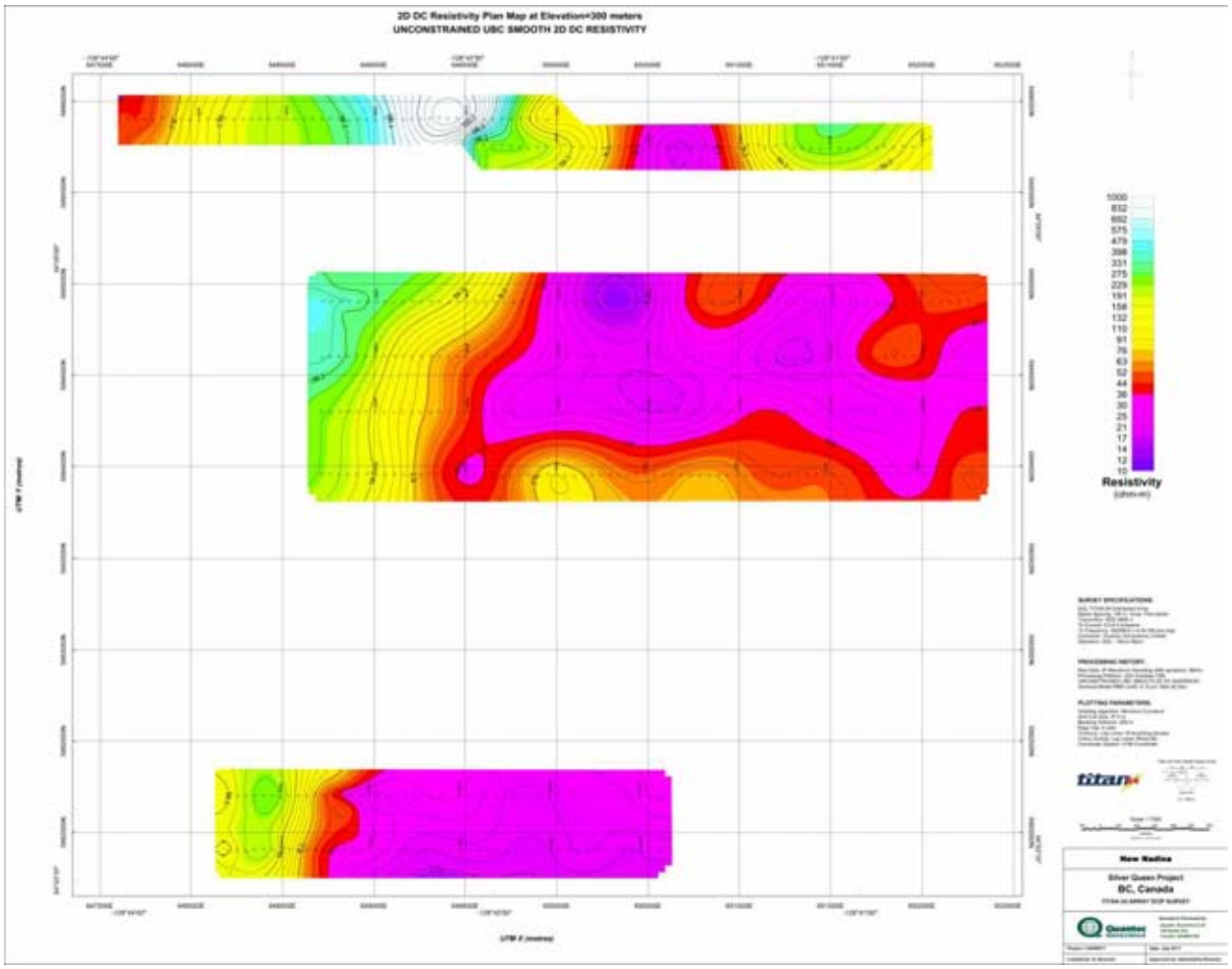

Plan Map at 300m Elevation of DC Resistivity.

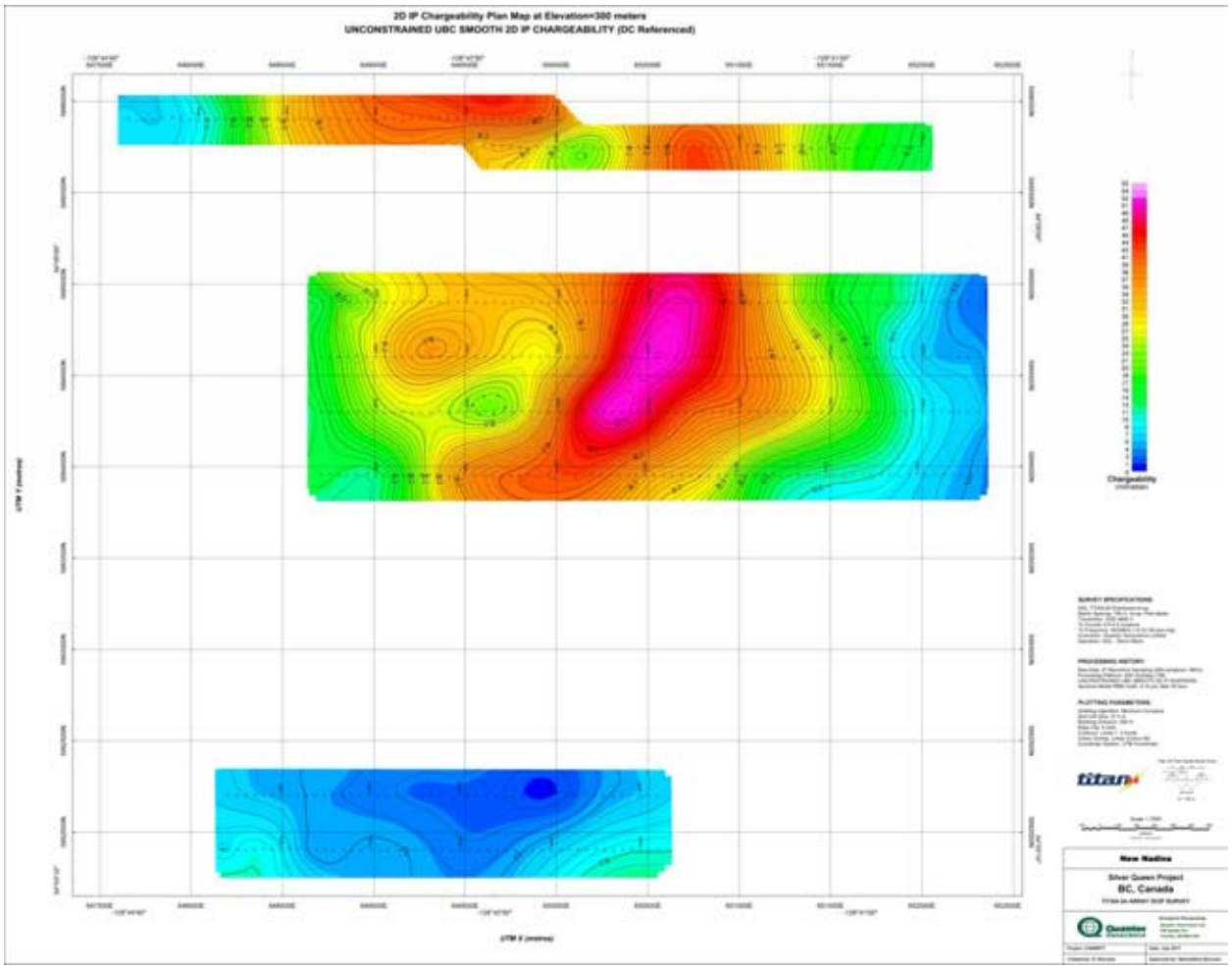

Plan Map at 300m Elevation of IP Chargeability.

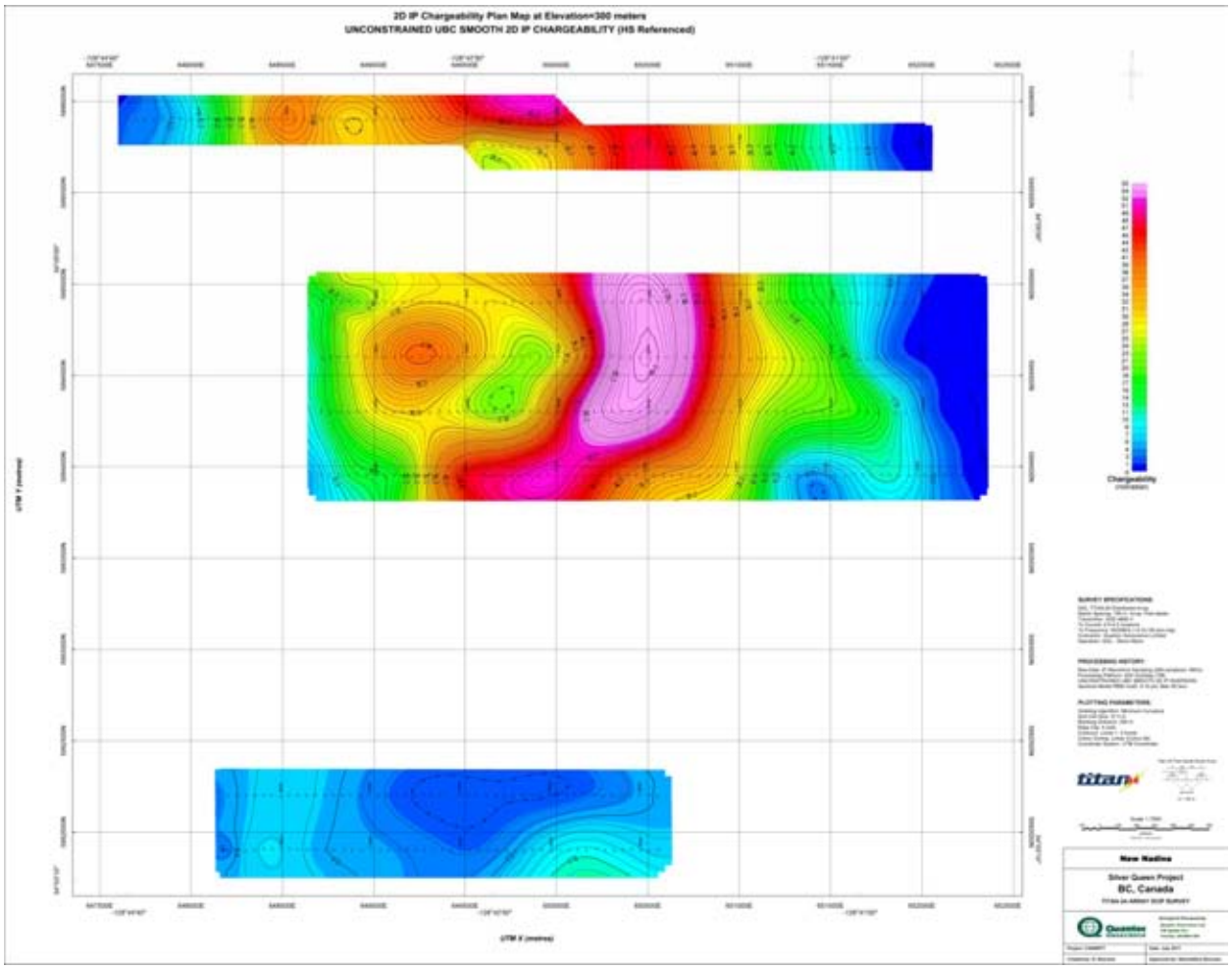

Plan Map at 300m Elevation of IP Chargeability.

K.13 PLAN MAP AT 400M ELEVATION

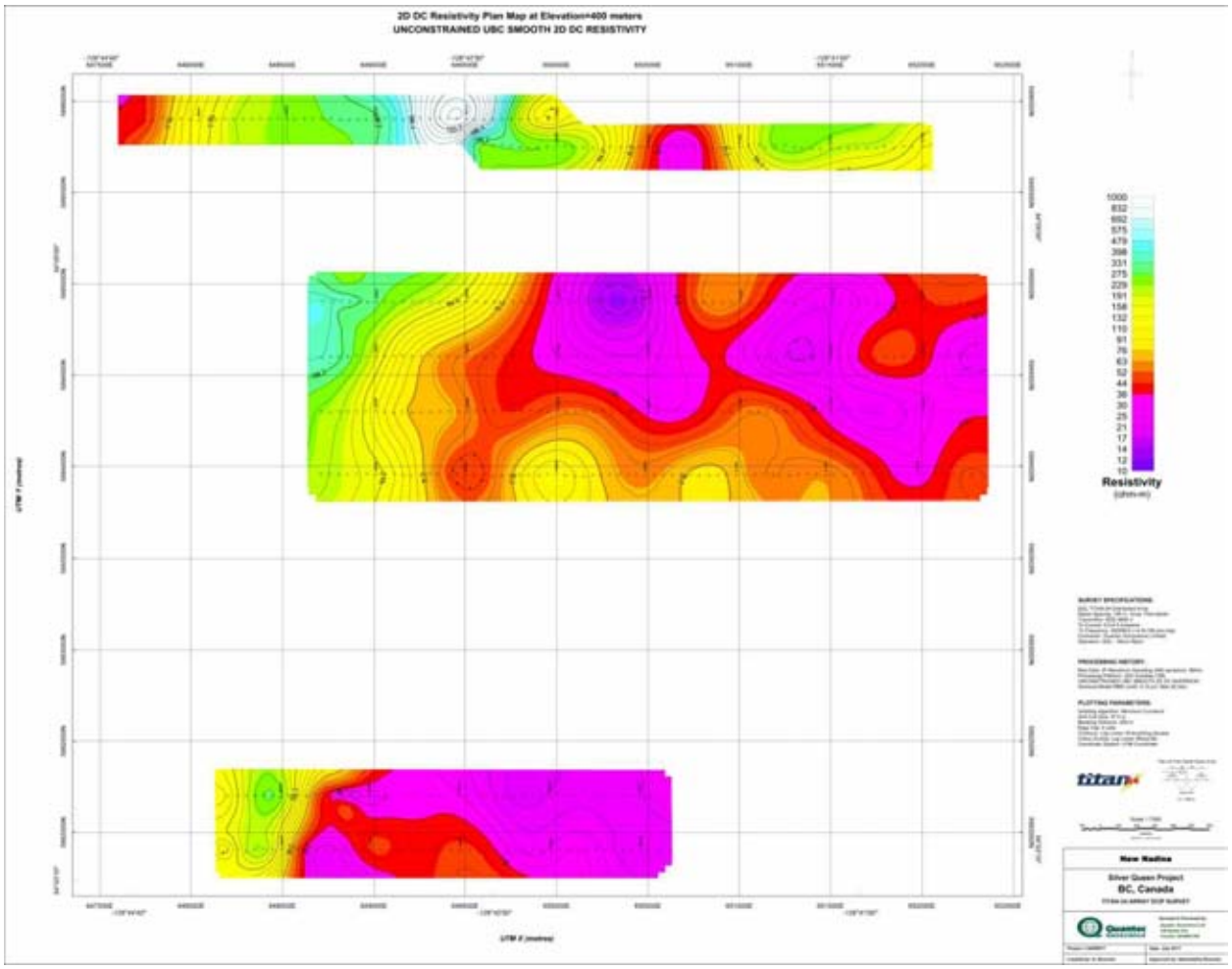

Plan Map at 400m Elevation of DC Resistivity.

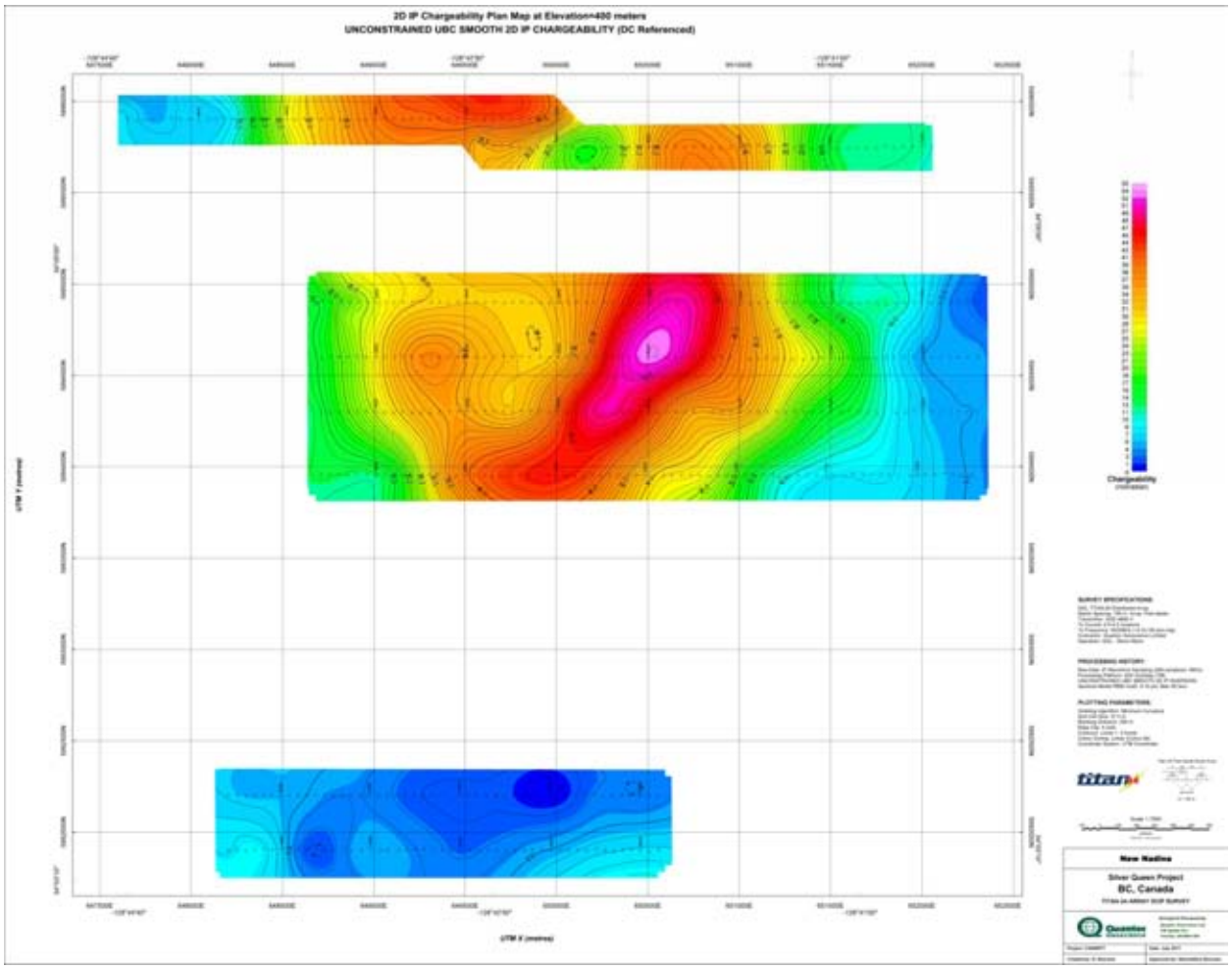

Plan Map at 400m Elevation of IP Chargeability.

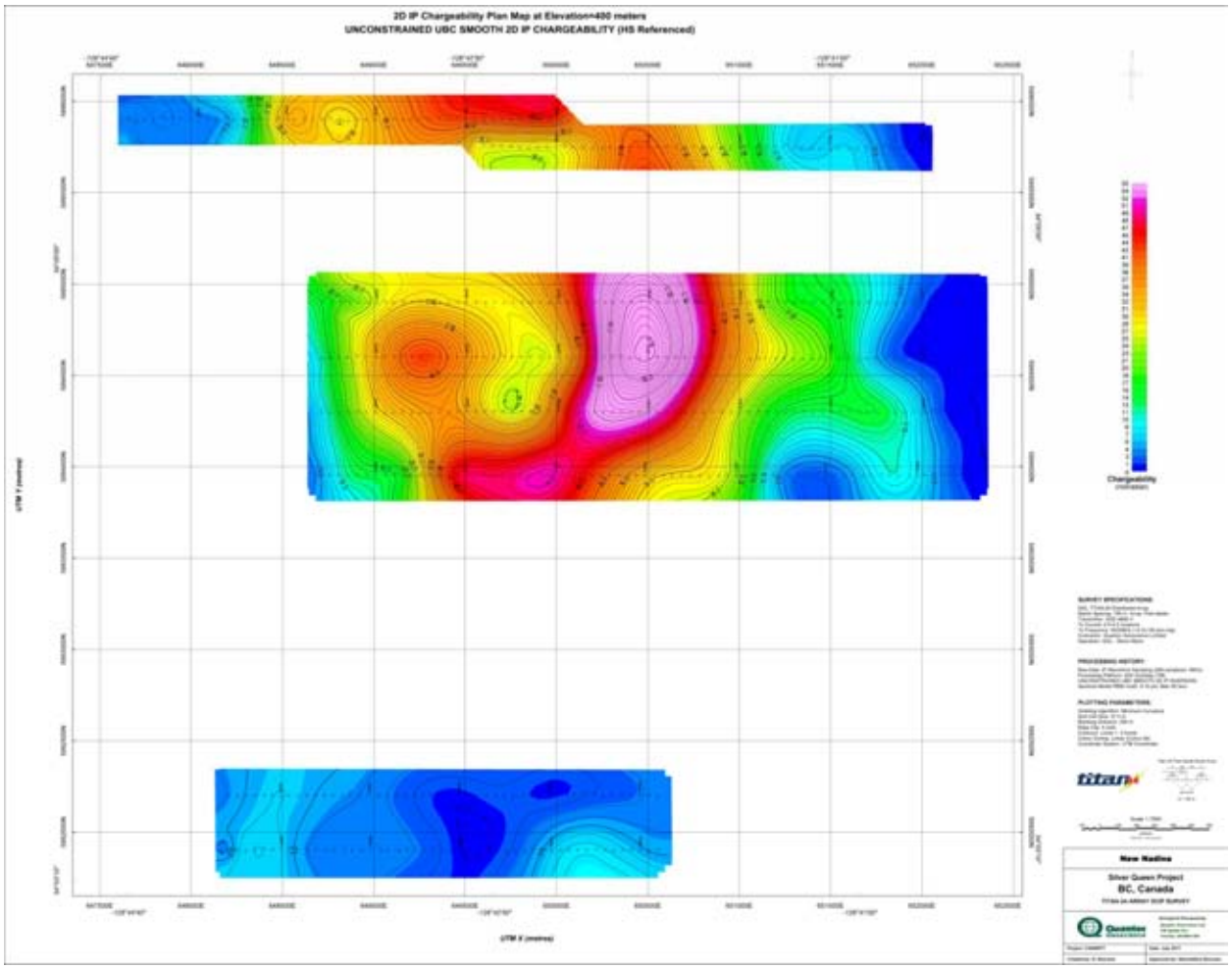

Plan Map at 400m Elevation of IP Chargeability.

K.14 PLAN MAP AT 500M ELEVATION

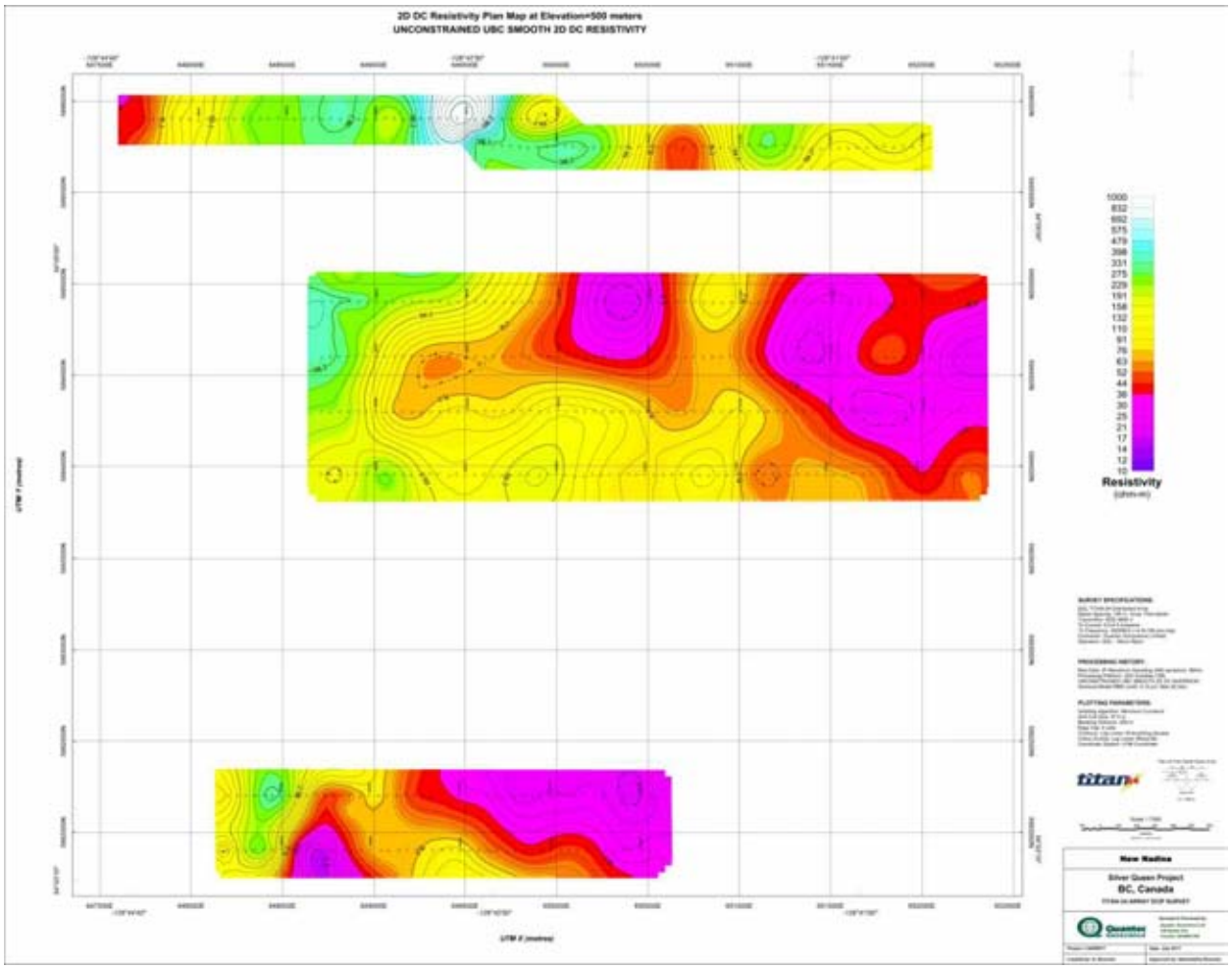

Plan Map at 500m Elevation of DC Resistivity.

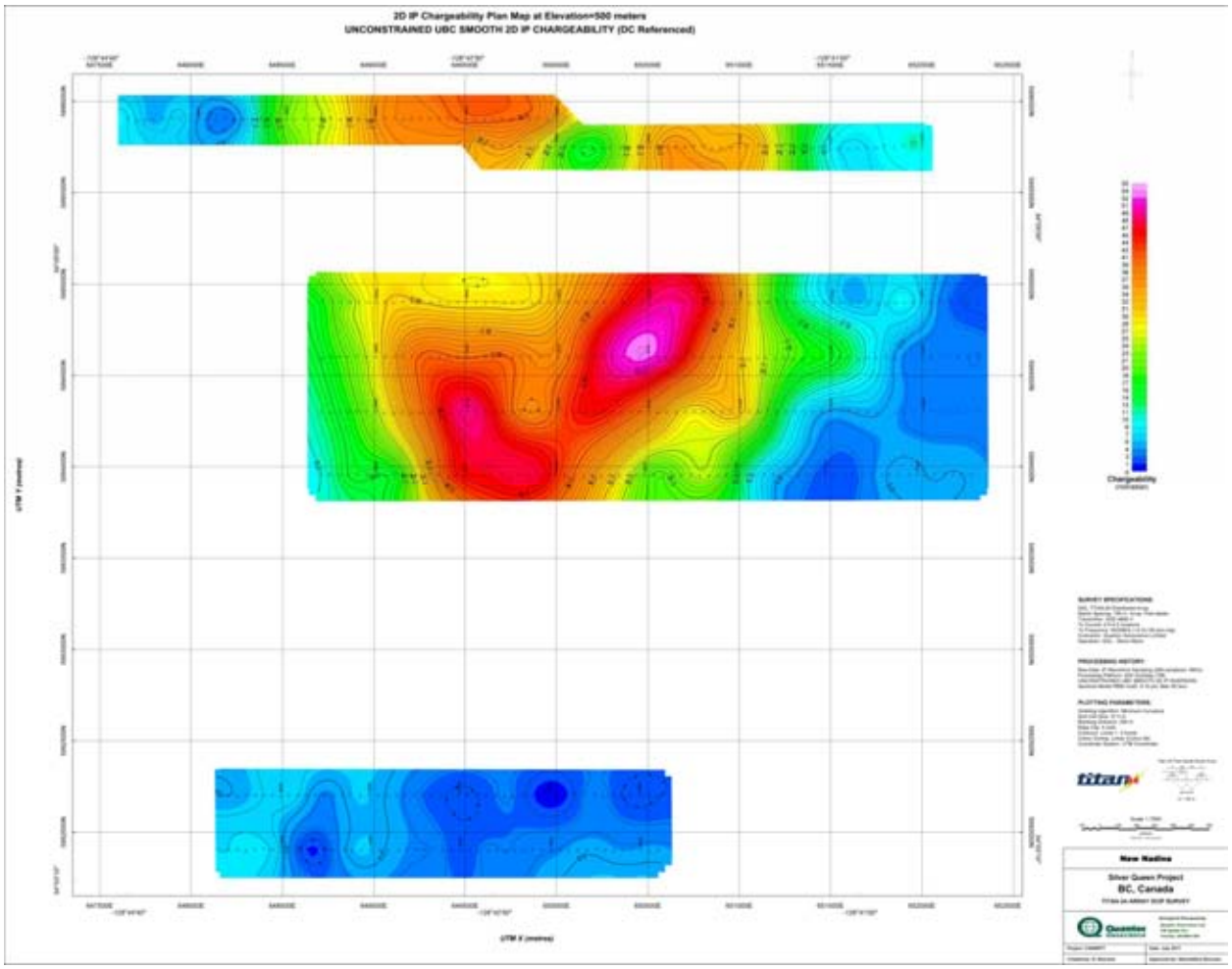

Plan Map at 500m Elevation of IP Chargeability.

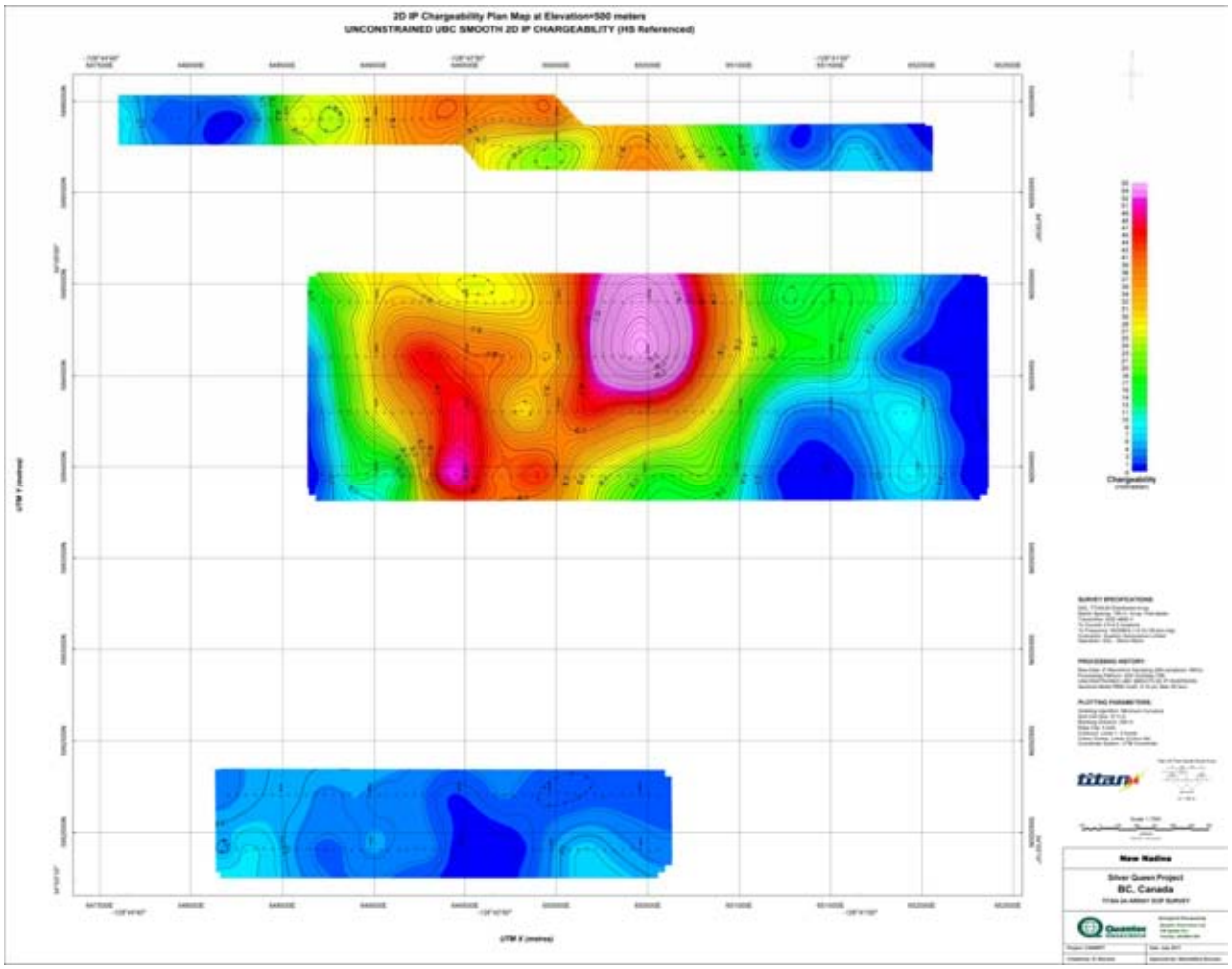

Plan Map at 500m Elevation of IP Chargeability.

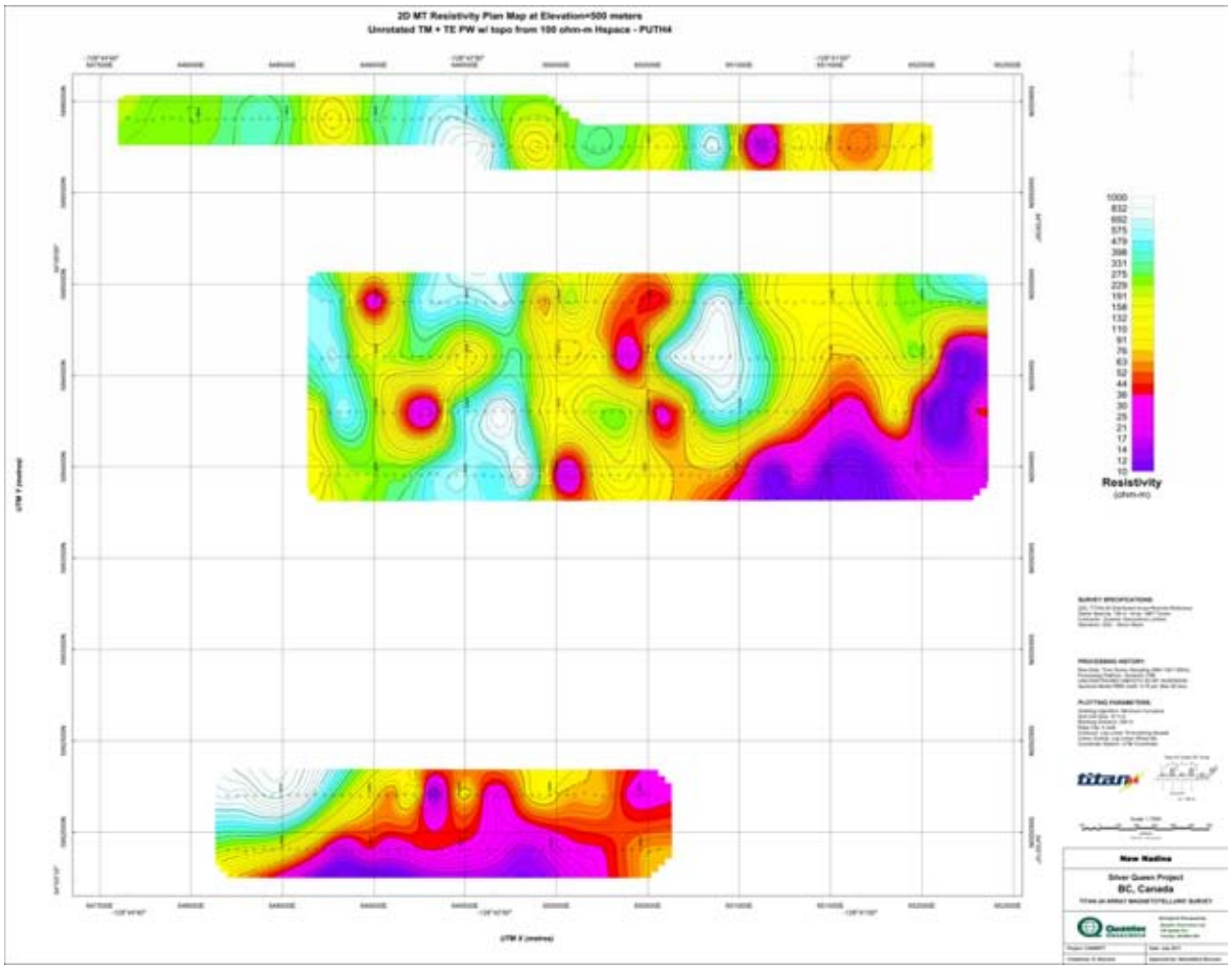

Plan Map at 500m Elevation of MT PWM Resistivity

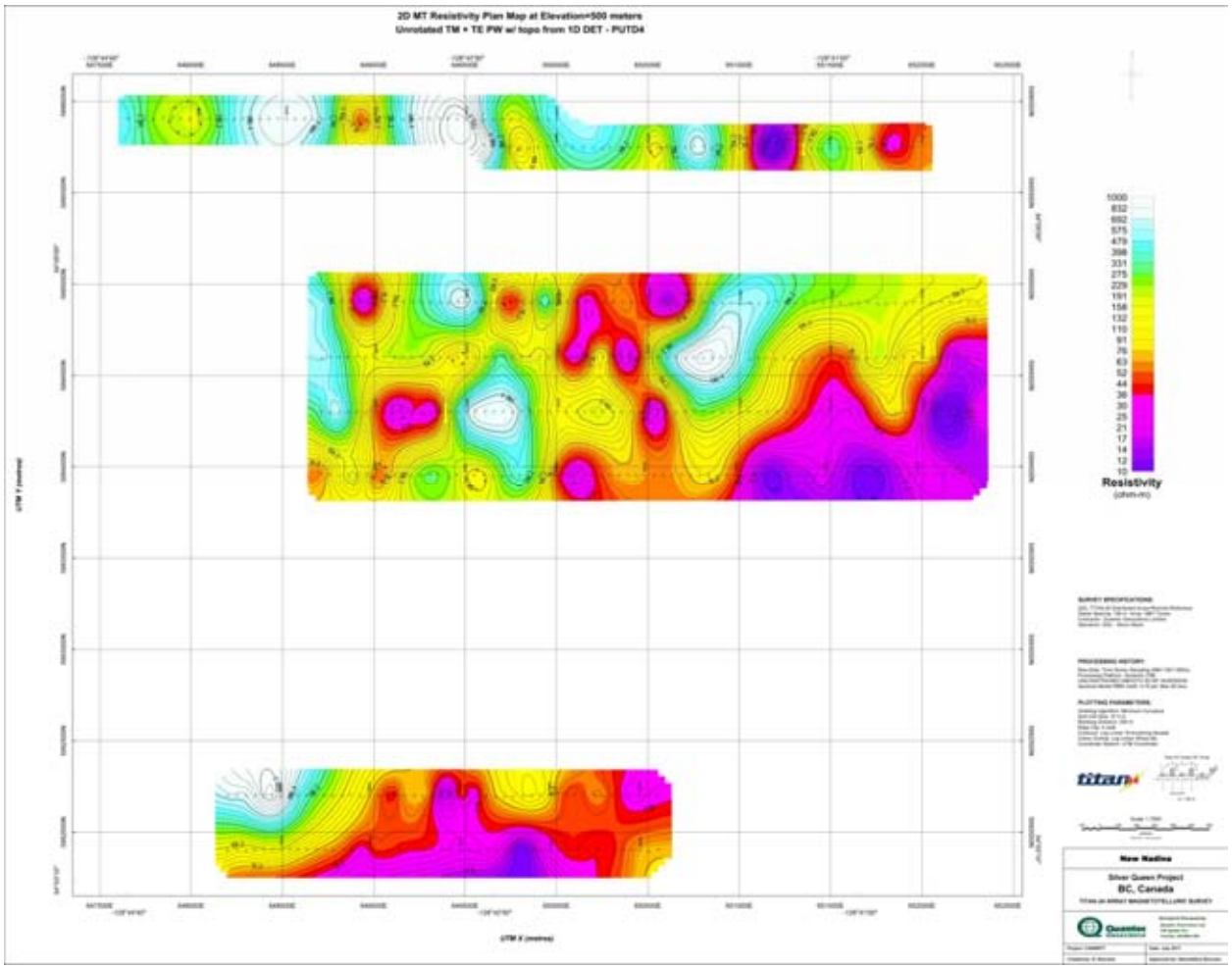

Plan Map at 500m Elevation of MT PWM Resistivity

K.15 PLAN MAP AT 600M ELEVATION

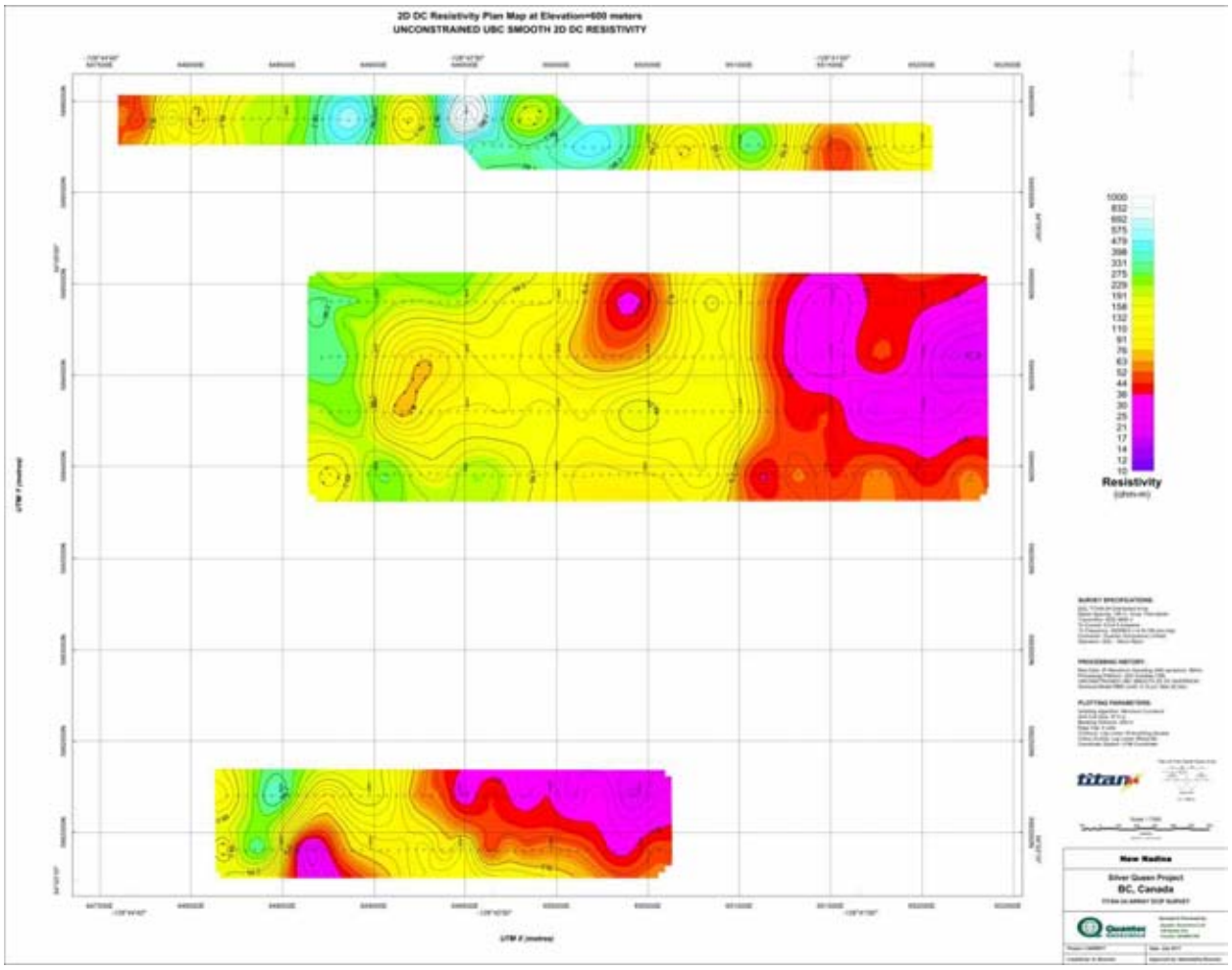

Plan Map at 600m Elevation of DC Resistivity.

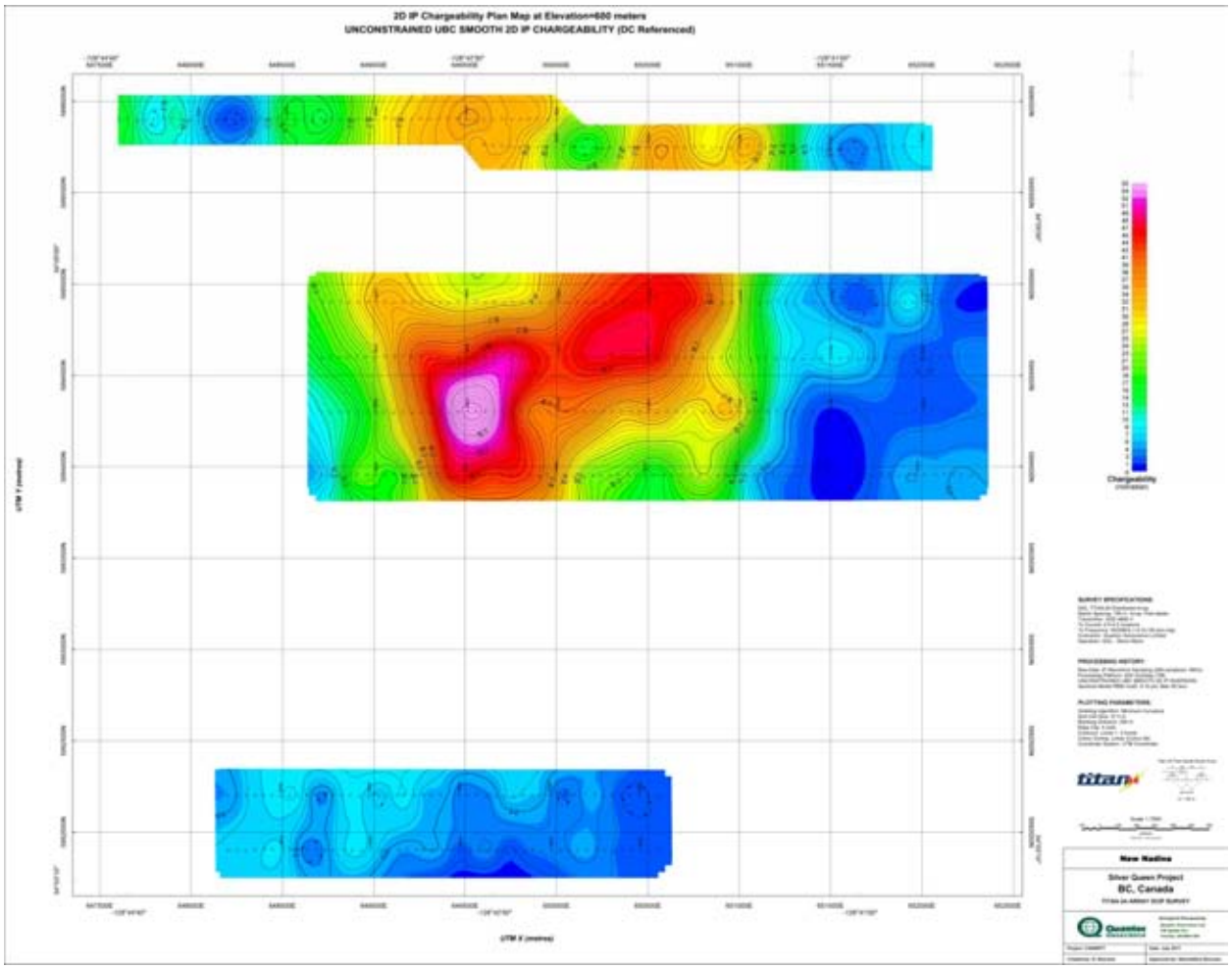

Plan Map at 600m Elevation of IP Chargeability.

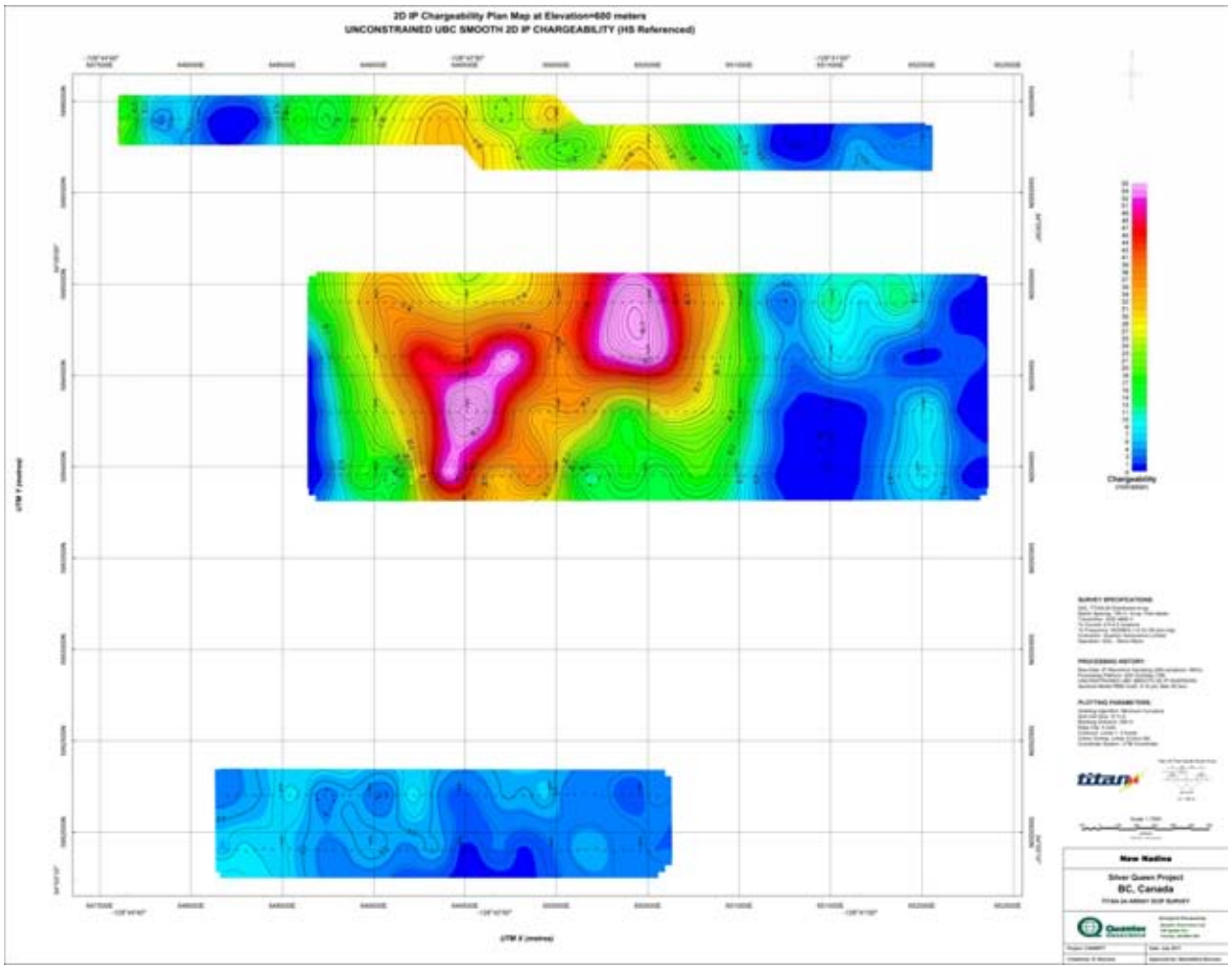

Plan Map at 600m Elevation of IP Chargeability.

K.16 PLAN MAP AT 700M ELEVATION

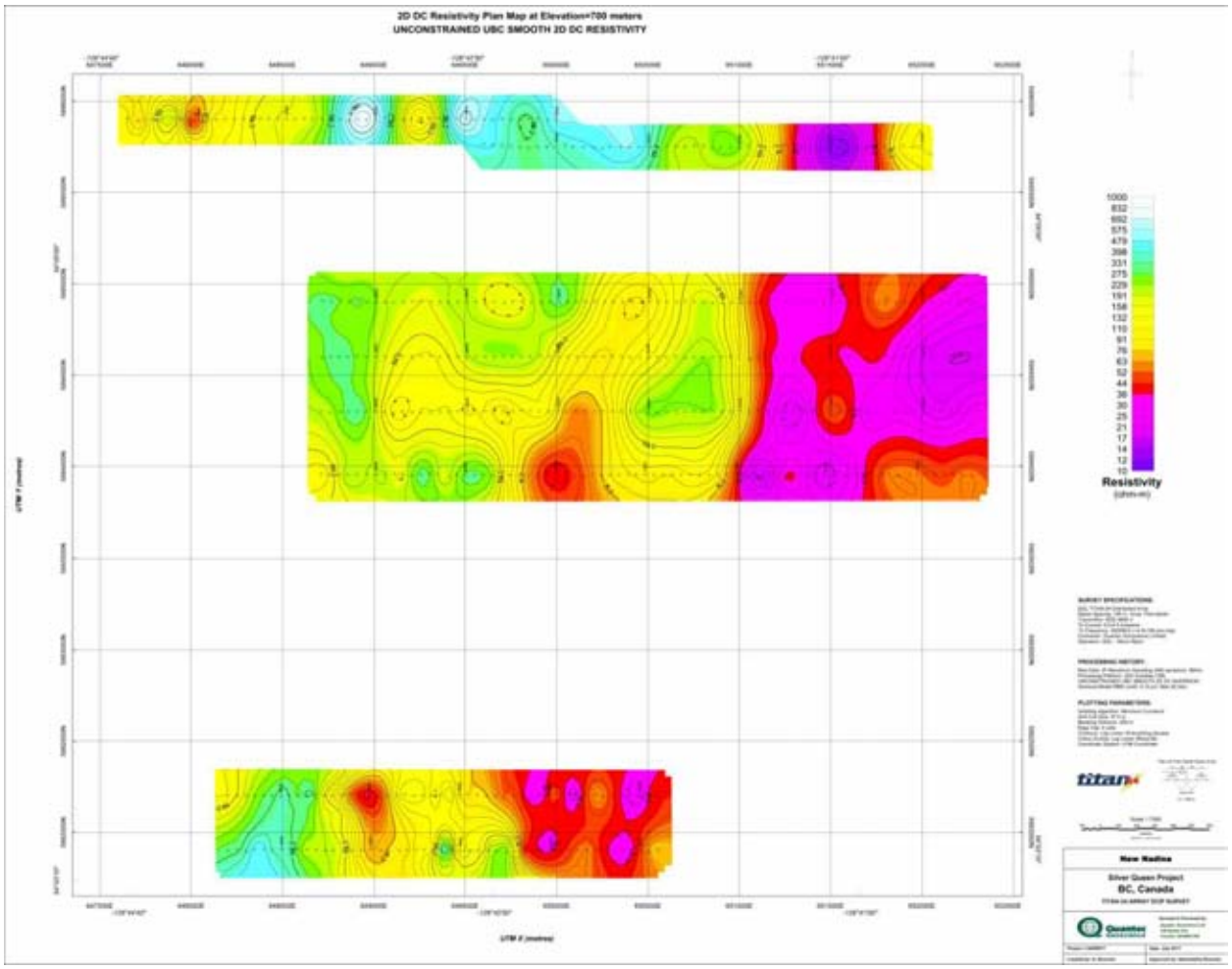

Plan Map at 700m Elevation of DC Resistivity.

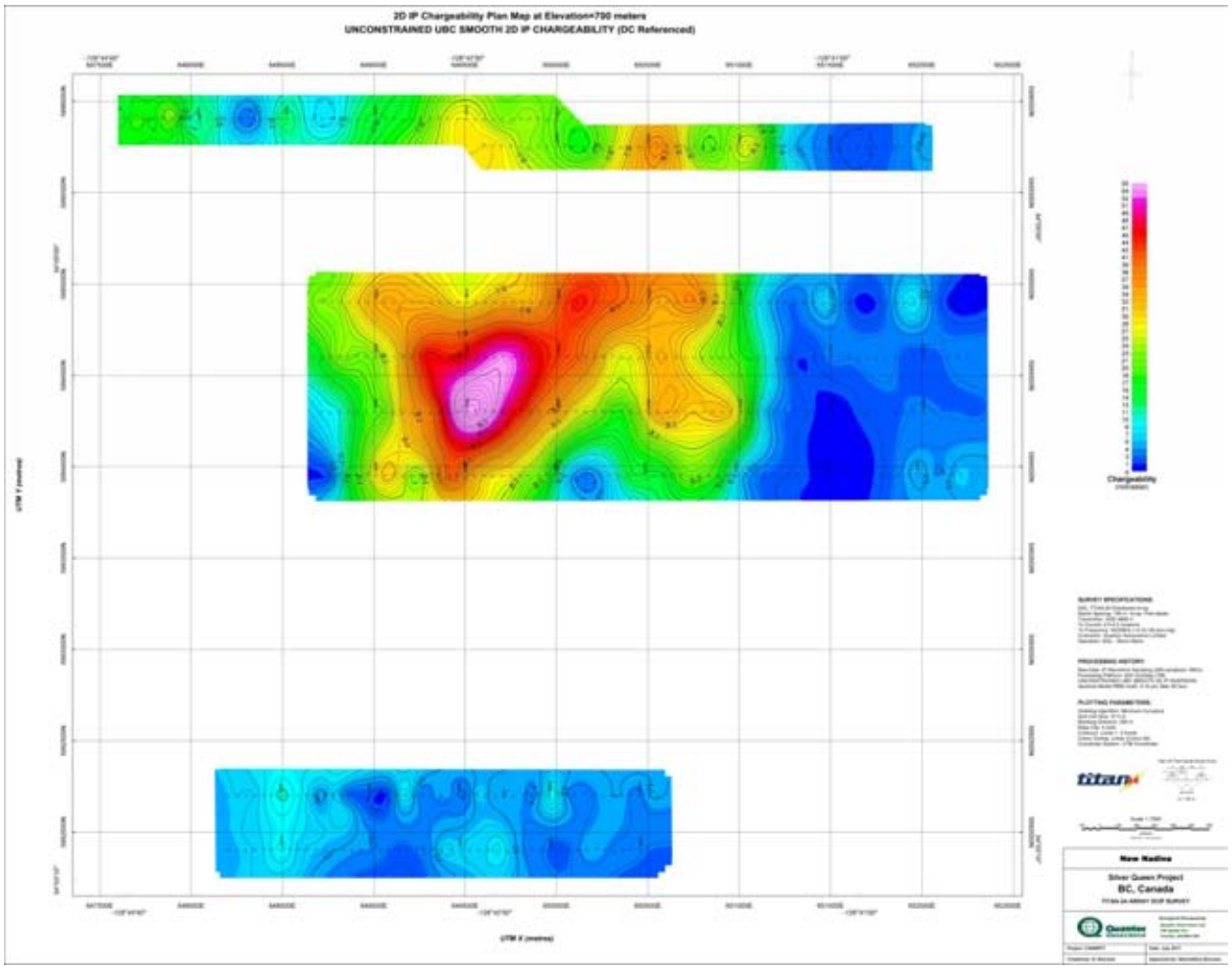

Plan Map at 700m Elevation of IP Chargeability.

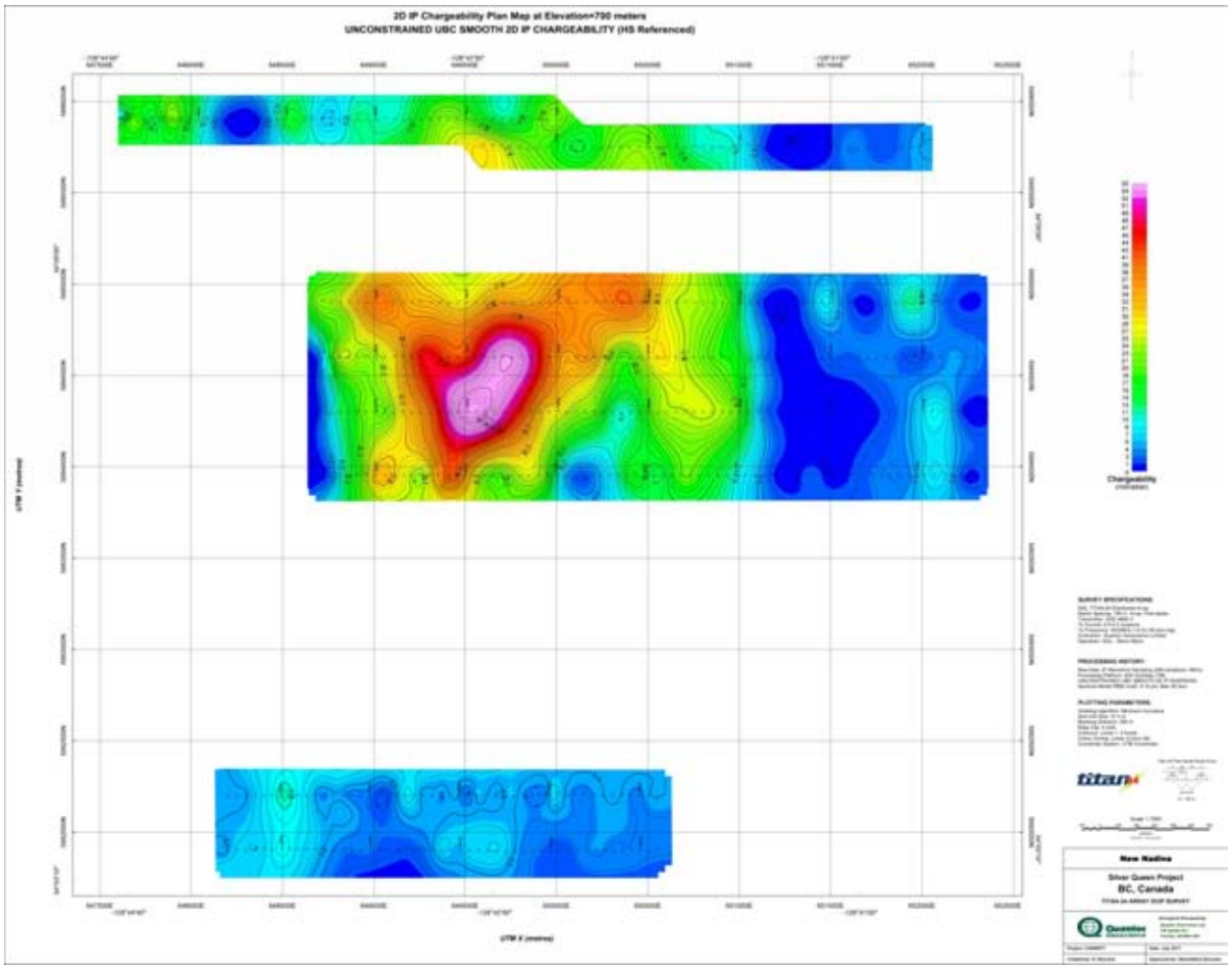

Plan Map at 700m Elevation of IP Chargeability.

K.17 PLAN MAP AT 750M ELEVATION

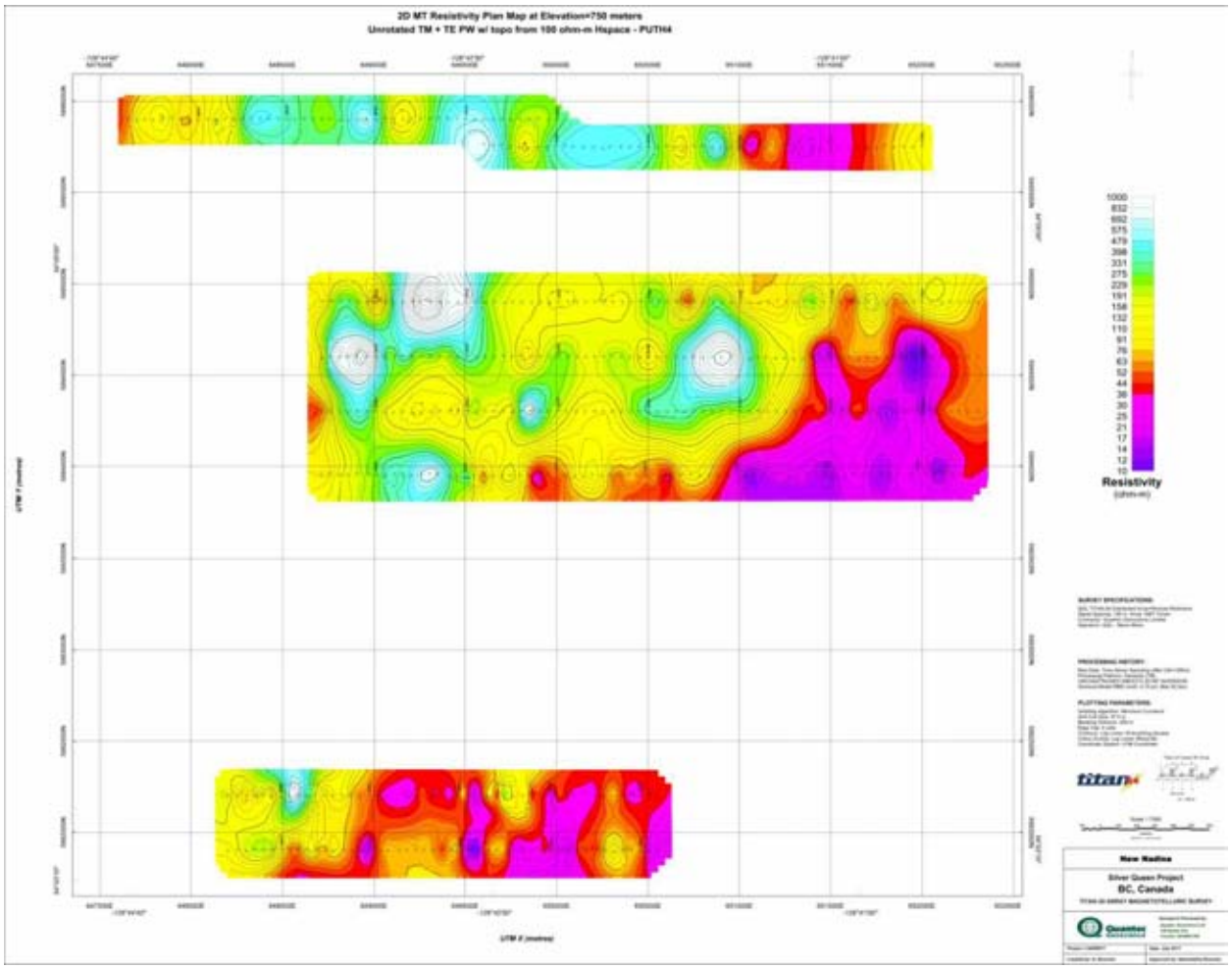

Plan Map at 750m Elevation of MT PWM Resistivity

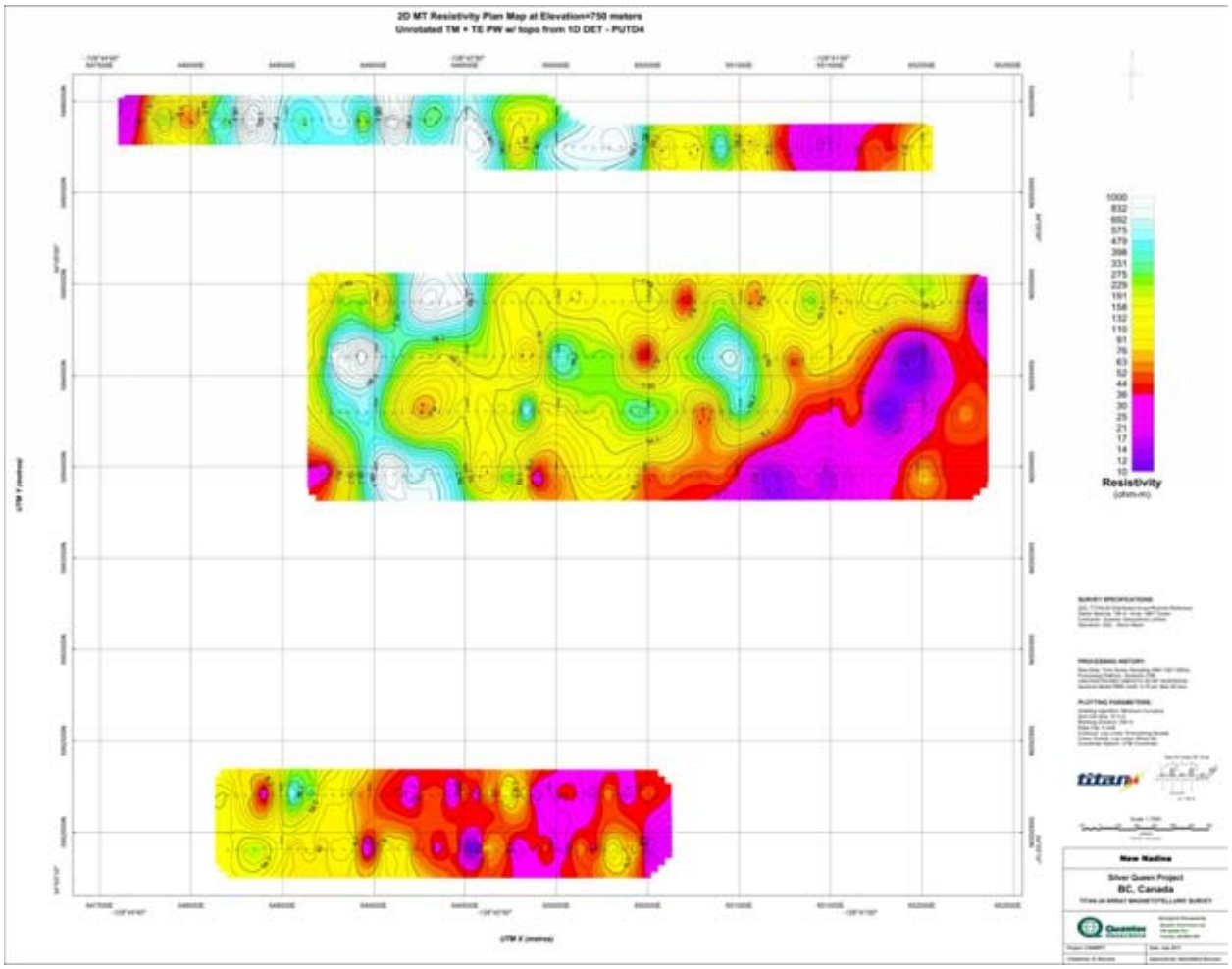

Plan Map at 750m Elevation of MT PWM Resistivity

K.18 PLAN MAP AT 800M ELEVATION

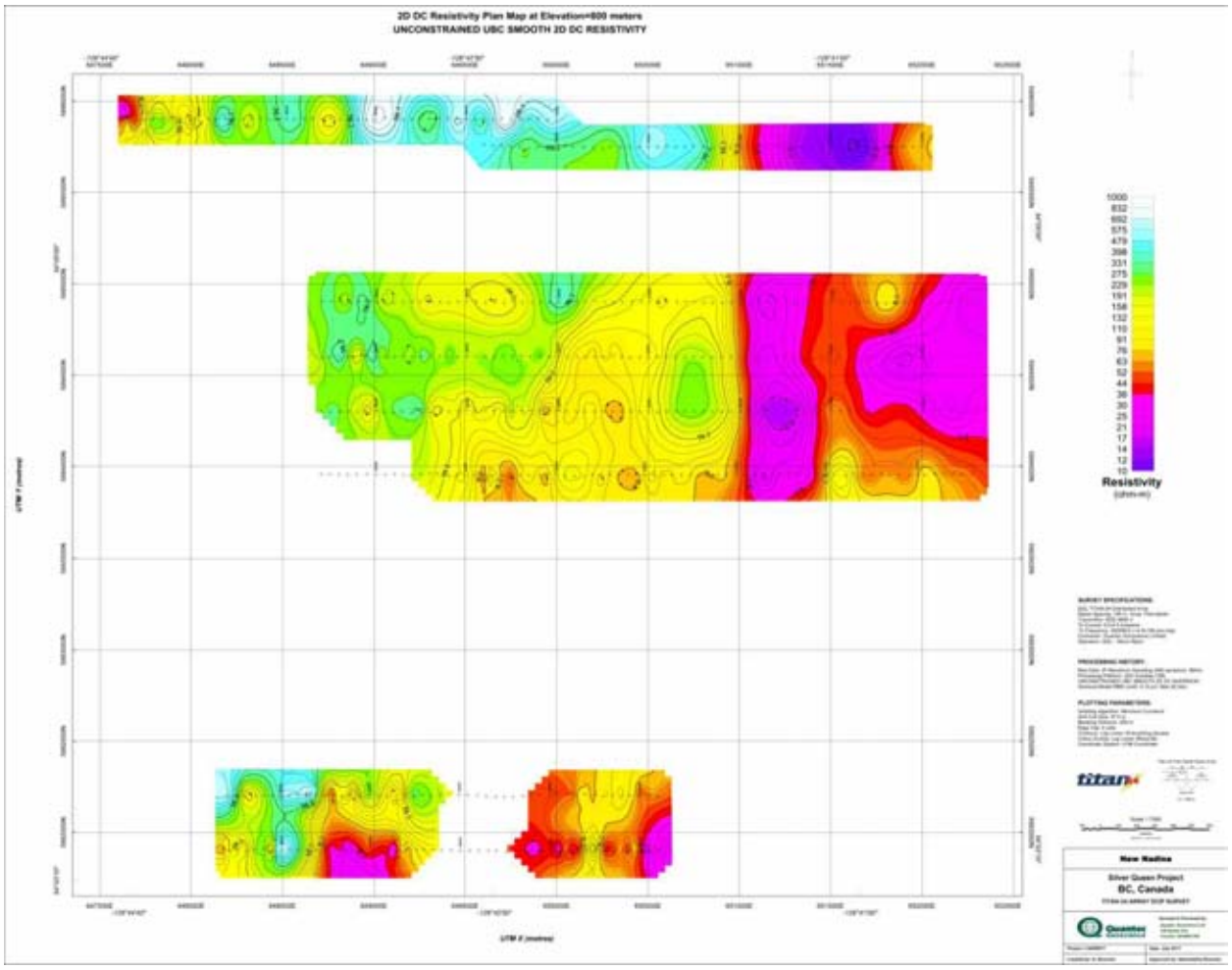

Plan Map at 800m Elevation of DC Resistivity.

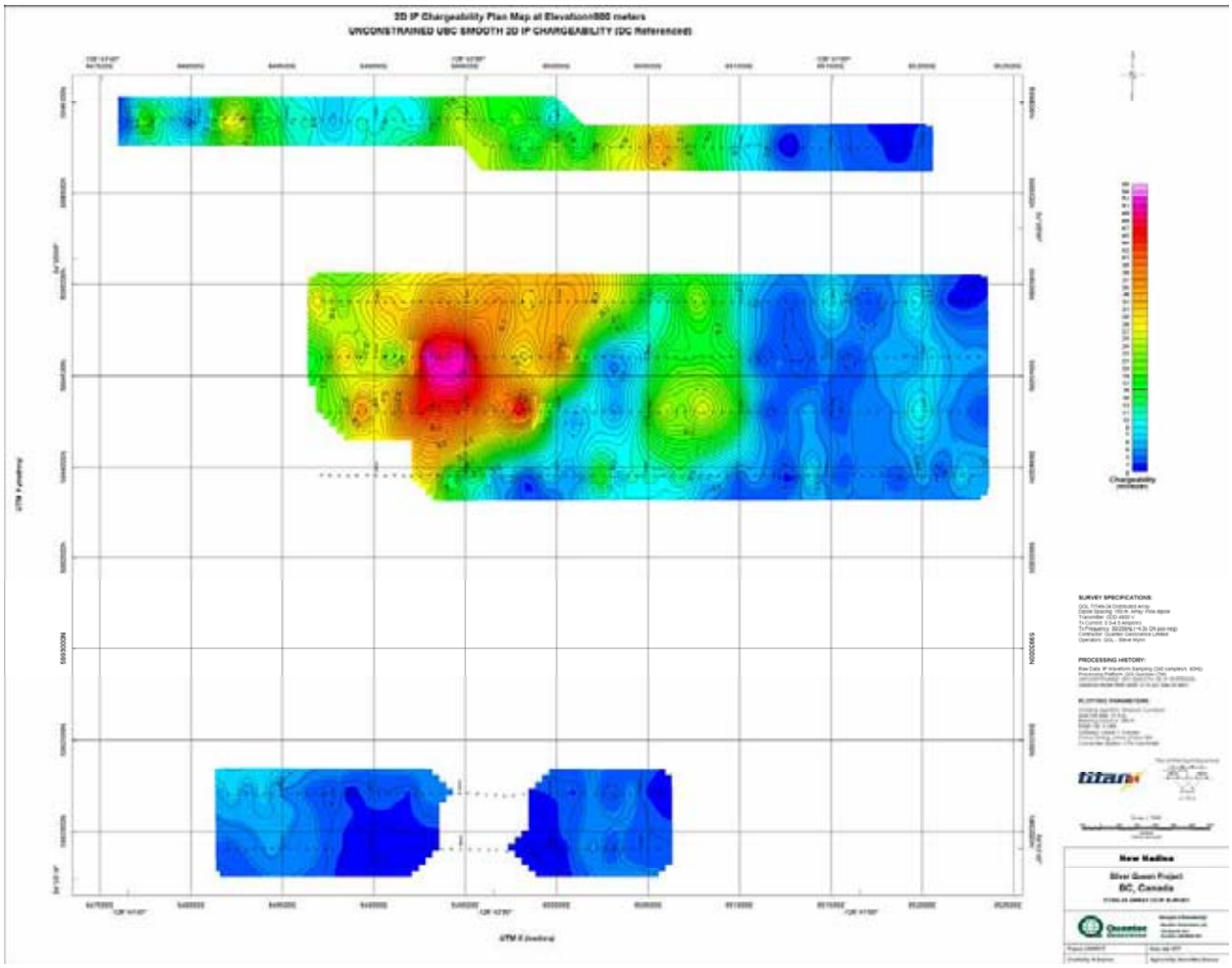

Plan Map at 800m Elevation of IP Chargeability.

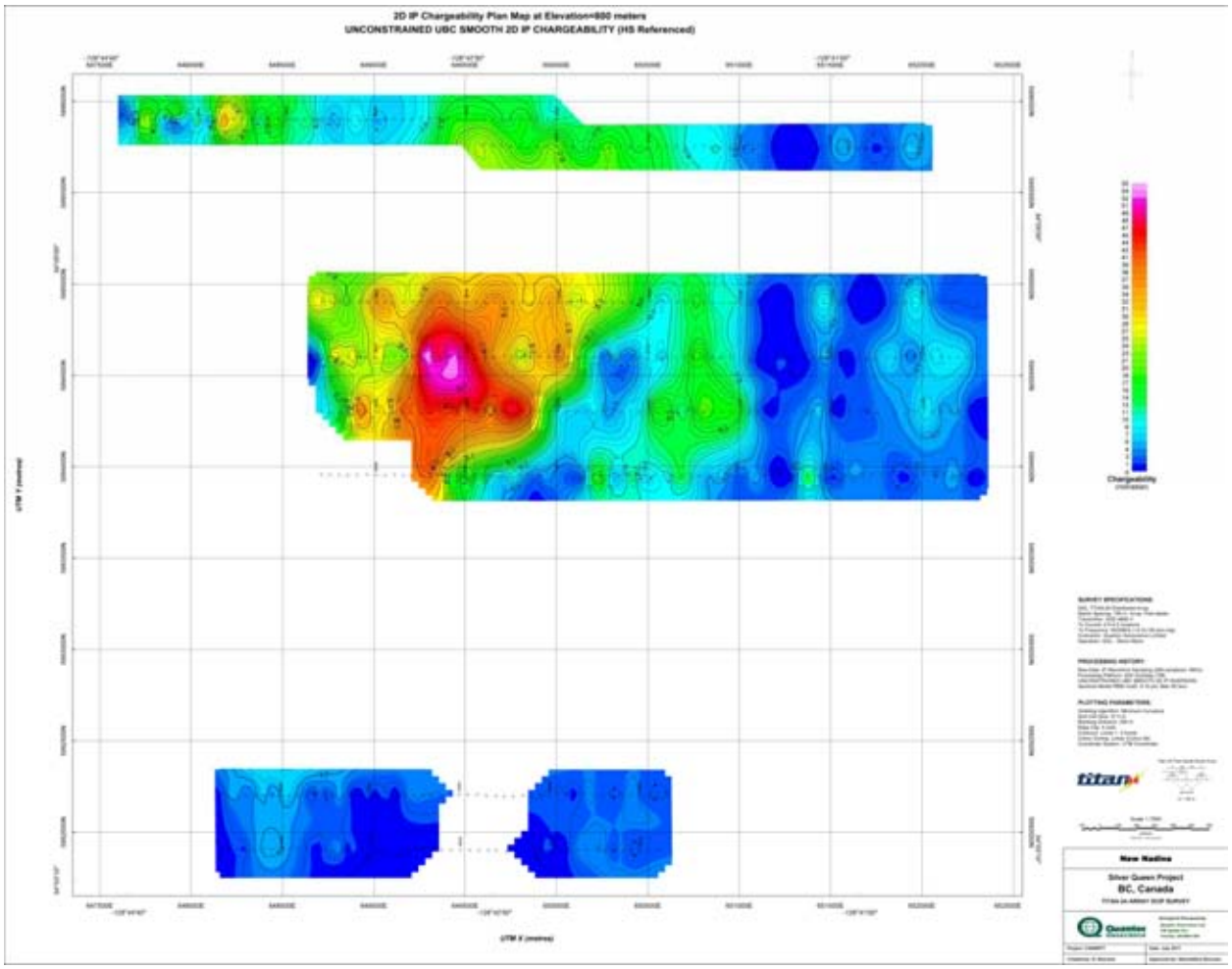

Plan Map at 800m Elevation of IP Chargeability.

L AN INTRODUCTION TO TITAN-24 DIRECT CURRENT (DC) RESISTIVITY AND INDUCED POLARISATION (IP) METHODS

L.1 INTRODUCTION

Titan-24 is a 24-bit multi-channel, distributed acquisition system that allows for the collection of high quality Direct Current (DC) Resistivity and Induced Polarization (IP) data (Sheard 1998). The system provides high multiplicity data sets and records full-waveform time-series utilizing 24-bit Sigma Delta Analog to Digital (A/D) conversion. Like other conventional resistivity methods, acquisition is performed by the injection of an artificial controlled source of current, usually a series of full duty cycle[13] square pulses, into the ground through the transmitter electrode. The voltages, normalized by the injected current, are measured at the receiver electrodes as time series.

The use of 24-bit A/D converter allows the Titan-24 system to record the full waveform at the receivers, thus permitting the accurate removal or deconvolution of the source effects from the recorded time series. What is left of the time series after the deconvolution consist of mainly the responses of the ground and noise.

DC resistivity method is quite sensitive to small variations in resistivity near surface, and its effectiveness will be limited by high level of noise in the presence of a shallow conductive layer in the ground. On the other hand, in the desert or coarse-grained sandy environments, DC resistivity method can suffer from poor electrical contact with the ground. As a result, very little or no current can be injected into the ground, and no meaningful data can be collected.

The resistivity is among the most variable of all geophysical parameters, with a range exceeding 10^6 ohm-m. The resistivity of rocks depends primarily on their porosity, permeability and particularly the salinity of fluids contained, according to Archie's Law. Therefore, DC resistivity method can be utilized in a wide variety of applications in mineral exploration, mainly for mapping of resistivity structures and locating of conductive targets.

The chargeability responds to the presence of polarisable minerals (metals, sub-metallic sulphides and oxides, and graphite), in minute amounts. Both the quantity of individual chargeable grains present and their distributions within subsurface current flow paths are significant in controlling the level of response. The IP method can be used to directly detect disseminated to massive sulphides.

More detailed descriptions on the theory and application of the DCIP method can be found in Telford et al. (1976).

[13] Duty cycle is the ratio between the pulse duration and the period of a square waveform.

L.2 TITAN-24 DCIP SURVEY

Titan-24 is a distributed DCIP acquisition system. A typical survey layout, or spread, is 2400m long and has 25 inline (Ex) 100m potential dipoles and the current injections sites. With current extensions, a typical Titan-24 spread can be stretched to 3600m. If requested, the dipole length can be changed to 50m or 200m, and the resulting length Titan-24 spread will be 1200m or 4800m. Also, cross line dipoles (Ey) can be deployed as well.

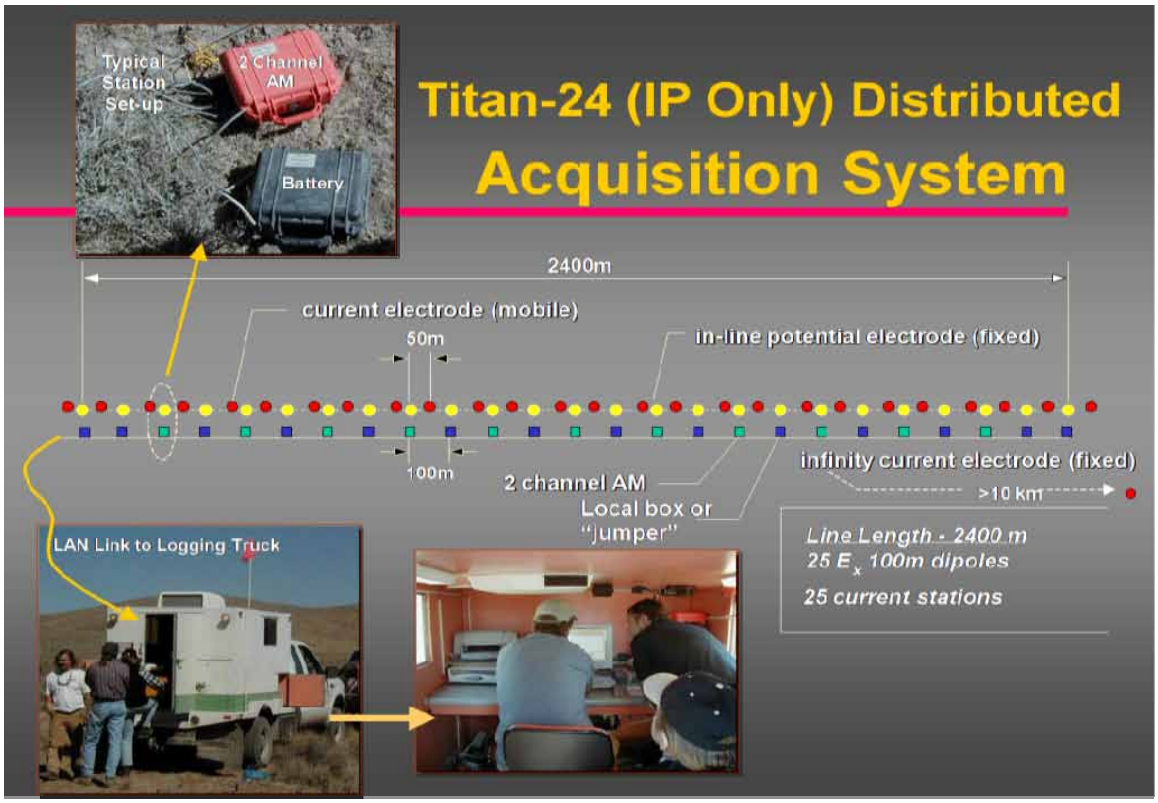

Titan-24 Distributed Acquisition System (IP-only) layout.

In a normal Titan-24 survey, the transmitter (Tx) and receiver (Rx) configuration is the pole-dipole-dipole array, combining pole-dipole right (PDR) and pole-dipole left (PDL). The current is injected at the mid-point between two potential electrodes. However, with special safety arrangements made to the system, the current can be injected at the potential electrode locations.

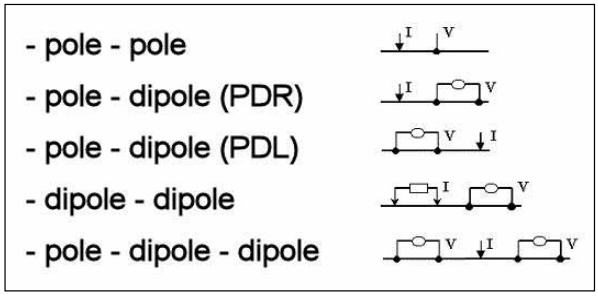

Titan-24 Transmitter (Tx) and Receivers (Rx) configurations.

L.3 TITAN-24 DCIP DATA PROCESSING

For one potential electrode pair, the data acquired with one current injection event is a time series of measured voltages at the electrodes normalized by the current, Vp in mV/A. A typical Titan-24 time series are shown below.

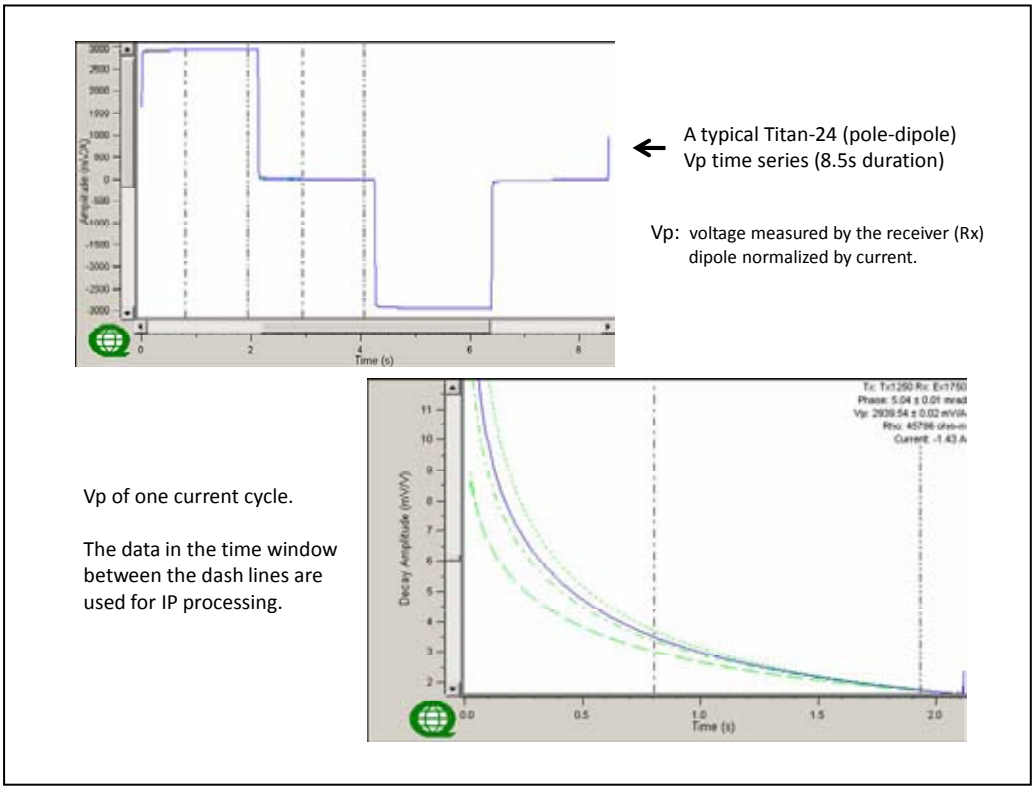

Typical Titan-24 DCIP time series.

A single injection event usually lasts approximately three minutes. The time series of an event are stacked twenty times per second in order to increase the signal to noise (S/N) ratio. The data processing is done in the frequency domain. Current waveform deconvolution and digital filtering of power line noise (60/50Hz, and their harmonics) are applied to the frequency domain data.

L.4 HALVERSON-WAIT CHARGEABILITY

Titan-24 IP chargeability are described using the Halverson-Wait spectral model (Halverson et al., 1981), which is not well known, but is similar to the Cole-Cole model proposed by Pelton et al. (1978) which is a simple relaxation model that fits complex (frequency-dependant) resistivity results.

The time domain chargeability, originally proposed by Siegel (1959), is defined (Telford et al., 1976) as:

$$M = \frac{1}{V_c}\int_{t1}^{t2} V(t)dt$$

where $V(t)$ is the residual or secondary voltage at a time t that is decaying after the current is cut off, between time t_1 and t_2 with the steady voltage V_c during the current flow interval. The ratio $V(t)/V_c$ is expressed in millivolts per volts (mV/V).

In the frequency domain, the "frequency effect" is defined as:

$$FE = \frac{(\rho_{DC} - \rho_{AC})}{\rho_{AC}}$$

where ρ_{DC} and ρ_{AC} are the apparent resistivity's measured at DC and "very high" frequency, usually in the 0.1 to 10 Hz range.

The Cole-Cole model for the chargeability m, as defined by Pelton et al. (1978) is given by the following:

$$Z(\omega) = R_0\left[1 - m\left(1 - \frac{1}{1+(i\omega\tau)^C}\right)\right]$$

where $Z(\omega)$ is the complex impedance with ω the angular frequency in Hz, R_0 the DC resistivity, m the chargeability in volts per volt, τ the time constant in seconds, and c is the frequency dependence (unit less). The latter two physical properties describe the shape of the decay curve in time domain or the phase spectrum in frequency domain, and commonly range between 0.01s to +100s and 0.1 to +0.5, respectively (Johnson, 1984).

The Halverson-Wait model was proposed by Halverson et al. (1981) as an extension to the Wait (1959) model of the impedance of "volume loading" of spheres, given by:

$$Z(\omega) = \frac{\rho}{G}\left[1 - 3\nu\left(1 - \frac{3\delta}{1+2\delta}\right)\right]$$

where G is a geometric factor, ρ the resistivity of the media, ν the volume loading (the volume fraction of chargeable "spheres"), δ the sphere surface impedance. The Wait model was designed to provide an explanation of the differences in the shape of decay curves from different polarisable targets, but does not describe very well the physical attributes of the rocks.

The Halverson-Wait model expands the Wait coated sphere IP model to include a new formulation of the sulphide-rock interface impedance, based on field studies and laboratory tests on samples. It is closely correlated to the Pelton et al. (1978) Cole-Cole model and is given by:

$$Z(\omega) = \frac{\rho}{G}\left[1 - 3\nu\left(1 - \frac{3/2}{1+r[i\omega]^K}\right)\right]$$

where r is the sphere radius and is equivalent to τ - the Cole-Cole time constant ($r = \tau^K$). The volume loading ν compares well to m, the Cole-Cole chargeability (see equation below), and the exponent K is equal to c, the Cole-Cole frequency dependence (Halverson et al., 1981). For sulphide systems, the r -factor reflects the size or inter-connectedness of the sulphide grains and the K -factor reflects the electrical characteristics of the sulphide surfaces.

An example of time domain Halverson-Wait model responses is shown below:

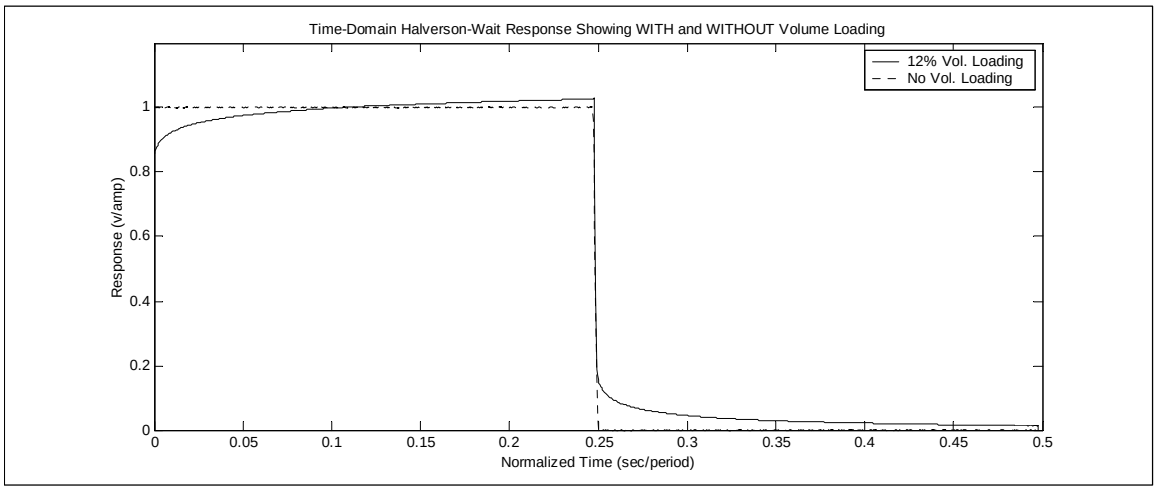

Polarisable versus Non-Polarisable TD-IP response using Halverson-Wait Model.

In the Halverson-Wait model the theoretical Percentage Frequency Effect (PFE)[14] (for infinite bandwidth), which equates to the theoretical chargeability in the Cole-Cole equation, is thereby defined by the volume loading:

$$\frac{PFE_0^{\infty}}{100} = m_0 = \frac{9v}{(2+3v)}$$

and m is output in units of milliradians (mrads).

L.5 TITAN-24 IP CHARGEABILITY DEFINITION (QTN001)

Quantec prefers to estimate IP responses using a time domain half-duty square-wave excitation standard, but convert those chargeability results to units of phase. The specific procedure and algorithm is as follows:

1. Determine the earliest time for which EM coupling has died out sufficiently. This time is called the averaging or integration *start time* t_0. A typical value for t_0 is 0.8s;
2. Determine the latest charge/decay time that is minimally affected by sigma-delta and low-pass (usually Hanning window moving average) filtering, called the averaging or integration *end time* t_1. A typical value for t_1 is 1.95s;
3. Adjust the *start time* (t_0) so that $t_1 - t_0$ (equated to number of samples) exactly spans an integer number of power-line signal periods. This can only be done for transmitted (fundamental) frequencies that are much lower than the power-line frequency;
4. Using the charge and decay sample numbers that equate to the averaging window[15] defined by t_0 and t_1, calculates the average charge and decay voltages. This average may

[14] The classical definition of PFE is $100 \times (\rho_0 - \rho_\infty) / \rho_0$.

[15] In practice this averaging window is tapered slightly to widen the stop-band notches and thereby provide enhanced power-line noise rejection.

involve a non-uniform weighting to further improve rejection of power-line noise;

5. Calculate the theoretical Halverson-Wait half-duty time-domain response using identical filtering to that applied to the measured data response estimate, and presuming the following spectral parameters:
   a. volume loading: 0.125 (this value is not important)
   b. r – value: 1.0
   c. k – value: 0.2
6. For the standard Halverson-Wait spectral parameters mentioned, the synthesized time-domain response and the $t_1 - t_0$ averaging window, convert all estimated/measured charge and decay voltages (using the specified averaging window) to chargeability (millivolts/volt) and then to phase (milliradians).

This is the algorithm used in the Titan-24 data processing. The relationship between Titan-24 chargeability unit, phase in milliradians, and other frequency domain systems is straightforward – Quantec's time-domain based phase equates to frequency domain based phase, see figures below.

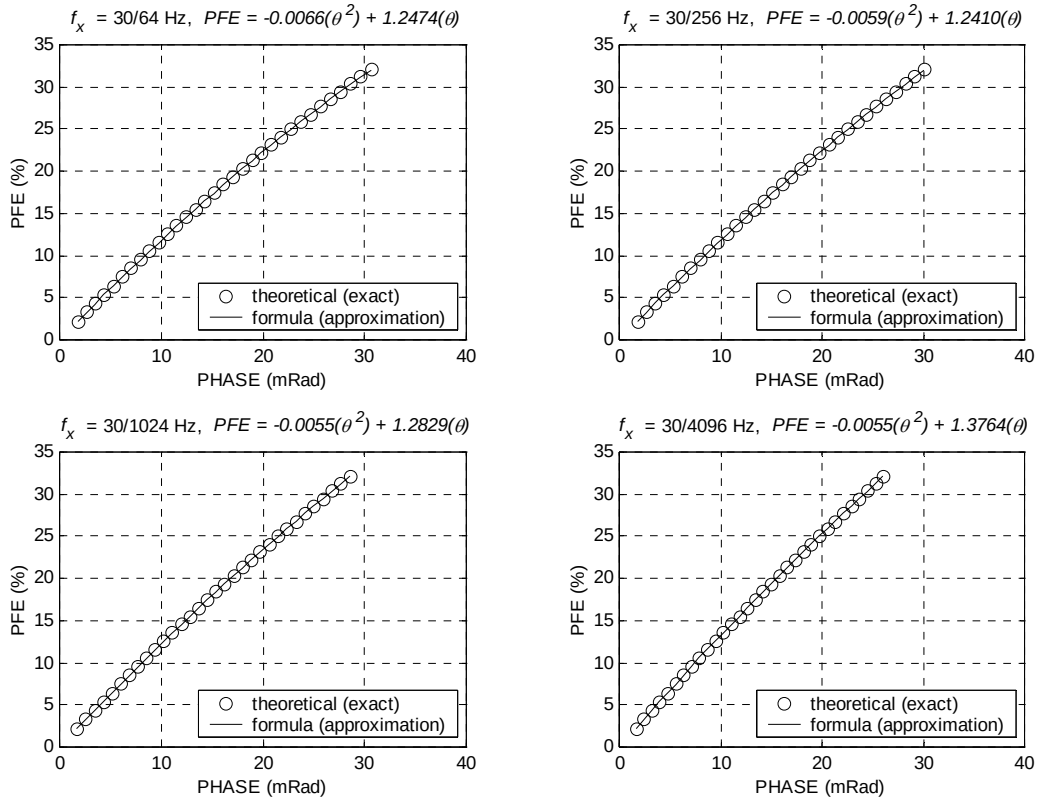

Phase vs. PFE for various pulse lengths and presuming standard Halverson-Wait spectral parameters (r-value = 1.0 and k-value = 0.2).

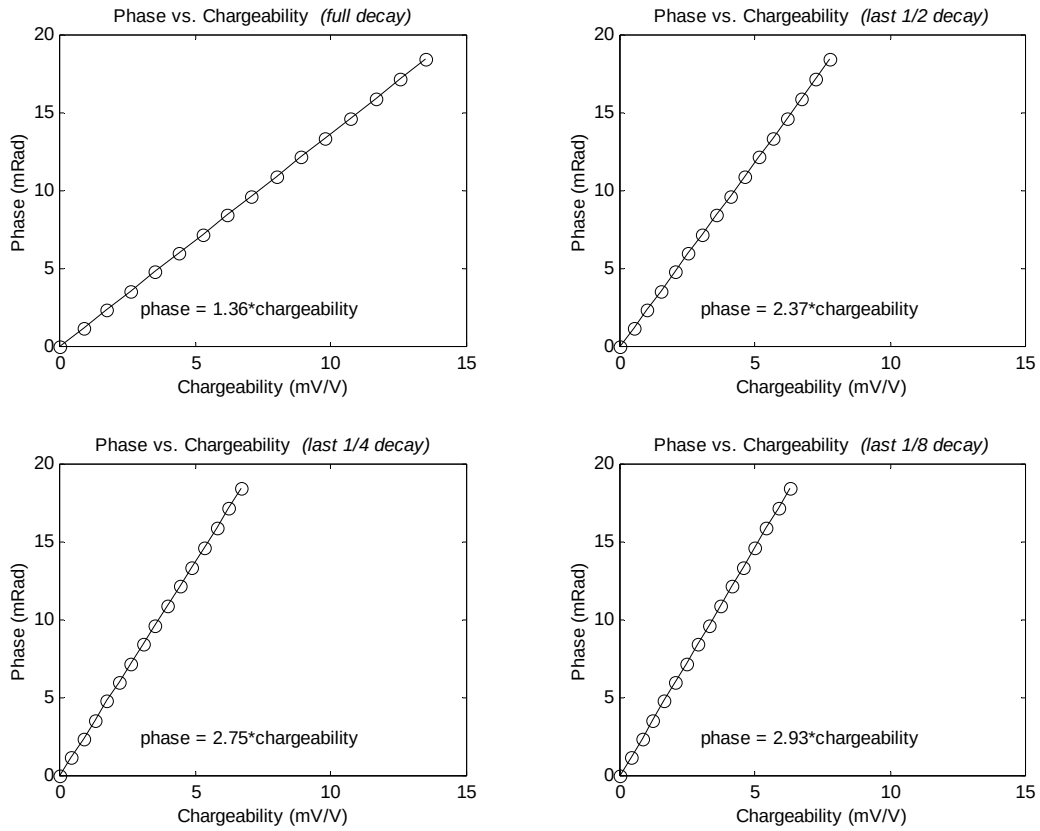

Illustration of the proportional relationship between phase (mrad) and chargeability (mV/V) for various charge/decay averaging windows

L.6 DCIP2D INVERSION

An excellent overview and introduction to both the theory and use of inversions in geophysics is available on the University of British Columbia (UBC) website (Oldenburg et al., 1998).

The DCIP2D inversion algorithms are developed by UBC-Geophysical Inversion Facility.

Mathematically, inversion is the process of fitting the observed data to a model through minimizing a function. The choice of which function to minimize ultimately defines the inversion model. In the inversion algorithm developed by UBC, this function is:

$$\phi = \phi_d + \beta \phi_m = (\text{misfit}) + \beta\,(\text{model norm})$$
$$0 < \beta < \infty \quad \text{is a constant}$$

The function to be minimized consists of a function, ϕ_d, that minimizes the data misfit, and a function ϕ_m that finds a "smooth" model. Beta, the regularization parameter, represents a relative weighting between fitting the data and smoothing the model.

Clearly, the data misfit function must be defined in more detail. One approach might be

$$\phi_d = \sum_{i=1}^{N} \left(\frac{F_i[m] - d_i^{obs}}{\varepsilon_i} \right)^2 .$$

This function defines the data misfit as the sum of the individual misfits squared (L2 norm), normalized by the errors associated with each data point. It is the least-squares definition of the data misfit.

The model misfit function must also be defined in more detail. One of the most flexible definitions is the one used by UBC

$$\phi_m(m,m_0) = \alpha_s \int_{vol} (m-m_0)^2 dv + \alpha_x \int_{vol} \left(\frac{\partial (m-m_0)}{\partial x} \right)^2 dv + \alpha_z \int_{vol} \left(\frac{\partial (m-m_0)}{\partial z} \right)^2 dv$$

In this definition there are three components to the "model norm" (or "smoothness" constraint, or "regularization"), each of which contains an α constant (α_s, α_x, α_z) that are commonly referred to as "alpha parameters", and a fourth variable m_o that refers to the starting or reference model – either a half-space or geophysical constraint – that also has a profound influence on the model-misfit.

The three "alpha" parameters represent a relative weighting of each component:

- the first component is simply an overall difference between the model and a "target" model;
- the second component is a horizontal smoothness;
- the third component is a vertical smoothness.

L.7 APPARENT RESISTIVITY OF UNIFORM HALF SPACE

From p.636, Telford et al. 1976, the apparent resistivity ρ_a is given as:

$$\rho_a = \frac{2\pi V_p}{G_f}$$

where G_f is the geometric factor defined as:

$$G_f = \left(\frac{1}{r_1} - \frac{1}{r_2}\right) - \left(\frac{1}{r_3} - \frac{1}{r_4}\right)$$

with:

r_1 the distance between current electrode P1 and potential electrode C1;

r_2 the distance between current electrode P2 and potential electrode C2;

r_3 the distance between current electrode P2 and potential electrode C1;

r_4 the distance between current electrode P2 and potential electrode C2;

L.8 DC INVERSION USING A SYNTHETIC MODEL

A synthetic resistivity model and its apparent resistivity pseudo section based on Titan-24 configuration are shown here. The model consists of a background of 1,000 ohm-m and a vertical dyke of 1 ohm-m. The synthetic DC data, V_p's, are computed using UBC's 2D forward modeling tool DCIPF2D

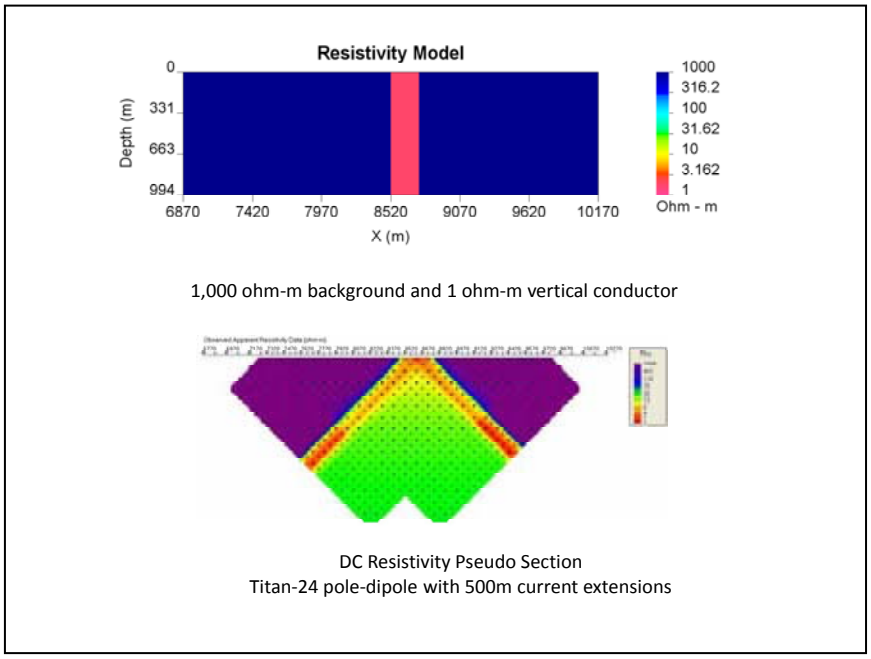

A synthetic model and its apparent resistivity pseudo section

The inverted resistivity model and the convergence curves are displayed below.

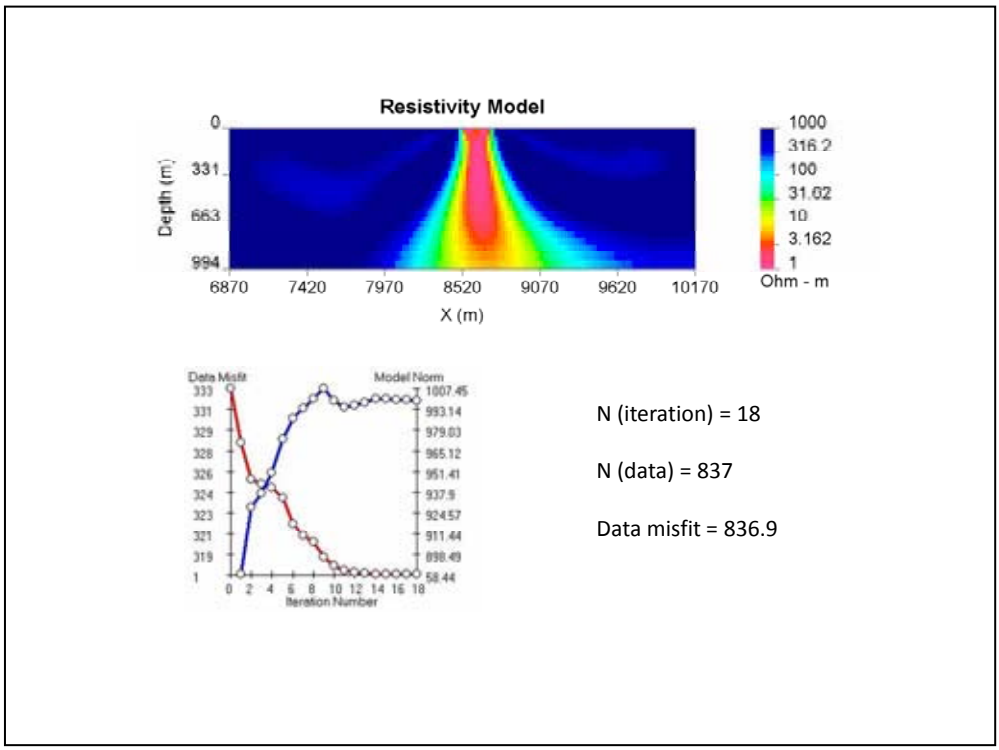

Inversion model, convergence curves and inversion statistics

L.9 IP INVERSIONS

For IP inversions, the apparent chargeability η is computed by carrying out two DC resistivity forward modeling with conductivity distributions $\sigma(x_i, z_j)$ and $(1-\eta)\sigma(x_i, z_j)$ (Oldenburg and Li, 1994), where (x_i, z_j) specifies the location in a 2D mesh.

The conductivity distributions used in IP inversions can be the inverted DC model or a half space of uniform conductivity. The IP inversion, generated through the use of a half space, is called the "NullCon" or "HSref" IP model

M INTRODUCTION TO THE MAGNETOTELLURIC METHOD

M.1 INTRODUCTION

The magnetotelluric (MT) method utilizes time-variations in the Earth's natural electric (E) and magnetic (H) fields to image the resistivity of the subsurface structure. The natural electromagnetic (EM) signals are assumed to be of plane-wave source over the frequency range with which the MT surveys are usually carried out. The plane-wave source is simpler to model compared with the complex transmitter geometries and signals used in the other EM methods. It makes the MT responses easier to understand and interpret with respect to the subsurface resistivity variations.

The E and H fields are measured over a broad range of frequencies. Typically, the frequencies can range from above 10 kHz to below 0.001Hz. Considering the conductivity of the Earth's materials and the frequency range over which the MT data are measured, the EM fields propagate in a diffusive regime. High frequency signals are attenuated more rapidly in the subsurface. Therefore, high frequency data are indicative of shallow resistivity structure while low frequency data are indicative of deep resistivity structure.

At frequencies below 1Hz the EM signal source is due to oscillations of the Earth's ionosphere as it interacts with the solar wind. At frequencies above 1Hz the signal source is due to worldwide lightning activities. There is a lack of natural signal around 1Hz, often referred to as the "hole". Modern 24-bit recording hardware and signal processing techniques, however, have largely eliminated the data quality degradations that have been traditionally seen around the 1Hz signal hole.

Between about 8Hz and 300Hz the signal from worldwide lightning activity propagates in a "resonant" cavity (the resistive atmosphere) between the conductive ionosphere and the conductive Earth's surface. Above 3 kHz the signal propagates as a ground wave. Between 300Hz and 3 kHz there is a "dead-band" where the signal does not propagate well. Despite hardware and signal processing improvements this dead-band remains problematic. When signal (atmospheric activity) is present within several hundreds of miles of the survey area the data quality improves. When no signal is being generated in the vicinity of the survey area the data quality is poor.

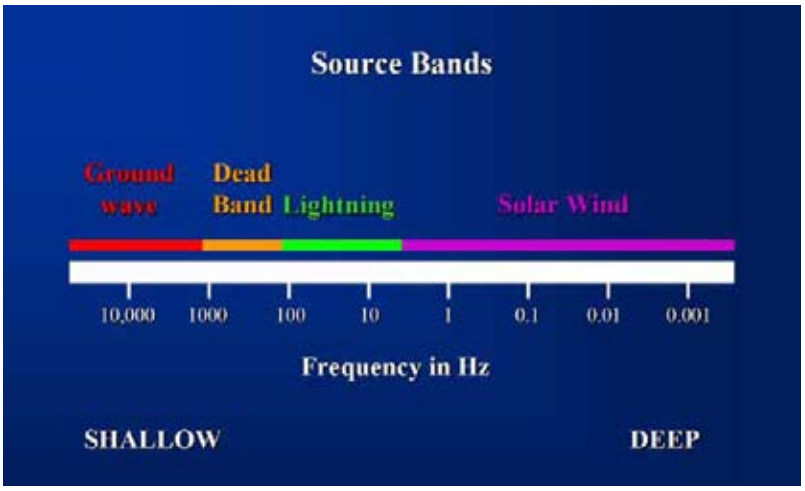

M.2 MEASUREMENTS

Both the electric and magnetic fields are measured at each site. The measured field strengths depend on the ionosphere and lightning activities and are essentially of random nature. While the E and H field strengths are random the ratio of these two fields depends on the frequency and the subsurface resistivity structure. For a homogeneous and a 1D earth resistivity structures, the magnetic field is perpendicular to the electric field. However, it is possible for a complex subsurface resistivity structure to rotate the fields. Therefore, full tensor data, including two perpendicular electric and two perpendicular magnetic fields, are usually measured.

In the field surveys, the electric and magnetic fields are measured as a function of time. The electric field is measured using two orthogonal grounded dipoles. The magnetic field is also measured using induction coils parallel to the electric dipoles.

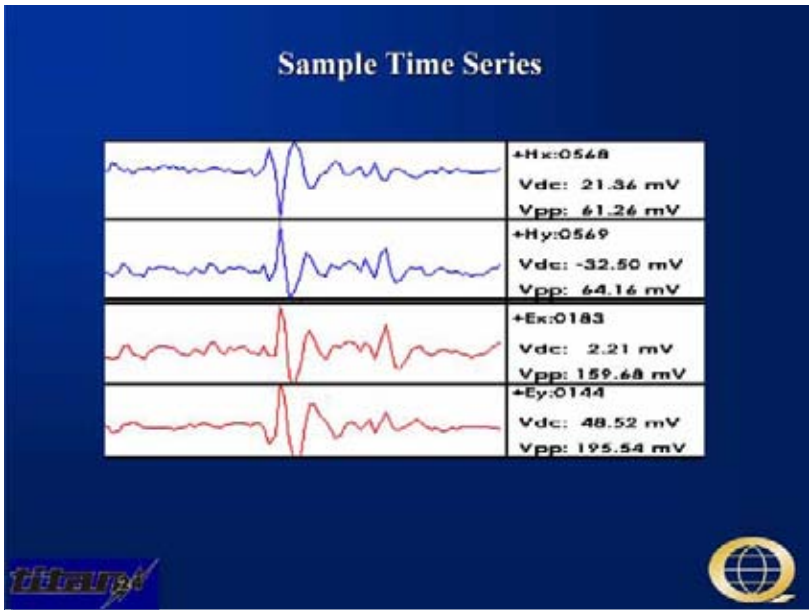

M.3 DATA PROCESSING

Extracting the subsurface resistivity structure from the measured magnetic and electric fields is a multi-step process. First, time series are transformed into frequency domain and sophisticated processing techniques are used to estimate the MT impedance tensor from the electric and magnetic fields. The impedance tensor is then used to calculate the apparent resistivity and phase data. In interpretation stage, inversion techniques are used to invert the apparent resistivity and phase data in to the subsurface true resistivity image. Finally, the resistivity image must be interpreted in terms of geologic units.

In time series processing, the measured magnetic and electric fields are Fourier transformed into the frequency domain. Calibration curves are applied to the measured fields to remove the acquisition system response. The Fourier coefficients represent the amplitude and phase of the electric and magnetic fields as a function of frequency.

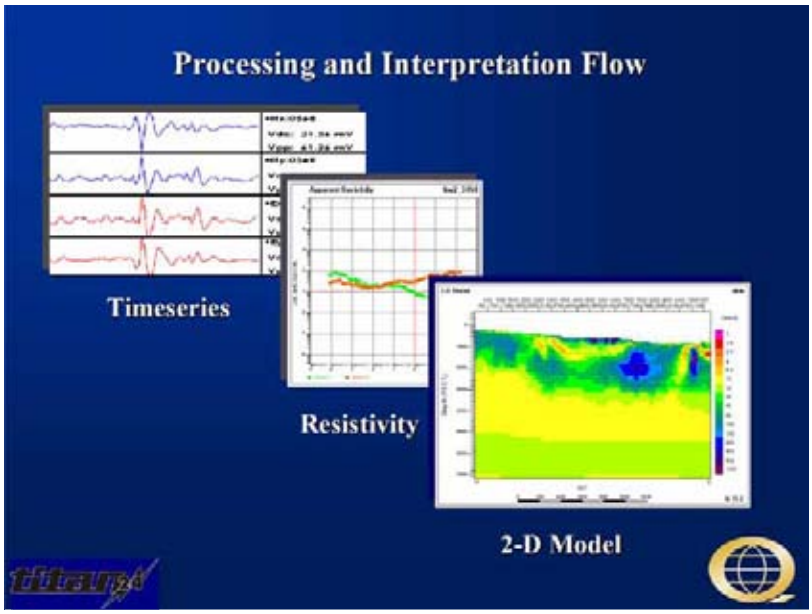

A variety of complex signal processing techniques are used to minimize noise and bias in the estimation of geophysical parameters from the measured fields. The approaches include:

- Spatial isolation of noise. A remote reference magnetic station is used to separate signal from local noise in the magnetic field data;
- Coherency sieves to find coherent signal. First the local and remote magnetic field measurements are compared and coherent signal are kept. Then the local magnetic and electric fields are compared for coherency;
- Frequency isolation of noise. Long Fourier transforms are used to provide extremely sharp isolation of noise in frequency;
- Time isolation of noise. Short Fourier transforms are used to remove noise that is isolated in time (noise spikes, or noise that is randomly turning off and on);
- Robust statistics that minimize biasing effects of a few isolated measurements.

The geophysical parameters are estimated after the processing is completed. In frequency domain, the ratio between the two measured components (E and H) is called electrical impedance (Z) and is defined as $|Z| = |E/H|$. The primary geophysical parameters are usually represented as plots of the apparent resistivity versus frequency and the phase versus frequency. The impedance values are used to calculate apparent resistivity and phase data as follows:

$$\rho_a(\Omega m) = \frac{1}{\mu\omega}|Z|^2 \quad \text{and} \quad \varphi = \arg(Z)$$

The apparent resistivity is a function of the frequency. The apparent resistivity can be considered as a volumetric weighted average of the resistivity and thickness of the rocks being sampled. Consequently, it is a smoothly varying function of the frequency. It can be shown theoretically that on a log-log plot of the apparent resistivity vs. frequency the curve cannot exceed a slope of +/- 45 degrees for a layered earth model. For a homogenous half-space or a one-dimensional (1D) earth the phase is related to the apparent resistivity through the Hilbert transform. This association does not exist for the 2D and the 3D earth models.

M.4 INTERPRETATION

Plots of apparent resistivity and phase data versus frequency in a log-log scale are a conventional way of looking at the data before interpretation. If the survey involves several MT sites located along a line pseudo-sections of the apparent resistivities and phases in both components provides a first impression of the resistivity variation of the subsurface along the survey line.

The depth of penetration of the EM signal depends on the frequency of the data and the resistivity of the subsurface. The depth at which the signal amplitude attenuates to 37% (1/e) of its initial value is called the electromagnetic skin depth (δ) and is defined as:

$$\delta(m) = \sqrt{\frac{2}{\mu\omega\sigma}} = 503\left(\sqrt{\frac{\rho}{f}}\right)$$

where δ (m) is the skin depth, μ the magnetic permeability, σ (S/m) the conductivity (1/resistivity), ω the angular frequency (=2πf), f (Hz) the frequency, and ρ (Ωm) the resistivity (1/conductivity)

The skin depth concept provides an estimation of the maximum depth of investigation of the MT data.

The following plots illustrate example of the apparent resistivity curves for two MT sites as well as the apparent resistivity cross-sections along a MT line over a simple geological model.

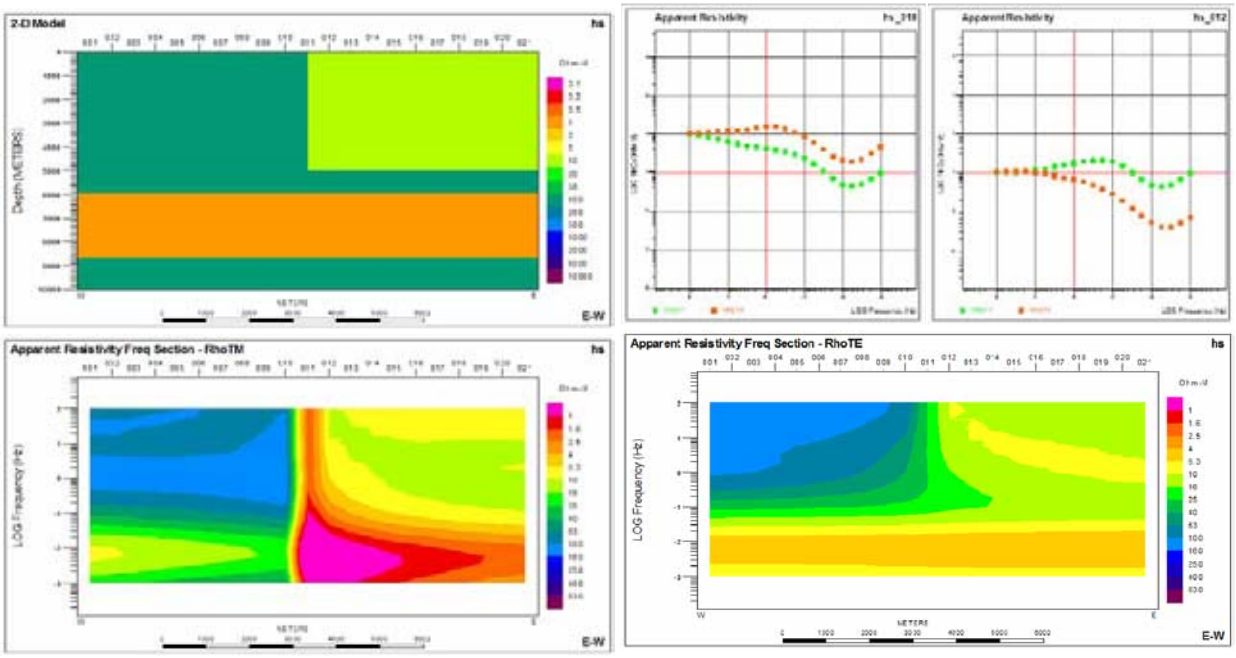

Interpretation of the MT data is performed using the maps of true resistivity of the subsurface. Inversion algorithms in one-dimension (1D), two-dimension (2D), and three-dimension (3D) are used to invert the apparent resistivity and phase data in to the maps of true resistivity of the subsurface. A simple layered subsurface structure generally can adequately be reproduced using the 1D inversion. In the case of more complex 2D or 3D structures, the MT response will be affected by lateral variations in resistivity. Consequently, a 2D or 3D inversion algorithm is required to allow the lateral resistivity variations.

In 1D earth assumption, off-diagonal elements of the impedance tensor are equal and of opposite signs and the diagonal elements are zero. The 1D inversion of the MT data produces a resistivity-depth profile

for each MT site. The results represent a first order approximation of the resistivity variations with depth using a layered-earth model.

If there are lateral variations in the resistivity of the subsurface along one direction only (perpendicular to the strike) then a 2D inversion and interpretation is required. In this case, for a data rotated to the strike direction, off-diagonal elements of the impedance tensor are of opposite signs but not equal and the diagonal elements are zero. Because the electrical conductivity is constant along the strike direction (for example x-direction) all derivatives with respect to x will be zero. Therefore, Maxwell's equations are simplified and can be separated into two distinct modes so-called Transverse Electric (TE) and Transverse Magnetic (TM). The TE-mode represents the condition where the electric field is parallel to the strike direction while the TM-mode represents the condition where the magnetic field is parallel to the strike direction.

A cross-section of the true resistivity variations perpendicular to the assumed strike direction is created in the 2D inversion and is used in interpretation. For more complex geological structures a 3D inversion is essential to adequately describe the resistivity variation of the subsurface. In this case, none of the elements in the impedance tensor are equal or zero.

One of the factors that can affect the multi-dimensional MT data and interpretation is "static shift". The apparent resistivity curves can be biased (shifted up or down) by lateral resistivity contrasts with dimensions smaller than the minimum wavelength of the EM fields. These small features cannot be resolved by the MT data and they introduce a DC shift on the log-log apparent resistivity plots. This effect can be recognized by examining the sounding resistivity curves from the neighbouring MT sites and most be treated before the interpretation. Note that there are no static shift effects in the phase data.

N REFERENCES

N.1 TITAN-24 METHOD AND APPLICATION

Donohue, J.G., and Sheard, S.N., 2001. Geophysics in North West Queensland – Improving the use of electrical geophysics. AIG Journal Paper 2001-01.

Garner, S., and Webb, D., 2000. Broadband MT and IP electrical property mapping with MIMDAS. SEG Technical Program Expanded Abstracts, 1085-1088.

Goldie, M., 2007. A comparison between conventional and distributed acquisition induced polarization surveys for gold exploration in Nevada. The Leading Edge, 26 (2), 180-183.

Hollyer, G, and Hearst, R., 2009. Deep exploration technologies for discovery in the shadow of head frames. First Break, 27 (July), 99-105.

Kingman, J., and Garner, S., 2003. Benefits of large channel capacity systems in electrical geophysics. ASEG 16th Geophysical Conference and Exhibition, Adelaide.

Legault, J., Carriere, D., and Petrie, L., 2008. Synthetic model testing and distributed acquisition dc resistivity results over an unconformity uranium target from the Athabasca Basin, northern Saskatchewan. The Leading Edge, 27 (1), 46-51.

Sheard, N., 1998. MIMDAS: A new direction in geophysics. Proceedings of the ASEG 13th International Conference, Hobart, Tasmania.

White, M., and Gordon, R., 2003. Deep imaging: New technology lowers cost of discovery. Canadian Mining Journal, April, 27-28.

L. Caron, 1996, 1995-1996 Compilation and interpretation of Data and Metallurgical Program- Final Technical Report, New Nadina Explorations Ltd.

JDS Energy & Mining Inc., 2011, Technical Report for the Silver Queen Property- New Nadina Explorations Ltd.

N.2 DIRECT CURRENT (DC) AND INDUCED POLARISATION (IP) METHODS

Halverson, M.O., Zinn, W.G., McAlister, E.O., Ellis, R., and Yates, W.C., 1981. Assessment of results of broad-band spectral IP field test. In: Advances in Induced Polarization and Complex Resistivity, 295-346, University of Arizona.

Johnson, I.M., 1984. Spectral induced polarization parameters as determined through time-domain measurements. Geophysics, v. 49, 1993-2003.

Li, Y., and Oldenburg, W., 2000. 3-D inversion of induced polarization data. Geophysics, v 65 (6), 1931-1945.

Loke, M.H., 2004. Tutorial: 2D and 3D electrical imaging surveys, Res2Dinv and Res3Dinv manual [www.geoelectrical.com].

Oldenburg, D., and Li, Y., 1994. Inversion of induced polarization data. Geophysics, 59, 1327-1341.

Oldenburg, D., Li, Y., and Jones, F., 1998. Tutorial: Inversion (Res/IP) Methodology. In: The UBC-GIF Tutorials [http://www.geop.ubc.ca/ubcgif].

Oldenburg, D., and Li, Y., 1999. Estimating depth of investigation in DC and IP surveys. Geophysics, 64, 403-416.

Pelton, W.H., Ward, S.H., Hallof, P.G., Sill, W.R. and Nelson, P.H., 1978. Mineral discrimination and removal of inductive coupling with multi-frequency IP. Geophysics, v.43, 588-609.

Quantec, 2009. Standard chargeability calculations in Titan-24 IP measurements. Quantec Technical Note 001.

Seigel, H., 1959. Mathematical formulation and type curves for induced polarization. Geophysics, 24, 547-565.

Telford., W.M., Geldart, L., Sheriff, R., and Keys, D., 1976. Applied Geophysics. Cambridge University Press, New York, NY.

Van Blaricom, R., 1992. Practical Geophysics for the Exploration Geologist. Nortwest Mining Association, Spokane, WA.

Wait, J., 1959. Overvoltage Research and Geophysical Applications. Pergammon Press.

N.3 MAGNETOTELLURIC (MT) METHOD

Bahr, K., and Simpson, F., 2005, Practical Magnetotellurics, Cambridge University Press.

Constable, S.C., Parker, R.L., and Constable, C.G., 1987. Occam's inversion - A practical algorithm for generating smooth models from electromagnetic sounding data. Geophysics, 52 (3), 289-300.

de Lugao, P.P., and Wannamaker, P.E., 1996. Calculating the two-dimensional magnetotelluric Jacobian in finite elements using reciprocity. Geophysical Journal International, 127, 806-810.

Marquardt, D.W., 1963. An algorithm for least-squares estimation of non-linear parameters. J. Sot. Ind. Appl. Math., 11, 431–441.

Nabighian, M.N., 1987. Electromagnetic Methods in Applied Geophysics, Volume 2: Application (Parts A and B). Society of Exploration Geophysicists (SEG), Tulsa.

Orange, A.S., 1989. Magnetotelluric exploration for hydrocarbons. Proceedings of the IEEE, 77, 287-317.

Rodi, W., and Mackie, R.L., 2001. Nonlinear conjugate gradients algorithm for 2D magnetotelluric inversions. Geophysics, 66, 174-187.

Siripunvaraporn, W., Egbert, G., Lenbury, Y., and Uyeshima, M., 2005. Three-Dimensional Magnetotelluric: Data Space Method. Physics of the Earth and Planetary Interiors, 150, 3-14.

Vozoff, K., 1972. The Magnetotelluric method in the Exploration of Sedimentary basins. Geophysics, 37, 98-141.

Wannamaker, P.E., Stodt, J.A., and Rijo, L., 1987. A stable finite-element solution for two-dimensional magnetotelluric modeling. Geophysical Journal of the Royal Astronomical Society, 88, 277-296.

Wight, D.E., 1987. MT/EMAP Data Interchange Standard, Revision 1.0. Society of Exploration Geophysicists (SEG). (Document available at the SEG web site: www.seg.org).

Quantec Geoscience Ltd Summary Table	
CLIENT	
Client / Company Name	New Nadina Explorations Ltd.
Client Main Location	(British Columbia, Canada)
Client Representative	Ellen Clements
Phone Number	(250) 445-2260
Fax Number	(250) 445-2259
Email Contact (if available)	Karine.brousseau@innovexplo.com
PROJECT	
Project Grid Name	Silver Queen Project
Project Grid Location	(British Columbia, Canada)
Survey Type	Titan-24 DC IP & MT
Survey Period (YY/MM/DD to YY/MM/DD)	2011/07/07 to 2011/07/20
Quantec Project Number	CA00857T
Responsible Geophysicist	Nasreddine Bournas
Data Processor	Joanne Cowburn
REPORT	
Report Date	03/10/2011
Quantec Template Version	2011.2